Wood Cellulose-Based New Materials: Functionalization and Applications

by

Xiaoyu Gong

A thesis submitted in partial fulfillment of the requirements for the degree of

Doctor of Philosophy

in

Food Science and Technology

Department of Agricultural, Food and Nutritional Science
University of Alberta

Abstract

Canada has great forest area with tremendous wood-based cellulose resource. However, the research effort for wood fibers to develop wood cellulose-based advanced materials is still limited. The overall objective of this research is to provide some feasible and efficient approaches for the functionalization and application of wood-based cellulose materials.

First, spruce cellulose was hydrolyzed by diluted sulfuric acid of various concentrations and hydrolysis times. The dissolution of these hydrolyzed samples was investigated in a NaOH/urea aqueous solution system considered environmentally "green". The effects of acid hydrolysis on the structure and properties of subsequent thermally induced gels were examined using scanning electron microscopy, swelling and reswelling experiments, and mechanical test. The molecular weight of spruce cellulose was significantly reduced by acid hydrolysis, whereas its crystallinity slightly increased because of the removal of amorphous regions. Hydrolyzed cellulose samples with lower molecular weight exhibited higher solubility. Rheological experiments showed these cellulose suspensions could form gels easily upon heating. A porous network structure was observed in which dissolved cellulose was physically crosslinked upon heating and then regenerated to form a 3D network, where the dispersed swollen cellulose fibers filled spaces to reinforce the structure. The swelling behavior and mechanical properties of these "matrix-filler" gels could be controlled by varying the mild acid hydrolysis conditions, which adjusts their degree of solubility.

Second, wood cellulose was consecutively oxidized to prepare oxidized cellulose nanocrystals followed with modification by phenyltrimethylammonium chloride to create hydrophobic domains comprised of phenyl groups. These modified oxidized cellulose nanocrystals were homogeneous/electrostatically stable in water and they can stabilize O/W Pickering emulsions.

The dispersed phase volume fraction (DPVF) of the Pickering emulsion was 0.7 at around 1.5 g/L, whereas the tween-20 control needed a 13-fold greater concentration to have a similar DPVR. In addition, these modified oxidized cellulose nanocrystal stabilized Pickering emulsions also showed good mechanical and thermal stability against centrifugation and heat, as well as size controllability.

Next, hydrocolloidally stable cellulose nanocrystals (CNCs) with zeta potentials lower than -30 mV at low electrolyte concentrations were prepared from wood-based cellulose. The cellulose nanocrystals were then homogeneously distributed in aqueous Poly(vinyl alcohol)(PVA) solutions and embedded evenly in the PVA matrix after crosslinking and freeze-drying. The morphology observations revealed the crosslinked CNCs/PVA aerogels had a strong, dense, and porous structure with cellulose nanocrystals percolated in the networks and supported by the crosslinked PVA matrix. The mechanical study showed small amount of cellulose nanocrystals (0.5-2.0 $^{w}/_{w}$%) can significantly increase the compressive modulus of the aerogels from 49.9±5.2 KPa to 200.9±8.0 KPa. Further compressibility studies graphically demonstrated the excellent shape recovery of the crosslinked CNCs/PVA aerogels and the aerogels could be cyclically compressed for ten times without significant variation in mechanical performance. Molecular interaction study by FTIR and crystallinity study by wide-angle x-ray diffraction indicated cellulose nanocrystals firstly formed the percolated network with each other by hydrogen bonding, and then strongly interacted with PVA matrix by hydrogen bonding. Meanwhile, the PVA matrix was further crosslinked by epichlorohydrin to form the strong, dense, and porous microstructures.

Finally, compressive aerogels were prepared from cross-linked poly(vinyl alcohol)/cellulose nanocrystals, followed by modification through thermal chemical vapor deposition of methyltrichlorosilane. With the 3D interconnected microstructure, the aerogels were highly porous

(porosity > 97.69%) and ultralight with density ranging from 22.50 to 36.13 mg/cm^3, and floatable on water surface. The wettability test revealed that the aerogel surfaces were highly hydrophobic with contact angles to water droplet up to 144.5°. In addition, the aerogels could be compressible up to 50 cycles without significant decrease in mechanical strength, thus demonstrated excellent robustness. The aerogels were capable of absorbing various oils and nonpolar solvents and efficiently separating them from water, with the absorption capacity up to 32.70 times of its original weight. Two simple approaches, including squeezing and rinsing, were applied to recycle the aerogels, demonstrating the aerogels could be cyclically used without obvious decrease of absorption capacity up to 10 times.

In summary, this research has developed several feasible approaches for the functionalization and application of wood-based cellulose materials. The hydrogels, Pickering emulsions, compressive aerogels, and oil absorbents fabricated from wood-based cellulose materials are potential for a wide range of applications.

Preface

Chapter 3 of this thesis has been published as Xiaoyu Gong, Yixiang Wang, Zhigang Tian, Xiang Zheng, Lingyun Chen, "Controlled production of spruce cellulose gels using an environmentally "green" system" in *Cellulose*, 2014, 21(3): 1667-1678. In this chapter, Xiaoyu Gong was responsible for the experimental design and conducting the experiments, data collecting and analysis, writing the manuscript. Dr. Yixiang Wang provided assistance in SEM observation and revising the manuscript. Zhigang Tian provided assistance in the characterization of the viscosity-average molecular weight of the hydrolyzed cellulose samples. Dr. Xiang Zheng contributed to the data analysis of the mechanical performance of the hydrogels. Dr. Lingyun Chen was the supervisor and corresponding author and contributed to the experimental design, data discussion, manuscript edits and submission.

Chapter 4 of this thesis has been published as Xiaoyu Gong, Yixiang Wang, Lingyun Chen, "Enhanced emulsifying properties of wood-based cellulose nanocrystals as Pickering emulsion stabilizer" in *Carbohydrate polymers*, 2017, 169: 295-303. In this chapter, Xiaoyu Gong was responsible for the experimental design and conducting the experiments, data collecting and analysis, writing the manuscript. Assistance was received from Dr. Yixiang Wang in obtaining the SEM images and revising the manuscript. Dr. Lingyun Chen was the supervisor and corresponding author and contributed to the experimental design, data discussion, manuscript edits and submission.

Chapter 5 of this thesis has been submitted as Xiaoyu Gong, Yao Huang, Jingqi Yang, Guangyu Liu, Weijuan Huang, Yixiang Wang, Lingyun Chen, "Robust and highly compressible aerogels based on cellulose nanocrystals percolated networks supported by crosslinked PVA matrix". In this chapter, Xiaoyu Gong was responsible for the experimental design and conducting the

experiments, data collecting and analysis, writing the manuscript. Dr. Yao Huang aided in SEM observations. Dr. Jingqi Yang provided assistance in WAXD characterization. Guangyu Liu and Weijuan Huang provided assistance in mechanical study and data discussion of SEM observations. Assistance was received from Dr. Yixiang Wang in experimental design, SEM image analysis. Dr. Lingyun Chen was the supervisor and corresponding author and contributed to the experimental design, data discussion, manuscript edits and submission.

Chapter 6 of this thesis has been submitted as Xiaoyu Gong, Yixiang Wang, Hongbo Zeng, Mirko Betti, Lingyun Chen, "Highly porous, hydrophobic, and compressible PVA/cellulose nanocrystals aerogels as recyclable absorbents for oil-water separation". In this chapter, Xiaoyu Gong was responsible for the experimental design and conducting the experiments, data collecting and analysis, writing the manuscript. Assistance was received from Dr. Yixiang Wang in obtaining the SEM images and data discussion. Drs. Hongbo Zeng, Mirko Betti, Lingyun Chen were supervisory authors. Dr. Zeng provided accessible lab equipment including FTIR and contact angle goniometer. Assistance was received from Drs. Hongbo Zeng and Mirko Betti for the data discussion. Dr. Lingyun Chen was the supervisor and corresponding author and contributed to the experimental design, data discussion, manuscript edits and submission.

Acknowledgements

I would like to thank my supervisor Dr. Lingyun Chen, who provided instruction and support to me during my PhD program. She offered this great opportunity to me, helped me adjust to a completely new environment, provided professional guidance for my research, encouraged me when I lost confidence, trained me to be a qualified and mature researcher. Without her enormous and continuous support, encouragement, guidance, and care, I can not get to this step in my program. I also thank Dr. Hongbo Zeng and Dr. Mirko Betti for being my supervisory committee members and all the valuable feedback they provided during my PhD program. Dr. Hongbo Zeng and Dr. Mirko Betti provided enormous patience, support, and encouragement all along these years. Many thanks go to Dr. Hongbo Zeng for providing accessible lab equipment including FTIR and contact angle goniometer. Special thanks go to Dr. Ning Yan and Dr. John Wolodko for being my external examiners in my final defense.

I am so grateful to my lovely group members and friends. It is a great experience to cooperate with them, to share ideas with them, and to encourage with each other in this group. They are excellent researchers in academic community and great friends in daily life.

I would like to give credit to the China Scholarship Council (CSC) for financial support of my PhD program and the Alberta-Pacific Forest Industries Inc. for their supply of the raw wood-based cellulose pulps.

Finally, I would like to thank my parents, my sisters, and my wife. My parents give me a life and bring me up with unconditional love and endless support, I am so proud to be their son. My sisters in China take care of my parents and support me all through these years. My wife, Jasmine Yijun Chen, is always there supporting and encouraging me. I am so appreciated that we can have this fantastic journey together to experience the ups and downs in our life.

Table of Contents

List of Tables

List of Figures

List of Abbreviations and Symbols

AC	Absorption capacity
AFM	Atomic force microscopy
AGU	Anhydroglucose unit
AMIMCl	1-Allyl-3-methylimidazolium chloride
ANOVA	Analysis of variance
APS	Ammonium persulfate
BC	Bacterial cellulose
BMIMCl	1-Butyl-3-methylimidazolium chloride
CI	Crystallinity index
CNCs	Cellulose nanocrystals
CNFs	Cellulose nanofibers
CP	Content of phenyltrimethylammonium
CVD	Chemical vapor deposition
DLS	Dynamic light scattering
DMAc	N, N-Dimethylacetamide
DMAEMA	N, N-(Dimethylamino)ethyl methacrylate
DMSO	Dimethyl sulfoxide
DP	Degree of polymerization
DPVF	Dispersed phase volume fraction
DSC	Differential scanning calorimetry
ECH	Epichlorohydrin
ESR	Equilibrium swelling ratio
FTIR	Fourier transform infrared spectroscopy
G'	Storage modulus
G''	Loss modulus
ha	Hectare
IC	Inclusion complex

ILs	Ionic liquids
M_n	Number-average molecular weight
M_w	Weight-average molecular weight
M_η	Viscosity-average molecular weight
m-O-CNCs	Modified oxidized CNCs
MTCS	Methyltrichlorosilane
NMR	Nuclear magnetic resonance
NMMO	N-methyl-morpholine-N-oxide
O-CNCs	Oxidized cellulose nanocrystals
O/W	Oil-in-water
PTAC	Phenyltrimethylammonium chloride
PVA	Poly (vinyl alcohol)
S_a	Solubility index
SEC	Size-exclusion chromatography
SEM	Scanning electron microscopy
RC	Regenerated cellulose
TDDS	Transdermal drug delivery system
TEM	Transmission electron microscopy
TEMPO	2,2,6,6-Tetramethylpiperidine 1-oxyl
W/O	Water-in-oil
WAXD	Wide-angle X-ray diffraction
ΔG_d	Gibbs free energy
θ	Contact angel
γ_{ow}	Tension at oil and water interface
γ_{po}	Tension at particle and oil interface
γ_{pw}	Tension at particle and water interface

Chapter 1 - Introduction

1.1 Introduction

Cellulose is a linear natural polymer, compositing of D-anhydroglucopyranose units linked by *β*-1,4-glucosidic bonds. It can be obtained from various sources, including higher plants (wood, cotton, bamboo, sisal, hemp, linin, etc.), several marine animals, algae, bacteria, fungi, invertebrates, and even amoeba (protozoa)[1]. With a rough estimation, cellulose is the most abundant biomaterial on the earth with an annual production of ~1.5×10^{12} tons[2-4], in which cotton and wood-based cellulose is mostly widely distributed[5]. Due to the specific requirement for geography and climate, cotton fibers are not readily available in cold areas, whereas wood fibers, as the largest source of cellulose, are abundant worldwide, especially in the countries with great forest area. Even though the content of cellulose in wood fibers (~50%) is lower than that in cotton fibers (up to 90%), recent techniques and industrial plants in wood pulping make it possible to extract cellulose from wood with high purity[6]. Therefore, a large-scale application of wood-based cellulose materials can be achieved.

However, currently, wood fibers are mainly used as the raw material for paper-making and lumbering, only 2% with high content of cellulose pulps are used to prepare regenerated cellulose fibers, films, and some cellulose derivatives (cellulose esters and cellulose ethers)[3]. The research effort for wood fibers to develop wood cellulose-based advanced materials is still limited, and the huge value behind wood-based cellulose needs to be unveiled.

1.1.1 Cellulose supramolecular structure

The three hydroxyl groups of the anhydroglucose unit (AGU) and the oxygen atoms in the D-glucopyranose and the glycosidic linkage can interact with each other within the chain or with another chain by forming intramolecular and intermolecular hydrogen bonds. FTIR[7, 8] and solid-

state NMR[9] revealed that the hydroxyl groups at C3 and the oxygen atom in the adjacent pyranose ring forms intramolecular hydrogen bonds in all cellulose molecules. The hydroxyl groups at C6 and the neighboring hydroxyl groups at C2 also form intramolecular hydrogen bonding[1]. Additionally, cellulose molecules are also connected with each other by intermolecular hydrogen bonding in the crystalline regions, especially for the hydroxyl groups at C6 and the oxygen atoms at an adjacent chain in native cellulose[10]. With the strong intra-/intermolecular interactions, multiple cellulose chains form the elementary fibrils and further assemble into larger microfibrils (5-50 nm in diameter and several microns in length)[6]. Due to the intra/inter-molecular hydrogen bonding network, as well as some other molecular interactions (van der Waals force, hydrophobic interactions), cellulose molecules are alternatingly arranged in a highly ordered (crystalline) regions and disordered (amorphous) regions within the cellulose fibrils[6]. This complicated supramolecular structure makes it challenging to process cellulose materials, since the supramolecular structure has a significant influence on the solubility of cellulose molecules, the reactivity of the three hydroxyl groups, the crystallinity, the rigidity of cellulose chains[1], etc.

1.1.2 Cellulose dissolution solvents

To functionalize and expand the applications of cellulose materials, the supramolecular structure of cellulose is always involved. Dissolution of cellulose materials in an efficient solvent and then regeneration into some advanced functional products is a promising way. Even though cellulose forms supramolecular structures by the strong intra-/intermolecular hydrogen bonds, making it insoluble in water and most common organic solvents[11, 12], cellulose can be dissolved in some specific solvent systems. The traditional CS_2/NaOH system has been employed to dissolve cellulose materials for a long time, in which raw cellulose is alkalized by NaOH and then reacted with CS_2 to form cellulose xanthogenate following with regeneration to form various cellulose

films, membranes, and sponges[13]. However, the traditional CS_2/NaOH system involves complicated procedures, high energy consumption, considerable amount of toxic gas (CS_2 and H_2S), discharge of great amount of alkaline water/acidic water/waste residue. Therefore, currently this approach has been abandoned in most countries. Some other solvent systems to dissolve cellulose materials include N-methyl-morpholine-N-oxide (NMMO)[14, 15], ionic liquids (ILs)[16, 17], N,N-dimethylacetamide (DMAc)/LiCl systems[18], etc. These approaches are not widely employed for the efficient dissolution of cellulose materials, due to the considerable by-products, high cost, toxicity, difficulty with scale-up, and environmental pollution, etc.

Recently, a new aqueous cellulose solvent, i.e., 7.0 $^{w}/_{w}$% NaOH/12 $^{w}/_{w}$% urea aqueous system has been developed that can effectively dissolve cotton linters with low viscosity-average molecular weight (M_η<11.4×10^4 Da) at -12.6 ℃ within 5 minutes[19]. Compared with the solvents above, this aqueous system is environmentally "green" and cost-effective without using any organic or toxic reagents. In this NaOH/urea system, cellulose chains are held in an inclusion complex (IC) involving a NaOH hydrate, urea hydrate and water cluster at low temperature, which can disrupt the intra-/intermolecular hydrogen bonding in cellulose chains and result in the dissolution of cotton-based cellulose[20].

However, this NaOH/urea solvent system was only reported and applied on cotton linters with low viscosity-average molecular weight (M_η<11.4×10^4 Da). For the countries like Canada in cold area, cotton-based cellulose is not readily available, whereas wood-based cellulose is abundant. Wood-based cellulose usually has high viscosity-average molecular weight (M_η>11.4×10^4 Da) and cannot be effectively dissolved in this solvent system. It is worthwhile to apply this environmentally "green" and cost-effective solvent system on wood-based cellulose and provide an avenue for the applications of wood-based cellulose materials.

1.1.3 Cellulose nanocrystals

Disintegration of cellulose chains is another potential approach to breakdown the supramolecular structure of cellulose materials for functionalization and applications. Since cellulose molecules are alternatingly arranged in a highly ordered (crystalline) regions and disordered (amorphous) regions within the cellulose fibrils, cellulose fibers can be disintegrated into rod-like cellulose nanocrystals that have the dimensions in nanoscale range with the diameter of 2-10 nm and length of 100-600 nm.

Generally, chemically induced disintegrating strategies are applied for cellulose nanocrystal preparation, in which the amorphous regions of cellulose are removed, and the highly crystalline regions are preserved, resulting in rigid rod-like cellulose nanocrystals without apparent defect[21]. Sulfuric acid hydrolysis is the most widely used method to prepare cellulose nanocrystals. When subjected into sulfuric acid, the surface hydroxyl groups of cellulose nanocrystals can react with sulfuric acid via an esterification process to form charged sulfate ester groups. This sulfate groups are randomly distributed along cellulose nanocrystals and form a negatively electrostatic layer covering the surface of cellulose nanocrystals, which promotes their dispersion in water[22]. Recently, (2,2,6,6-tetramethylpiperidine 1-oxyl)-mediated (TEMPO-mediated) oxidation of cellulose materials has also been studied to prepare the carboxylated cellulose nanocrystals, due to its high selectivity of oxidation on the surface of cellulose chains[23-28], in which only the hydroxylmethyl groups of cellulose are oxidized to the carboxyl groups, and the secondary hydroxyl groups remain intact. Based on this TEMPO-mediated processing, Yang et al. (2012) developed a new method with three steps of oxidation to prepare highly electrosterically stable cellulose nanocrystals. The obtained rod-like cellulose nanocrystals have similar dimensions to

those prepared by acid hydrolysis but a much larger charge density. Therefore, this TEMPO-oxidised cellulose nanocrystal suspension is highly electrosterically stable[29].

1.1.4 Cellulose hydrogels based on NaOH/urea aqueous system

Hydrogels are physically or chemically crosslinked polymer networks that are able to absorb large amount of water[30]. They have attracted much attention since they have wide applications in biomedicine, pharmaceutical engineering, separation technology, electronic devices, biosensors, agricultural industry, contact lenses, food packaging, cosmetic industry, etc[31]. Cellulose materials have some excellent merits, such as low density, renewability, biodegradability, biocompatibility, and nontoxicity, etc[2]. Additionally, cellulose materials are highly hydrophilic due to the abundant hydroxyl groups on the surface of the molecules, which endows cellulose-based hydrogels the great potential to hold large amount of water. Meanwhile, the abundant hydroxyl groups on the cellulose molecules facilitate the physical or chemical crosslinking of the molecules during the preparation of the cellulose-based hydrogels. Furthermore, cellulose materials exhibit outstanding mechanical properties (elastic modulus ~100-200 GPa[22]), which is essential for the fabrication of cellulose-based hydrogels with excellent mechanical strength. Therefore, cellulose materials are ideal candidates for the fabrication of versatile and robust hydrogels.

Currently, cotton-based cellulose materials have been prepared into hydrogels by both physical and chemical crosslinking methods in the NaOH/urea aqueous system. Cai & Zhang (2006) studied the gelation behavior of cotton-based cellulose molecules in the NaOH/urea aqueous system and found the cellulose hydrogels could be formed via destructing the stability of cellulose solution by increasing the temperature to 50 ℃ or reducing it to -20 ℃[32]. This physical crosslinking involves a process of breaking the hydrogen bonding system of the inclusion complex (IC) of cellulose/NaOH hydrate/urea hydrate/water cluster and rebuilding the system with new hydrogen

bonding networks. Rheological test further revealed the influence of cellulose molecular weight, concentration, and temperature on the gelation behavior, indicating the gelation temperature was decreased with the increase of the cellulose concentration and its molecular weight. Moreover, Zhou et al. (2007) studied the cellulose hydrogels prepared from cotton-based cellulose in the NaOH/urea aqueous system using epichlorohydrin as crosslinker. As a result, the mechanical properties of the obtained hydrogels were significantly increased[33].

However, wood-based cellulose materials have not been reported to be dissolved in the NaOH/urea aqueous system yet, since this NaOH/urea aqueous solvent is not applicable to some native celluloses with high viscosity-average molecular weight (M_η>11.4×10^4 Da)[19]. It would be useful to adapt this environmentally "green" solvent to wood-based cellulose to produce materials with different attributes and applications compared to those from cotton linters.

1.1.5 Cellulose materials as Pickering emulsion stabilizer

Pickering emulsions are the emulsions stabilized by solid colloids instead of traditional surfactants. These solid colloids include TiO_2 nanoparticles, chitin nanocrystals, starch particles, flavonoid particles, etc[34-37]. Depending on whether the particles are predominantly hydrophilic or hydrophobic, the systems may be either oil-in-water (O/W) emulsions or water-in-oil (W/O) emulsions[38]. Compared to the traditional surfactants, these solid colloids are usually biocompatible, biodegradable and environmentally friendly. In addition, the solid colloids can also form an effective steric/electrostatic shield at the oil and water interface, which prevents the emulsion droplets from coalescence so as to improve the stability of the emulsions[38].

Recently, cellulose materials have attracted great attention for the stabilization of Pickering emulsions. Andresen & Stenius (2007) prepared the hydrophobilized microfibrillated cellulose by surface silylation and then applied the modified microfibrillated cellulose for Pickering emulsion

preparation, suggesting the feasibility of cellulose materials in stabilization of Pickering emulsions[39]. Afterwards, cellulose nanocrystals obtained by hydrolysis of various sources have been used to stabilize Pickering emulsions. However, both the hydrophobilized microfibrillated cellulose and acid-hydrolysed cellulose nanocrystals are apt to aggregate in aqueous medium, due to either their enhanced hydrophobic interactions between the microfibrillated cellulose[40], or due to the weakened electrostatic repulsions between the cellulose nanocrystals[41]. Therefore, it is challenging to prepare stable Pickering emulsions with cellulose materials.

More recently, highly homogeneous, and electrostatically stable oxidized cellulose nanocrystals (O-CNCs) were obtained by consecutive oxidation to introduce carboxyl groups onto the surface of oxidized cellulose nanocrystals[29]. These oxidized cellulose nanocrystals have similar dimensions to cellulose nanocrystals prepared by acid hydrolysis, but have a larger charge density, and thus are mostly homogeneous and electrostatically stable in aqueous medium[29]. Their nanoscale size and rod-like morphology make them suitable to be adsorbed to the oil-water interface, indicating them as potential Pickering emulsion stabilizer[42-44]. However, oxidized cellulose nanocrystals have limited interfacial activity due to their hydrophilic nature, and surface modification of the oxidized cellulose nanocrystals to enhance their interfacial properties will be a promising and interesting opportunity to prepare stable Pickering emulsions.

1.1.6 Compressive aerogels based on cellulose materials

Compressible aerogels have been of increasingly important for the high demand of next generation of products, such as super absorbents[45, 46], electrode substrate for batteries and supercapacitors[47, 48], catalyst supports[49], and chemical and biological sensors[50, 51], etc. Many of these applications require the aerogel materials to be strong yet compressible and capable of reversible deformation under large strain[52]. Traditional aerogels are mostly fabricated from silica

materials featured with large porosity (up to 99.8%), low density (4-500 mg/cm^3), and large surface area (100-1,000 m^2/g)[53, 54]. There are considerable studies on silica-based aerogels for various applications, including thermal and acoustic insulator[55, 56], optical applications[57], batteries[58, 59] and capacitor electrodes[60, 61], nuclear waste storage[62] and catalysis[63], etc. However, the traditional silica-based aerogels usually suffer from fragility, and they are too brittle to meet the mechanical robustness as compressive materials[64].

Recently, aerogels prepared from Poly(vinyl alcohol)(PVA) have drawn great attention since these polymeric molecules are generally less brittle, more flexible, and easy-processable[65], in addition to their excellent merits such as cost-effectiveness, nontoxicity, biocompatibility, and biodegradability[66-68]. However, PVA aerogels are neither mechanically strong nor highly compressible, which limits their applications as compressible materials. So far, PVA aerogels reinforced by carbon nanotubes and graphene materials with good mechanical strength and high compressibility have been reported[53, 69, 70]. However, those carbon-based materials are not readily available due to the high cost of equipment/raw materials, and the sophisticated procedures, which limit their large-scale applications[64].

Cellulose materials could be an alternative for carbon nanotubes and graphene materials to prepare the mechanical strong yet highly compressive PVA aerogels, due to their readily availability, low cost, good mechanical properties, low density, and excellent biocompatibility. So far, cellulose nanofibers (CNFs) have been incorporated with PVA to form the PVA/CNFs aerogels[71]. However, these aerogels were not elastic enough and deformed permanently when the compression strain was higher than 20%[71]. Cellulose nanocrystals, on the other hand, are highly ordered rod-like nanoparticles, and they are generally considered as effective fillers in aerogels to reinforce networks[72], due to their intrinsic rigidity and excellent mechanical strength (elastic

modulus~100-200 GPa[22]). Hence, there are considerable studies on the reinforcement of the mechanical strength of PVA aerogels with cellulose nanocrystals. However, even though these CNCs/PVA aerogels showed significantly improved mechanical strength, they have poor compressibility.

1.2 Hypotheses

In the light of previous studies, this thesis research will test the following hypotheses:

Hypothesis 1: The NaOH/urea solvent can be applied to dissolve wood cellulose, and further facilitate the fabrication of wood cellulose hydrogel (Chapter 3).

Hypothesis 2: The cellulose nanocrystals prepared from TEMPO-mediated oxidation of wood cellulose can disperse in deionized water with high stability. Further surface modification on oxidized cellulose nanocrystals can be successfully carried out. The Pickering emulsions stabilized by the modified oxidized cellulose nanocrystals can be successfully prepared with good mechanical/thermal stability (Chapter 4).

Hypothesis 3: The crosslinked CNCs/PVA aerogels can be successfully prepared with excellent mechanical strength and good compressibility (Chapter 5).

Hypothesis 4: The highly compressive CNCs/PVA aerogels can be successfully fabricated and used as oil/organic solvent absorbent with robust mechanical strength, good absorption capacity and recyclability (Chapter 6).

1.3 Objectives

The overall objective of this research is to provide some feasible and efficient approaches for the functionalization and application of wood-based cellulose materials. This overall objective can be detailed into 3 specific objectives:

Objective 1: To hydrolyze wood-based cellulose materials in a controlled manner, and to apply the environmentally "green" NaOH/urea solvent on wood-based cellulose materials for the preparation of wood-based cellulose hydrogels (Chapter 3).

Objective 2: To prepare oxidized cellulose nanocrystals by TEMPO-mediated oxidation and to modify the oxidized cellulose nanocrystals for enhanced interfacial properties. To prepare Pickering emulsions using the modified oxidized cellulose nanocrystals and to evaluate the mechanical/thermal stability of the Pickering emulsions (Chapter 4).

Objective 3: To prepare cellulose nanocrystals by sulfuric acid hydrolysis and to fabricate the highly compressive CNCs/PVA aerogels, and to investigate the feasibility of the obtained aerogels as efficient absorbents for oil/organic solvent removal (Chapter 5 and 6).

Chapter 2 - Literature review

2.1 Cellulose

Dated back to thousand years ago, cellulose has been used by human beings in the form of wood, cotton, and other plant fibers for energy source, building materials, and for clothing. Two centuries ago, the French chemist Anselme Payen firstly discovered a fibrous and resistant material when he treated various plant tissues with acid and ammonia. After further extraction, he obtained a solid material and determined the molecular formula of that material to be $C_6H_{10}O_5$ by elementary analysis, which he named "cellulose" in a report of the French academy in 1839[3].

Since the discovery of cellulose as a chemical raw material, it has been extensively investigated for about 150 years. Researchers gained increasingly knowledge about this natural polymer, regarding its sources, structural features, physical and chemical properties, derivatives, processing approaches, and its applications. Cellulose is the most ubiquitous and abundant biomaterial on the earth with an estimated annual production of ~1.5×10^{12} tons[2, 3], which is considered as an almost inexhaustible resource for the increasing demand of environmentally friendly and biocompatible products[3]. Cellulose materials are now considered as potential alternatives for the traditional petroleum/fossil-based materials to lower the impact on environment, owing to their excellent merits including the abundance in nature, low density, appealing mechanical properties, biodegradability, biocompatibility, and nontoxicity, etc.

2.1.1 Cellulose source materials

As illustrated in **Fig. 2-1**, cellulose is widely distributed through nature in higher plants (such as wood, bamboo, cotton, sisal, hemp, linin, etc.), in several marine animals (for example, tunicates), and in algae, bacteria, fungi, invertebrates, and even amoeba (protozoa)[1]. Cellulose is a structural element in the complex architecture of the cell walls of plants. It can exist in pure form

in some sources, such as bacterial cellulose. However, in most of the case, it is usually accompanied with hemicellulose, lignin, and some other extractives in plants. As a raw estimation, an impressive amount of cellulose is produced each year, from a wide variety of sources, i.e., wood fiber from trees (ca. 1,750,000 kt), cotton linters (18,450 kt), bamboo (10,000 kt), jute (2,300 kt), flax (830 kt), sisal (378 kt), hemp (214 kt), and ramie (100 kt)[5].

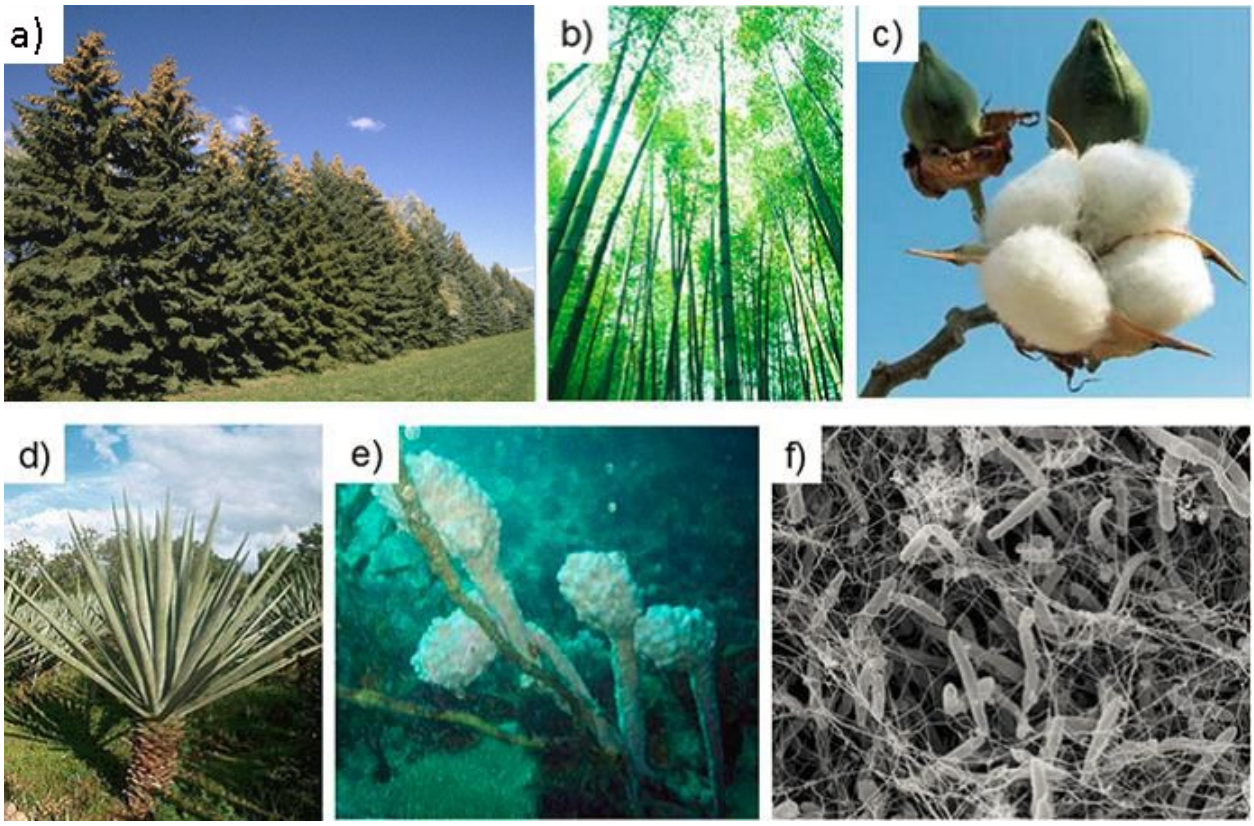

Figure 2- 1 Selection of important cellulose sources: (a) hard wood (spruce tree), (b) bamboo, (c) cotton, (d) sisal, (e) tunicine, and (f) gluconacetobacter xylinum[1]. Adapted with permission from Ref. 1. Copyright (2015) Springer Nature.

Wood: cellulose is widely existed as polysaccharide in wood cell walls. Wood as cellulose source has many advantages. Most importantly, it is abundant, which is an inexhaustible resource.

Especially for the countries with great forest area (for example, Russia: 795,090K ha; Brazil: 485,802K ha; Canada: 331,285K ha)[73], wood-based cellulose could be a great potential natural resource for industry. Currently, considerable numbers of industrial plants for wood harvesting, processing, and handling are existing[6], including the pulp and paper, packaging, green energy, and pharmaceutical industries, etc. Generally, wood contains about 50% of cellulose, 30% of hemicellulose, and 20% of lignin, in which hardwood usually has higher content of cellulose than softwood[74]. Wood pulp which is the most important raw material for processing of cellulose, is usually prepared by chopping bulk wood into small pieces, following with removing lignin with sulfites or removing hemicellulose in alkaline at high temperature and pressure. Currently, most of the wood pulp are used to produce paper and carboard, only 2% with high content of cellulose are used to prepare cellulose regenerated fibers, films, and some cellulose derivatives (cellulose esters and cellulose ethers)[3]. Hence, the potential of wood cellulose-based materials for value-added processing is still unveiled yet.

Cotton: cotton contains the highest amount of cellulose (ca. 87-90%) in all plant fibers. Cotton fibers are usually obtained from two sources: pure cotton fiber, which can be used directly as textile raw materials; and cotton linters, which are fine, silky fibers adhered to the seeds of the cotton plant after ginning. Due to their high content of cellulose (up to 93%), cotton linters are widely used to prepare regenerated cellulose, cellulose derivatives, pharmaceutical and chemical engineering raw materials, coating materials, and some explosives. However, cotton can only be planted in some specific areas (such as the valley along the River Nile, mid-Asia, China, south part of the United States), due to its geographical and climatic requirement for growing. Cotton resource is limited in cold areas, such as Russia and Canada.

Bacterial cellulose (BC): bacterial cellulose is secreted extracellularly from some small molecules (glucose and various other carbon sources) by some specific bacteria. Recent studies find the genera *Acetobacter*, *Agrobacterium*, *Alcaligenes*, *Pseudomonas*, *Rhizobium*, and *Sarcina* can synthesize bacterial cellulose, in which *Acetobacter xylinum*, a gram-negative strain of the *Acetobacter*, is the mostly widely investigated[75, 76]. *Acetobacter xylinum* has the highest efficiency to synthesize bacterial cellulose, which has been used as a model to study the biosynthesis, crystallization, and structure-functionality of bacterial cellulose. Bacterial cellulose is secreted directly as a pure fibrous network without lignin, pectin, and hemicellulose. It is highly crystallized (crystallinity index up to 84-89%[77]) and has a relatively higher degree of polymerization (DP). Bacterial cellulose is a good material with high purity, functionality, and properties. However, the large-scale production of bacterial cellulose is limited, due to the high requirement of the industrial plant to incubate the specific bacterial and low yield.

2.1.2 Structure of cellulose

2.1.2.1 Molecular structure

As shown in the molecular structure of cellulose in **Fig. 2-2**, cellulose is a linear polymer, compositing of D-anhydroglucopyranose units linked by β-1,4-glucosidic bonds. In other words, it is a β-1,4-D-glucan[78]. The D-glucopyranose rings are in the $^4C_1$-chair configuration, which is the lowest energy confirmation. The β-1,4-glucosidic bonds result in an alternate turning around the cellulose chain axis by 180° at each glucose unit, thus, the repeated unit of cellulose is cellobiose with a length of 1.3 nm[1]. Each anhydroglucose unit (AGU) within the cellulose chain possess three reactive hydroxy groups, in which one is primary hydroxyl group (C6), two are secondary hydroxyl groups (C2, C3). These hydroxyl groups can undergo the typical reactions of primary and secondary hydroxyl groups, such as esterification, etherification, and oxidation[1]. The chain

ends of the cellulose molecule behave chemically differently. One end contains an anomeric C atom linked by β-1,4-glucosidic bonds (nonreducing end), whereas the other end has a glucopyranose unit in equilibrium with the aldehyde function (reducing end)[79].

Cellulose has degrees of polymerization (DPs) that depend on sources and treatments. Krässig et al. (2000) studied the degree of polymerization of celluloses from different sources[80]. In general, native celluloses have higher DP values than that of the regenerated celluloses[81] and some processing, including purification, hydrolysis, oxidation, reduces the relatively high DP values[82]. Theoretically, the molecular weight of cellulose can be calculated according to the DP value, namely M_w=162$\times$DP. However, since cellulose samples are always polydisperse, the DP value of cellulose must be considered as average value. The molecular weight of cellulose, as well as its molecular weight distribution, apparently influence the mechanical properties, the dissolution behaviors (solubility, viscosity, rheology), the degradation, aging, and chemical reactions of cellulose materials. There are several techniques to obtain information about the molar masses and their distribution, including viscosity and osmotic pressure measurements, size-exclusion chromatography (SEC) and light scattering[1]. Accordingly, viscosity-average molecular weight (M_η), number-average molecular weight (M_n), weight-average molecular weight (M_w) are used to characterize cellulose molecular weight. The viscosity-average molecular weight (M_η), calculated from the Mark-Houwink Equation in different solvent systems, is widely accepted as a simple and efficient approach to characterize cellulose.

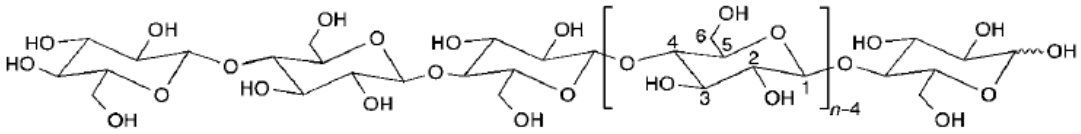

Figure 2- 2 Molecular structure of cellulose (n=DP)[3]. Reprinted with permission from Ref. 3. Copyright (2005) John Wiley and Sons.

2.1.2.2 Supramolecular structure

Crystal polymorphs: so far, six cellulose crystal polymorphs have been studied, including the cellulose I type (I, III_I, and IV_I), and cellulose II type (II, III_{II}, and IV_{II}). All native cellulose material is cellulose I, while all the other five polymorphs are modified celluloses. As illustrated in **Fig. 2-3**, the cellulose crystal polymorphs can transfer between each other by chemical or thermal treatment. Cellulose II is usually obtained by two approaches: (1) regeneration, which involves the dissolution of cellulose I in aqueous solvents; (2) mercerization that treats native cellulose I with a concentrated alkaline swelling agent. Cellulose III is obtained by swelling cellulose I or II in amines or liquid ammonia and then removing the swelling agent[83, 84]. Cellulose IV is formed by annealing cellulose III in glycerol[85].

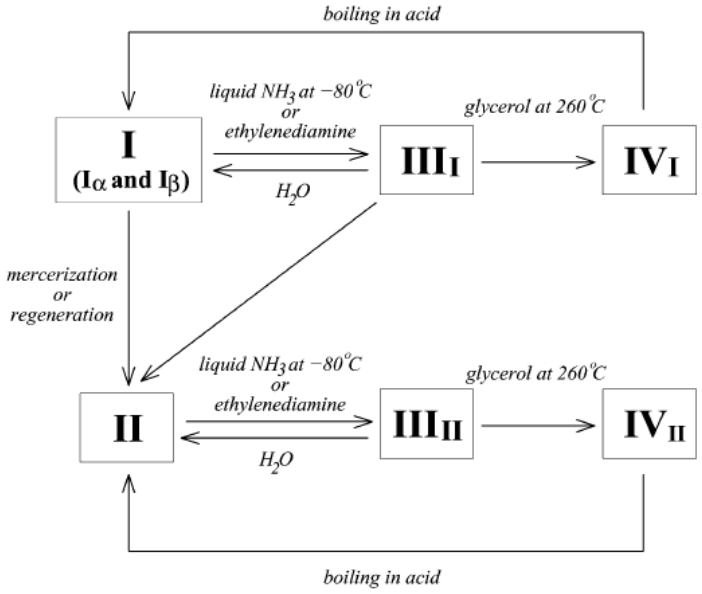

Figure 2- 3 Polymorphs of cellulose[86]. Reprinted with permission from Ref. 86. Copyright (2004) American Chemical Society.

To understand the supramolecular structure of cellulose, it is important to study the structure of the crystal polymorphs. Even though these polymorphs all have the same chemical composition, they have different properties due to their different crystal structures. As shown in **Fig. 2-4** and **Fig. 2-5**, The difference between these crystal polymorphs is revealed by X-ray diffraction and solid state ^{13}C-NMR spectra[87]. Almost all native celluloses have similar X-ray diffraction patterns. Further study of cellulose I by solid-state ^{13}C-NMR revealed two crystalline allomorphs, namely cellulose I_α and I_β[88], in which cellulose I_α is triclinic while cellulose I_β is monoclinic[89]. These two allomorphs of cellulose I may coexist in one cellulose sample[90], or even in the same microfibrils[89]. Cellulose I_α are mainly distributed in algal and bacterial cellulose, whereas cellulose I_β are widely present in higher plant cellulose[91, 92]. It is noted that I_α phase is metastable and can be converted to the thermodynamically stable I_β by annealing in aqueous sodium hydroxide or various organic solvents[93-95].

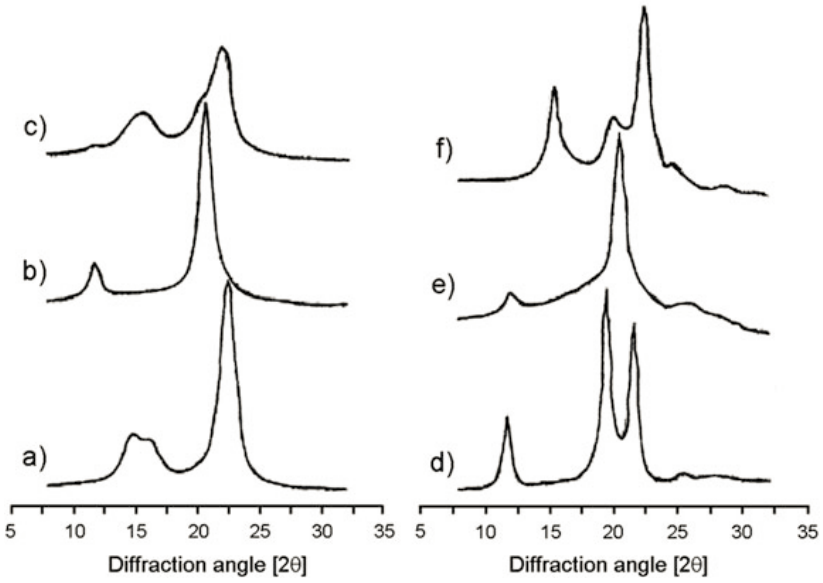

Figure 2- 4 X-ray diffraction patterns of (a) cellulose I_{β}, (b) cellulose III_{I}, (c) cellulose IV_{I}, (d) cellulose II, (e) cellulose III_{II}, and (f) cellulose IV_{II}[1]. Reprinted with permission from Ref. 1. Copyright (2015) Springer Nature.

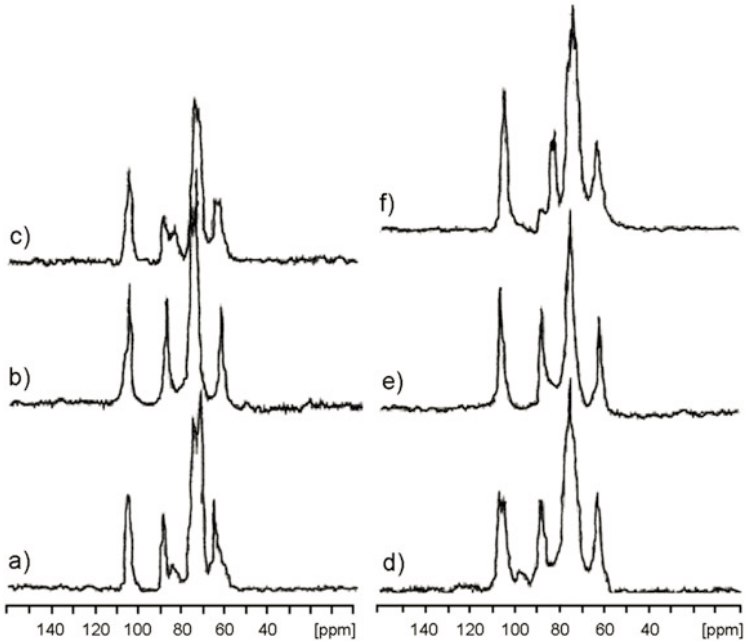

Figure 2- 5 Solid state ^{13}C-NMR spectra of (a) cellulose I_β, (b) cellulose III_I, (c) cellulose IV_I, (d) cellulose II, (e) cellulose III_{II}, and (f) cellulose IV_{II}[1]. Reprinted with permission from Ref. 1. Copyright (2015) Springer Nature.

Celluloses which are dissolved and regenerated or treated with a concentrated alkaline swelling agent and washed with water consist of cellulose II. **Table 2-1** gives the data of the unit cells and diffraction planes of cellulose polymorphs. The major distinction between cellulose I and cellulose II lies in the layout of their atoms: cellulose I has antiparallel packing while its counterpart packs parallelly[96]. Cellulose II has more intermolecular hydrogen bonding and the crystals are highly packed, which is the most thermodynamically stable crystalline form[96, 97]. Therefore, the transformation from cellulose I to cellulose II is irreversible.

Table 2- 1 Unit cells and diffraction planes of cellulose polymorphs.

Poly morph	Chain No.	Unit cell (Å)						Diffraction angle 2θ[92]			
		a	b	c	α	β	γ	1 $\bar{1}$0	110	020	012
I_α[90]	1	6.74	5.93	10.4	117	113	81				
I_β[98]	2	7.85	8.27	10.4	90	90	96.3	14.8	16.3	22.6	
II[99]	2	8.1	9.05	10.3	90	90	117.1	12.1	19.8	22	
III_I[84]	2	10.25	7.78	10.3	90	90	122.4	11.7	20.7	20.7	
IV_I[85]	2	8.03	8.13	10.3	90	90	90	15.6	15.6	22.2	
IV_{II}[85]	2	7.99	8.1	10.3	90	90	90	15.6	15.6	22.5	20.2

Hydrogen bonding: there are three active hydroxyl groups in each AGU of the cellulose molecule, resulting in strong intramolecular and intermolecular hydrogen bonding system (**Fig. 2-6**). It is now widely accepted this hydrogen bonding network has a significant influence on the structure and properties of cellulose materials, including the supramolecular structure, the crystalline domains, the limited solubility in most solvents, and the reactivity of the hydroxyl groups, etc.

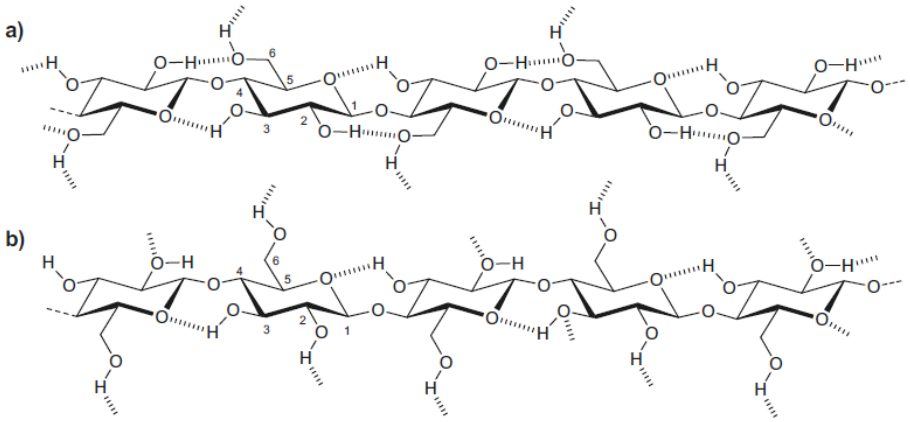

Figure 2- 6 Cellulose hydrogen bonding system of (a) cellulose I, (b) cellulose II[1]. Reprinted with permission from Ref. 1 Copyright (2015) Springer Nature.

The three hydroxyl groups of the AGU and the oxygen atoms in the D-glucopyranose and the glycosidic linkage are able to interact with each other within the chain or with another chain by forming intramolecular and intermolecular hydrogen bonds. There are several methods to characterize the hydrogen bonding network in cellulose, including FTIR[92, 100], solid-state NMR[91, 101], X-ray diffraction[102], DSC[103]. FTIR[7, 8] and solid-state NMR[9] revealed that the hydroxyl groups at C3 and the oxygen atom in the adjacent pyranose ring forms intramolecular hydrogen bonds in all polymorphs of cellulose molecules. The hydroxyl groups at C6 and the neighboring hydroxyl groups at C2 can also form intramolecular hydrogen bonding. This intramolecular hydrogen bonding, together with the glycosidic covalent linkage, are responsible for the rigidity of cellulose chains[1].

In the crystalline regions, cellulose molecules are connected with each other by intermolecular hydrogen bonding, especially for the hydroxyl groups at C6 and the oxygen atoms at an adjacent chain in native cellulose (cellulose I). As a result, these cellulose molecules are connected in a layer, and the layers are assembled by hydrophobic interactions, weak C-H-O bonds, and the intermolecular hydrogen bonding between the layers[10]. Cellulose II on the other hand forms intermolecular hydrogen bonding between hydroxyl groups at C6 in one chain and hydroxyl groups at C2 in another chain. Moreover, the intramolecular hydrogen bonding at C2 are avoided and intermolecular hydrogen bonding between hydroxy groups at C2 of two chains are formed[104]. As a result, cellulose II molecules are more densely packed and more strongly bonded. Therefore, the cellulose II molecules are less reactive.

As illustrated in **Fig. 2-7**, multiple cellulose chains form the elementary fibrils and further assemble into larger microfibrils (5-50 nm in diameter and several microns in length)[6]. Due to the intra/inter-molecular hydrogen bonding network, as well as some other molecular interactions (van

der Waals force, hydrophobic interactions), cellulose molecules are alternatingly arranged in a highly ordered (crystalline) regions or disordered (amorphous) regions within these cellulose fibrils. The supramolecular structure makes it difficult to modify and process cellulose materials. It has a significant influence on the solubility of cellulose, the reactivity of the three hydroxyl groups of the AGU unit, as well as their crystallinity, etc. To explore the application of cellulose, it is critical to search for the feasible methods to break down the supramolecular structure of cellulose, so as to process, derivatize or regenerate cellulose and fabricate new cellulose functional products.

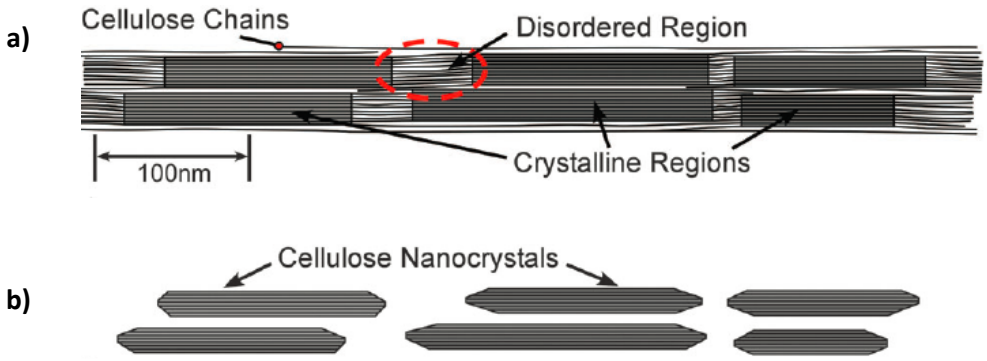

Figure 2- 7 The alternatingly arrangement of the crystalline and amorphous regions of cellulose fibrils (a) and cellulose nanocrystals after acid hydrolysis dissolved the disordered regions (b)[6]. Adapted with permission from Ref. 6. Copyright (2011) The Royal Society of Chemistry.

2.1.3 Cellulose dissolution systems

Cellulose forms supramolecular structures by the strong intra-/intermolecular hydrogen bonds, making it insoluble in water and most common organic solvents[11, 12]. This structural feature of

cellulose impedes the development of cellulose functional products. As for industrial concerns, search for a cost-effective solvent to dissolve cellulose is a key technique for cellulose applications.

The traditional **CS_2/NaOH system** has been employed to dissolve cellulose materials in the Viscose Rayon process, in which raw cellulose is alkalized by NaOH and then reacts with CS_2 to form cellulose xanthogenate followed by regeneration to form various cellulose fibers, films, membranes, and sponges[13]. However, the traditional CS_2/NaOH system involves complicated procedures, high energy consumption, and considerable amount of toxic gas (CS_2 and H_2S).

N-methyl-morpholine-N-oxide (NMMO) is used as a commercial, environmentally acceptable and non-derivative cellulose solvent in the Lyocell process[11, 14]. Due to its strong N-O dipole moment and molecule size breaking the hydrogen bonding system, cellulose materials can be dissolved by the strong interaction of hydrogen bonding between NMMO, water, and the polymers[13]. However, considerable by-products form in the cellulose/NMMO/water system by homolytic, heterolytic and thermal degradation process, which leads to some detrimental effects such as degradation of cellulose, decreased product performance, increased consumption of stabilizer, etc[15]. In addition, the relatively high cost of NMMO has also limited the large-scale application of this approach.

Ionic Liquids (ILs) are also investigated for cellulose dissolution including 1-butyl-3-methylimidazolium chloride (BMIMCl) and its anion-substituent (Br^-, SCN^-, and $[BF4]^-$, $[PF6]^-$), and 1-allyl-3-methylimidazolium chloride (AMIMCl) as well[11, 16, 17]. It is reported that $BMIM^+X^-$ can only dissolve cellulose with high molecular weight (DP≈1,000) on heating to 100-110 ℃[11]. Zhang et al. (2005) proposed that AMIMCl can be dissociated to individual Cl^- and $AMIM^+$ ions above the critical temperature, of which free Cl^- ions associate with cellulose hydroxyl proton and $AMIM^+$ forms complex with cellulose hydroxyl oxygen, to further disrupt the hydrogen bonding

in cellulose and dissolve cellulose[12, 105]. However, although ILs is powerful as a cellulose solvent, the relatively high cost to synthesize ILs has limited their applications. Moreover, the toxicity of ILs should also be addressed before the large-scale applications[16].

N,N-Dimethylacetamide (DMAc)/LiCl system can also dissolve cellulose by heating or refluxing to obtain transparent cellulose solution[12, 18]. It is reported that the N,N-dimethylketeniminium ions present in DMAc/LiCl at elevated temperature can cleave the glucosidic bonds of cellulose, resulting in the dissolution of cellulose[18]. This method is only limited to laboratory use because of the high price of LiCl. Additionally, cellulose solution can also be prepared in **heavy metal-amine complex** (such as Cuoxam, Ni-tren, Cd-tren and so on). Due to the increasing concern of environmental issues, none of these approaches can be commercialized for large-scale applications[106].

Recently, a new aqueous cellulose solvent, i.e., 7.0 $^{w}/_{w}$% NaOH/12 $^{w}/_{w}$% urea aqueous system has been developed that can effectively dissolve cotton linters at -12.6 ℃ within 5 minutes[19]. Compared with the solvents above, this aqueous system is environmentally "green" and cost-effective without using organic or toxic reagents. As described in **Fig. 2-8**, when cotton linters are immersed in the pre-cooled NaOH/urea aqueous system, NaOH hydrates, urea hydrates, and free water surround the cellulose molecules (**Fig. 2-8a**)[19], which then penetrate into the cellulose chains and destroy the original intra-/intermolecular hydrogen bonding at low temperature (**Fig. 2-8b**)[19]. In such scenario, the cellulose molecules are held in an inclusion complex (IC) consisted of an overcoat of NaOH hydrates, urea hydrates, and free water, resulting in the dissolution of cellulose molecules and the formation of the transparent solution(**Fig. 2-8c**)[19, 20]. It would be useful to adapt this "green" solvent to wood cellulose to produce materials with different attributes and applications compared to those from cotton linter. However, this NaOH/urea aqueous solvent is

not applicable for some native cellulose with high viscosity-average molecular weight (M_η>11.4×10^4 Da)[19], thus wood cellulose needs to be broken down partially to achieve a good solubility.

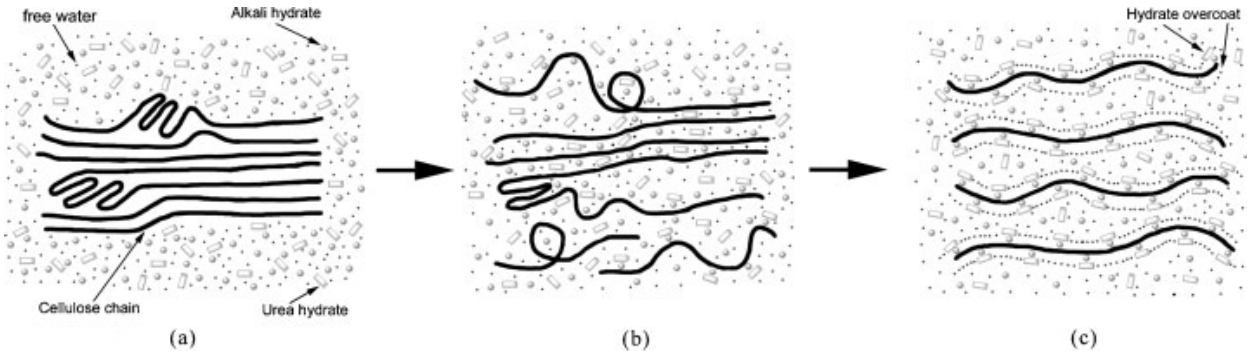

Figure 2- 8 Schematic dissolution process of the cellulose in NaOH/urea aqueous solutions at low temperature: (a) cellulose bundle in the solvent, (b) swollen cellulose in the solution, (c) transparent cellulose solution[19]. Reprinted with permission from Ref. 19. Copyright (2005) John Wiley and Sons.

2.1.4 Cellulose products from NaOH/urea solutions

A great amount of new functional materials from cellulose have been developed for a broad range of applications, due to the increasing demand for environmentally friendly and biocompatible products. Cai & Zhang (2006) studied the gelation behavior of cotton linters in the NaOH/urea aqueous system, and found the obtained cellulose hydrogels could be formed via destructing the stability of cellulose solution by increasing the temperature to 50 ℃ or reducing it to -20 ℃[32]. This physical crosslinking involves a process of breaking the hydrogen bonding system of the inclusion complex (IC) of cellulose/NaOH hydrate/urea hydrate/water cluster and rebuilding the system with new hydrogen bonding networks. Rheological test further revealed the influence

of cellulose molecular weight, concentration, and temperature on the gelation behavior. The gelation temperature was decreased with increase of the cellulose concentration and its molecular weight. Moreover, Zhou et al. (2007) prepared chemically crosslinked cellulose hydrogels from cotton linters using epichlorohydrin as a crosslinker. As a result, the mechanical properties of the obtained hydrogels were significantly increased[33].

In addition to cellulose hydrogels, regenerated cellulose (RC) films were also prepared from cotton linters in the NaOH/urea aqueous system by casting method followed by regeneration with coagulate reagents such as acetic and sulfuric acids. The obtained cellulose films had a typical cellulose II crystalline form and the degree of crystallinity was lower than the original cellulose I[107] with smaller apparent crystal size. Yang et al. (2011) reported high oxygen barrier properties for the regenerated films, which are promising bio-based food packaging materials[108]. Qi et al. (2009) further prepared the transparent and photoluminescent cellulose films by adding the fluorescent dyes and photoluminescent pigments in the fabrication process[109]. Moreover, cellulose filament fibers can be fabricated from cotton linters in NaOH/urea solution. Cai et al. (2004, 2007) dissolved cotton linters in the NaOH/urea system and converted the cellulose solution into multifilament fibers using wet-spinning processing. The obtained cellulose filament fibers featured a circular cross-sectional shape and a smooth surface as well as good mechanical properties[110, 111].

2.2 Cellulose nanocrystals

Since the French chemist Ränby firstly found cellulose nanocrystals can be obtained by subjecting native or mercerized wood cellulose into sulfuric acid[112, 113], cellulose nanocrystals have attracted increasing attention as a novel and multi-functional nanomaterial. Transmission electron microscopy (TEM) reveals the dried cellulose nanocrystals are rod-like particles that have

the dimensions in nanoscale range with the diameter of 2-10 nm and length of 100-600 nm. The aspect ratio of cellulose nanocrystals, defined as the ratio of the length to the width (***L/w***), is usually in the range of 10-100. Wood fibers and plant fibers are both good sources to prepare cellulose nanocrystals due to their abundance in nature. Generally, chemically induced disintegrating strategies are usually applied for cellulose nanocrystals preparation, in which the amorphous regions of cellulose fibers are removed, and the highly crystalline regions are preserved, resulting in rigid rod-like cellulose nanocrystals without apparent defect[21].

2.2.1 Preparation of cellulose nanocrystals

Natural cellulose fibers can be disintegrated by various top-down methods, including mechanical degradation, enzymatic hydrolysis, acid hydrolysis, and oxidation, etc. Mechanical degradation of cellulose materials, usually includes high-pressure homogenization[114-116], grinding/refining[117], cryocrushing[118], high intensity ultrasonic treatment[119], and microfluidization[120]. These physical processing generally produces high intensity of shear force that cause transverse cleavage along the longitudinal axis of the cellulose fibers, leading to the breakup of some amorphous regions, whereas the highly crystalline regions stay intact. Therefore, these processes usually generate cellulose nanofibers (CNFs) with both crystalline and amorphous regions. The CNFs chains usually have length more than 1 μm and width ranging from 10 to 100 nm depending on the cellulose source[21]. Thus, CNFs are relatively soft with long chains and easy to entangle with each other. Enzymatic hydrolysis of cellulose materials is less aggressive, comparing with mechanical degradation and chemical treatment. However, this method has not been widely employed in industry due to the high requirement for the reaction conditions, high cost and low yield. For academic research, enzymatic processing is usually combined with mechanical method or chemical treatment, for a controlled fibrillation of cellulose fibers[115]. As for

the preparation of cellulose nanocrystals, chemically induced disintegration is preferred, in which the amorphous regions of cellulose chains are preferentially broken down by either acids or oxidants, whereas the highly crystalline regions are preserved due to their higher resistance to acid or oxidation.

Acid hydrolysis: the release of cellulose nanocrystals from cellulose fibers usually involves an acid-induced disintegrating process, in which the small acid molecules diffuse into the amorphous regions of cellulose fibers, resulting in the cleavage of the glycosidic bonds. In this process, cellulose fibers are subjected into strong acid under strict control of temperature, stirring speed, and reaction time before quenched by diluting the acid with large amount of water (usually 10-folds). The obtained cellulose suspension colloids are then washed with water by successive centrifugations, followed by dialysis against deionized water to remove any excess acid. A sonication process is usually performed to disintegrate the aggregates and a complete cellulose nanocrystal dispersion is obtained.

Different acids have been investigated to disintegrate the amorphous regions and release the highly crystalline cellulose nanocrystals from cellulose fibers, including sulfuric[121, 122], hydrochloric[123, 124], phosphoric[125, 126], and hydrobromic acids[127], etc, in which sulfuric and hydrochloric acids are the most extensively used. When prepared by hydrolysis in hydrochloric acid, the obtained cellulose nanocrystals usually have limited dispersibility and they are unstable with a tendency to flocculate, owing to their almost neutral surface. However, when subjected into sulfuric acid, cellulose fibers react with sulfuric acid via an esterification process to form charged sulfate ester groups. These sulfate groups are randomly distributed along the obtained cellulose nanocrystals and form a negatively electrostatic layer covering the surface of cellulose nanocrystals, which promotes their dispersibility in water[22].

The concentration of sulfuric acid used to hydrolyze cellulose fibers is usually 65 $^{w}/_{w}$%. Whereas a wider temperature range can be employed to prepare cellulose nanocrystals (from room temperature up to 70 ℃), and the hydrolysis time varies from 30 min to overnight depending on the hydrolysis temperature[112]. As for the cellulose nanocrystals prepared from hydrochloric acid hydrolysis, the reaction is usually taken place in a reflux apparatus, and the concentration of hydrochloric acid is usually between 2.5 M and 4 M for various reaction times depending on the source of the cellulose fibers[112].

TEMPO-mediated oxidation: (2,2,6,6-tetramethylpiperidine 1-oxyl)-mediated (or TEMPO-mediated) oxidation of cellulose materials has been studied in recent years, due to its high selectivity of oxidation of cellulose chains[23-28, 128]. As illustrated in **Fig. 2-9**, in the presence of NaBr and NaOCl, TEMPO-mediated oxidation process can convert the hydroxylmethyl groups of cellulose to the carboxyl groups at pH 9-11, while the secondary hydroxyl groups are remained intact. To avoid undesirable side reactions under alkaline conditions, TEMPO/NaClO/$NaClO_2$ system is further developed under neutral or slightly acidic conditions[23]. Based on this TEMPO-mediated processing, Yang et al. (2012) developed a new method with three steps of oxidation to prepare cellulose nanocrystals: (i) periodate oxidation selectively oxidizes C2 and C3 hydroxyl groups to 2,3-dialdehyde units on the cellulose chain; (ii) chlorite oxidation converts the 2,3-dialdehyde groups to dicarboxyl groups; (iii) TEMPO-mediated oxidation converts primary hydroxyl groups on C6 to carboxyl groups[29]. The obtained cellulose nanocrystals have similar dimensions to those prepared by acid hydrolysis but a large charge density. Therefore, the obtained cellulose nanocrystal suspension is highly electrosterically stable[29].

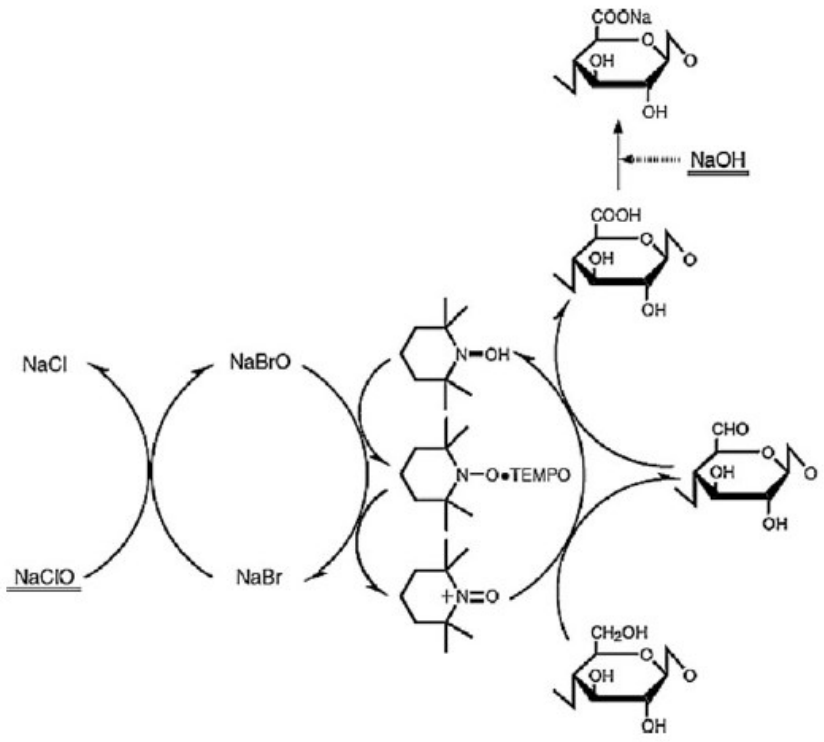

Figure 2- 9 Scheme of TEMPO-mediated oxidation of cellulose materials[28]. Reprinted with permission from Ref. 28. Copyright (2006) American Chemical Society.

APS oxidation: ammonium persulfate (APS), an oxidant with high water solubility and low cost, has also been investigated for cellulose nanocrystals preparation. This process involves heating cellulose materials at 60 ℃ in 1 M APS solution under vigorous stirring for various times. The reaction time is substrate-dependent, ranging from 3 h for bacterial cellulose and 16 h for complex cellulose substrates such as hemp, flax. Atomic force microscopy (AFM) and transmission electron microscopy (TEM) reveal the uniform cellulose nanocrystals with diameter of ~3-6 nm and length of ~88-148 nm. It is proposed the free radical $SO_4\cdot^-$ is formed when the solution containing persulfate is heated ($S_2O_8^{2-}$ + heat → $2SO_4\cdot^-$). Meanwhile, hydrogen peroxide is also formed ($S_2O_8^{2-} + 2H_2O \rightarrow 2HSO_4^- + H_2O_2$) under the acidic condition (pH 1.0). These free radicals and

H_2O_2 then penetrate into the amorphous regions of cellulose fibers and break down the amorphous structure to form cellulose nanocrystals[129]. In this process, a large number of oxidants are usually consumed, and the reaction time is much longer for most of the cellulose materials[130]. Moreover, the great amount of water and energy consumption also increased the cost of cellulose nanocrystals production.

2.2.2 Morphology of cellulose nanocrystals

The geometrical dimensions (length, *L*, and width, *w*) of cellulose nanocrystals are different, not only depending on the source of cellulose fibers, but also on the preparation conditions (reaction time, stirring speed, temperature, and feed ratio) employed to disintegrate cellulose chains. The effect of acid hydrolysis conditions on the dimensions and crystallinity of the obtained cellulose nanocrystals has been investigated. Dong et al. (1998) found the longer hydrolysis time resulted in shorter cellulose nanocrystals and higher surface charge[131]. Beck-Candanedo et al. (2005) found the hydrolysis time and acid-to-pulp ratio had significant influence on the properties of the obtained cellulose nanocrystals from both softwood and hardwood pulps[132]. When the reaction time was too long, cellulose was completely digested into sugar molecules while the shorter hydrolysis resulted in large and indispensable fibers, as well as aggregates[133]. The geometrical dimensions of cellulose nanocrystals from various sources are presented in **Table 2-2**. And the morphology of cellulose nanocrystals from different sources are shown in **Fig. 2-10**.

Table 2- 2 Dimensions of cellulose nanocrystals from various sources[112]. Adapted with permission from Ref. 112. Copyright (2010) American Chemical Society.

Source	*L*(nm)	*w*(nm)	technique	ref
soft wood	100-200	3-4	TEM	134
	100-150	4-5	AFM	132
hard wood	140-150	4-5	AFM	132
cotton	100-150	5-10	TEM	135
	70-170	~7	TEM	131
	200-300	8	TEM	136
	255	15	DLS	137
cotton linter	100-300	10-20	SEM	138
	25-320	6-70	TEM	139
	300-500	15-30	AFM	140
ramie	150-250	6-8	TEM	141
	50-150	5-10	TEM	142
bacterial	100-1,000	10-50	TEM	143

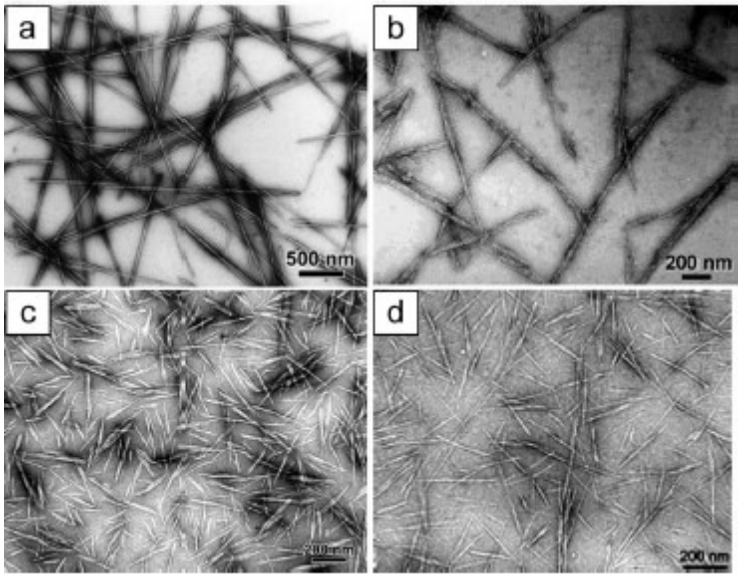

Figure 2- 10 Transmission electron microscopy images from diluted suspension of cellulose nanocrystals from (a) tunicate (b) bacterial, (c) ramie, and (d) sisal[112]. Reprinted with permission from Ref. 112. Copyright (2010) American Chemical Society.

2.2.3 Mechanical properties and potential nanoreinforcement

It is extremely challenging to understand the intrinsic mechanical properties of cellulose nanocrystals, due to the small particle size and the limited metrology techniques to characterize these nanoscale materials along multiple axes. Additionally, several other factors may also influence the measured mechanical properties, and the reported data may distribute widely, not only between different cellulose nanocrystal types, but also for a given specific specimen. These factors include: crystal type (I_α, I_β, II), crystallinity index (CI), anisotropy, defects, and the measurement methods and techniques[6].

The elastic modulus of cellulose nanocrystals has been investigated by either theoretical evaluations or by experimental measurements (X-ray diffraction, Raman spectroscopy, and atomic force microscopy). Some data of the longitudinal elastic modulus of cellulose nanocrystals are summarized in **Table 2-3**. The studies of transverse modulus of cellulose nanocrystals are limited, and the reported values of transverse modulus are much lower than that of the longitudinal elastic modulus[22]. As shown in **Table 2-3**, the values of elastic modulus of cellulose nanocrystal are different, depending on the crystal type (I_α, I_β, II), and the processing techniques.

Table 2- 3 Longitudinal Modulus (E_L) of cellulose nanocrystals[22]. Adapted with permission from Ref. 22. Copyright (2014) John Wiley and Sons.

Methods	Materials	E_L(GPa)	Ref.
Calculation	Cellulose I	136±6	[144]
		167.5	[145]
		134–135	[146]
	Cellulose I_α	127.8	[147]
		136–155	[148]
	Cellulose I_β	124–155	[149]
		156	[150]
	Cellulose II	162.1	[145]
		155	[151]
X-ray diffraction	Cellulose I	134	[152]
		138	[153]
	Cellulose II	106–112	[154]
Raman	Cellulose I_β	143	[155]
Inelastic X-ray scattering	Cellulose I	220	[156]
AFM	Cellulose I_β	145–150	[117]

It is accepted that the elastic modulus of cellulose nanocrystals varies from 100-200 GPa. which is similar to Kevlar (60-125 GPa) and could be comparable to steel (200-220 GPa). Actually, the specific Young´s modulus of cellulose nanocrystals, which defines as the ratio between the Young´s modulus and their density, is around 85 J/g, whereas it´s around 25 J/g for steel[22]. These excellent mechanical properties endow cellulose nanocrystals an ideal nanoreinforcement to composite with other polymers and improve the properties of a targeted host material due to their excellent intrinsic properties, including nanoscale dimensions, high surface area, unique

morphology, low density (~1.61 g/cm^3 for pure cellulose nanocrystals I_β), appealing mechanical strength (elastic modulus ~100-200 GPa), renewability and biodegradability.

The first study about the nanoreinforcement effect of cellulose nanocrystals was reported by Favier et al. (1995), in which a significant increase of the storage modulus of the poly(styrene-co-butylacrylate)-based nanocomposites was reported even when low amount of cellulose nanocrystals was added[157]. Since then, cellulose nanocrystals have been incorporated into a wide range of polymer materials, including polysiloxanes[158], polysulfonates[159], poly(caprolactone)[128], poly(oxyethylene)[160], poly(styrene-co-butylacrylate)[157], cellulose acetate butyrate[161], carboxymethyl cellulose[162], poly(vinyl alcohol)[163], poly(vinyl acetate)[164], polyethylene[142], and water-borne polyurethane[165], etc.

This excellent reinforcing effect is ascribed to a mechanical percolation phenomenon[99]. It is explained by the formation of a rigid percolating filler network that was connected by hydrogen bonding in cellulose nanocrystals nanocomposites[166]. Such rigid percolating filler network was confirmed by electrical measurements on nanocomposites consisted of polypyrrole-coated cellulose nanocrystals[167]. It is believed that there is a percolation threshold for the cellulose nanocrystals-reinforced nanocomposites. Above the percolation threshold, the cellulose nanocrystals connect and form a 3D continuous network throughout the nanocomposite, due to the strong intermolecular hydrogen bonds between cellulose nanocrystals[99]. There are several variables that mainly influence the percolation threshold, including the shape of cellulose nanocrystals (size and aspect ratio[168]), the orientation of cellulose nanocrystals in the matrix[169], and the interactions between cellulose nanocrystals[170]. The mechanical properties of nanocomposites prepared from cellulose nanocrystals are mainly influenced by the formation of

the percolated network. Therefore, the mechanical properties can be controlled by the dimensions of cellulose nanocrystals and their interfacial interactions (between them or with the host matrix)[112].

2.2.4 Applications of cellulose nanocrystals

2.2.4.1 Pickering emulsion stabilizer

Pickering emulsions are the emulsions stabilized by solid colloids instead of traditional surfactants. These solid colloids include TiO_2 nanoparticles, chitin nanocrystals, starch particles, flavonoid particles[171-174], etc. Depending on whether the particles are hydrophilic or hydrophobic, the systems may be either oil-in-water (O/W) emulsions or water-in-oil (W/O) emulsions[175]. These solid colloids are usually biocompatible, biodegradable and environmentally friendly. In addition, the solid colloids can form an effective steric/electrostatic shield at the oil and water interface, which prevents the emulsion droplets from coalescence so as to improve the stability of the emulsions[176].

As illustrated in **Fig. 2-11** for the idealized case of spherical particles wetted by water, the location of an individual solid particle with respect to the oil/water interface in Pickering emulsion is defined by the contact angel θ (θ<90°). Once a particle of radius r is attached to the oil/water interface with θ not too close to 0° or 180°, it can be regarded as being irreversibly adsorbed, due to the fact that the Gibbs free energy of spontaneous desorption of the particle, ΔG_d, is extremely high compared with the thermal energy:

$$\Delta G_d = \pi r^2 \gamma_{ow} (1 - |cos\theta_{ow}|)^2 \qquad \textbf{(2-1)}$$

Where ΔG_d is the Gibbs free energy of spontaneous desorption of solid colloids from the interface, γ_{ow} is the interfacial tension (the particles is initially in one phase and subsequently adsorbed at the interface), $\theta_{ow}$is the contact angle and r is the particle radius[177]. The Gibbs free energy (ΔG_d) of spontaneous desorption of the solid colloids is influenced by the composition of the oil and

aqueous phases. But apart from the contact angle and interfacial tension, the most important factor controlling the binding energy is particle size. As estimated by Dickinson[38], the theory predicts the binding energy of a spherical microparticle (r=1 μm) of ΔG_d~$10^6 \kappa T$, even for smaller particles (r=5~10 nm), ΔG_d>>$10\kappa T$ (κT: thermal energy, κ: Boltzmann's constant, T: absolute temperature). Thus removing these solid colloids from the interface needs significant energy[38] and the solid colloids are considered irreversibly adsorbed at the oil-water interface, rather than the reversible balance of adsorption/desorption of traditional surfactants such as Tween and Span. Therefore, Pickering emulsions have some distinctive benefits in terms of superior stability, biocompatibility, biodegradability[178], and free from surfactants[179].

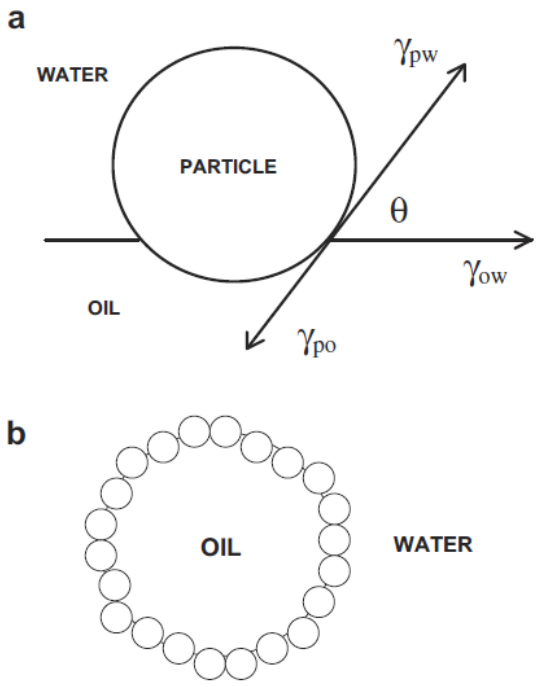

Figure 2- 11 O/W Pickering emulsion stabilized by spherical particles. (a) Single hydrophilic particle at the oil/water interface, with contact angle θ. Quantities γ_{po}, γ_{ow} and γ_{pw} are the tensions at the three boundaries. (b) Monolayer of equal-sized particles at surface of dispersed oil droplet[38]. Reprinted with permission from Ref. 38. Copyright (2012) Elsevier.

Recently, cellulose materials have attracted great attention for the stabilization of Pickering emulsions. Andresen & Stenius (2007) prepared the hydrophobilized microfibrillated cellulose by surface silylation and then applied the modified microfibrillated cellulose for Pickering emulsion preparation. The results suggested the feasibility of cellulose materials in stabilization of Pickering emulsions[39]. Afterwards, cellulose nanocrystals obtained by hydrolysis of various sources have been used to stabilize Pickering emulsions. However, both the hydrophobilized microfibrillated cellulose and acid-hydrolyzed cellulose nanocrystals are apt to aggregate in aqueous medium, due to the enhanced hydrophobic interactions between microfibrillated cellulose[40], and the weakened electrostatic repulsions between the cellulose nanocrystals[41]. Therefore, it is challenging to prepare stable Pickering emulsions with cellulose materials.

More recently, highly homogeneous, and electrostatically stable oxidized cellulose nanocrystals were obtained by consecutive oxidation to introduce carboxyl groups onto the surface of oxidized cellulose nanocrystals[29]. These oxidized cellulose nanocrystals have similar dimensions to cellulose nanocrystals prepared by acid hydrolysis, but have a larger charge density, and thus are mostly homogeneous and electrostatically stable in aqueous medium[29]. Their size and rod-like morphology are suitable to be adsorbed to the oil-water interface, making them potential Pickering emulsion stabilizer[42-44]. However, oxidized cellulose nanocrystals have limited interfacial activity due to their hydrophilic nature. Thus, surface modification of the oxidized cellulose nanocrystals will be required to enhance their interfacial properties for Pickering emulsion formation.

2.2.4.2 Compressive aerogels based on cellulose materials

Compressible aerogels have been of increasingly important for the high demand of next generation of products, such as super absorbents[45, 46], electrode substrate for batteries and supercapacitors[47, 48], catalyst supports[49], and chemical and biological sensors[50, 51] etc. Many of

these applications require the aerogel materials to be strong yet compressible and capable of reversible deformation under large strain[52]. Traditional aerogels are mostly fabricated from silica materials featured with large porosity (up to 99.8%), low density (4-500 mg/cm^3), and large surface area (100-1,000 m^2/g)[53, 54]. There are considerable studies on silica-based aerogels for various applications, including thermal and acoustic insulator[55, 56], optical applications[57], batteries[58, 59] and capacitor electrodes[60, 61], nuclear waste storage[62] and catalysis[63] etc. However, the traditional silica-based aerogels usually suffer from fragility, and they are too brittle to meet the mechanical robustness as compressive materials[64].

Recently, aerogels prepared from Poly(vinyl alcohol)(PVA) have drawn great attention since these polymeric molecules are generally less brittle, more flexible, and easy-processable[65], in addition to their excellent merits such as cost-effectiveness, nontoxicity, biocompatibility, and biodegradability[180-182]. However, PVA aerogels are neither mechanically strong nor highly compressible, which limits their applications as compressible materials. So far, PVA aerogels reinforced by carbon nanotubes and graphene materials with good mechanical strength and high compressibility have been reported[53, 69, 70]. However, those carbon-based materials are not readily available due to the high cost of equipment/raw materials, and the sophisticated procedures, which limit their large-scale applications[64].

Cellulose materials could be an alternative for carbon nanotubes and graphene materials to prepare the mechanical strong yet highly compressive PVA aerogels, due to their readily availability, low cost, good mechanical properties, low density, and excellent biocompatibility. So far, cellulose nanofibers (CNFs) have been incorporated with PVA to form the PVA/CNFs aerogels[71]. However, these aerogels were not elastic enough and deformed permanently when the compression strain was higher than 20%[71]. Cellulose nanocrystals, on the other hand, are highly

ordered rod-like nanoparticles, and they are generally considered as effective fillers in aerogels to reinforce networks[72], due to their intrinsic rigidity and excellent mechanical strength (elastic modulus~100-200 GPa[22]). Hence, there are considerable studies on the reinforcement of the mechanical strength of PVA aerogels with cellulose nanocrystals. However, even though these CNCs/PVA aerogels showed significantly improved mechanical strength, they have poor compressibility.

2.3 Summary

Canada has large forest area with abundant wood-based cellulose resources. However, wood fibers are mainly used for paper-making and lumbering, only 2% pulps with high content of cellulose are used to prepare regenerated cellulose fibers, films, and cellulose derivatives. Thus, research efforts are still required to develop applications of wood cellulose to add their values.

Two strategies (dissolution and disintegrating) can be applied for the functionalization and application of cellulose materials. As for dissolution, the recently developed NaOH/urea system is relatively environmentally "green" and has been applied to dissolve cotton linters. Wood-based cellulose has high molecular weight and cannot be effectively dissolved in this solvent system. It would be interesting to study if partial hydrolysis could promote the dissolution of wood-based cellulose in the NaOH/urea solvent system that could be further developed into some functional products, such as wood cellulose hydrogels. Additionally, wood-based cellulose materials can be disintegrated into cellulose nanocrystals either by oxidation or by acid hydrolysis. Due to their large surface area, low density and excellent mechanical properties, wood-based cellulose nanocrystals can be used as renewable and biodegradable materials for a wide range of applications. Since cellulose nanocrystals prepared from TEMPO-mediated oxidation are electrostatically stable,

further surface modification of the oxidized cellulose nanocrystals to enhance their interfacial properties could be a promising and interesting opportunity to prepare stable Pickering emulsions. Moreover, cellulose nanocrystals showed excellent mechanical properties and potential nanoreinforcement in various nanocomposites, they could be an alternative for carbon nanotubes/graphene materials to prepare the mechanical strong yet highly compressive aerogels. After these value-added processing, some wood cellulose-based new materials could be developed, and the value behind wood cellulose could be unveiled.

Chapter 3 - Controlled production of spruce cellulose gels using an environmentally "green" system*

3.1 Introduction

Cellulose is the most abundant biomass on the earth with an estimated annual production of ~1.5×10^{12} tons[3, 4, 78]. Especially wood-based cellulose, with a dominant status in Canada, has received much attention in the field of green energy, paper, textile, materials, environmental and biomedical engineering. It possesses a high strength and stiffness, and is renewable, biodegradable and biocompatible[78, 183, 184]. However, cellulose forms supramolecular structures by strong intra-/ intermolecular hydrogen bonds, making it insoluble in water and most common organic solvents[11, 12]. Accordingly, wood cellulose is difficult to process. Searching for a cost-effective and efficient solvent to dissolve wood cellulose is a key challenge in its industrial applications.

Polymers can be dissolved only if the polymer-polymer interactions are overcome by stronger polymer-solvent interactions[78]; otherwise, they are just swollen rather than dissolved. Overall, there are several cellulose solvent systems of interest including N-methyl-morpholine-N-oxide (NMMO), ionic liquids (ILs) and N,N-Dimethylacetamide (DMAc)/LiCl systems[11, 12, 14-18]. Recently, a new aqueous cellulose solvent based on NaOH/urea system has been developed which can efficiently dissolve cotton linters at low temperature (-12.6 ℃) in 2 min[19, 20]. Here, cellulose chains are held in an inclusion complex involving a NaOH hydrate, urea hydrate and water cluster, disrupting the intra-/intermolecular hydrogen bonds and leading to the dissolution of cellulose[20]. This solvent system is environmentally "green", and relatively cost-effective since no organic

* A version of this chapter has been published: Xiaoyu Gong, Yixiang Wang, Zhigang Tian, Xiang Zheng, Lingyun Chen, "Controlled production of spruce cellulose gels using an environmentally "green" system" in *Cellulose*, 2014, 21(3): 1667-1678.

solvents or toxic reagents are required. It would be useful to adapt this "green" solvent to wood cellulose to produce materials with different attributes and applications compared to those from cotton linters. Since this NaOH/urea aqueous solvent is not applicable to some native cellulose with high viscosity-average molecular weight (M_η>11.4×10^4 Da)[19], wood cellulose needs to be broken down partially to achieve a good solubility.

Various multifunctional products, such as cellulose films, gels, micro/nano-particles and fibers, have been fabricated from cellulose/NaOH/urea aqueous solutions targeting a wide range of applications[33, 107, 110, 111]. Cellulose hydrogels have especially shown potential in the creation of bioengineering and biomedical materials such as tissue engineering scaffolds and drug delivery formulations[185]. In our previous work, physically crosslinked all-cellulose composite gels were prepared from cotton linter through a convenient and time-saving process involving a rapid thermal-induced phase separation followed by a regenerating process. These gels demonstrated a capacity to steadily release bioactive compounds in the simulated body fluid[186]. This current research aimed to study the effects of acid-hydrolysis on the molecular structures of spruce cellulose and subsequently its dissolution in NaOH/urea aqueous solution. Then, the potential applications of thermal-induced gels fabricated from the resultant spruce cellulose suspensions were evaluated, and gel structure-function relationships were discussed in detail.

3.2 Materials and methods

3.2.1 Materials

Spruce cellulose (bleached kraft pulp) with β-cellulose content of 87.3% was provided by Alberta-Pacific Forest Industries Inc. (AB, Canada). Its viscosity-average molecular weight (M_η) was determined with an Ubbelohde viscometer in LiOH/urea aqueous solution at 25±0.1 ℃ and

calculated to be 40 $\times 10^4$ Da[187]. Sulfuric acid solutions with different concentrations were prepared via dilution of concentrated sulfuric acid (Fisher Scientific, Canada). Sodium hydroxide, lithium hydroxide and urea were purchased from Sigma-Aldrich Canada Ltd. (Oakville, ON, Canada), and were used as received.

3.2.2 Acid hydrolysis of spruce cellulose

Spruce cellulose (10.0 g) was hydrolyzed in a beaker by diluted sulfuric acid under continuous stirring (600 rpm) at 30 ℃. The ratio of cellulose to sulfuric acid was $3^{w}/_{v}$%. The acid concentrations were set to 10, 15 and 20 $^{w}/_{w}$%, while the hydrolysis times were 6, 12 and 24 h. As a result, 9 hydrolyzed cellulose samples were obtained and coded as *X*-*Y*-Cellulose (*X*: acid concentration; *Y*: hydrolysis time). The yield of acid hydrolysis was higher than 94.4% and the content of hemicellulose in the resultant samples was lower than 6.7 $^{w}/_{w}$% (**Table 3-1**).

Table 3- 1 Viscosity-average molecular weight (M_η), solubility index (S_a), yields and hemicellulose content of the cellulose samples hydrolyzed at different conditions.

Samples	Acid concentration ($^{w}/_{w}$%)	Hydrolysis time (h)	$M_\eta \times 10^{-4}$	Sa%	Yields ($^{w}/_{w}$%)	Hemicellulose ($^{w}/_{w}$%)
10%-6-Cellulose	10%	6	18.6	44	97.5	6.7
15%-6-Cellulose	15%	6	16.9	55.5	97.2	6.2
20%-6-Cellulose	20%	6	10.6	76.2	97	5.8
10%-12-Cellulose	10%	12	15.2	56.3	97.3	5.8
15%-12-Cellulose	15%	12	13.8	76.2	96.9	4.3
20%-12-Cellulose	20%	12	9	77.2	96.8	3.7
10%-24-Cellulose	10%	24	10.6	63.5	96.5	3
15%-24-Cellulose	15%	24	7	86.7	95.8	1.5
20%-24-Cellulose	20%	24	5.8	92.5	94.4	0.4

3.2.3 Cellulose structure characterizations

In our preliminary experiment, hydrolyzed spruce cellulose could not be dissolved completely in NaOH/urea aqueous solution, although a well-dispersed system was obtained, whereas both spruce cellulose and its hydrolysate could be completely dissolved in LiOH/urea system at diluted concentrations[19]. The intrinsic viscosity *[η]* of the hydrolyzed cellulose in 4.6% LiOH/15% urea aqueous solution was measured with an Ubbelohde viscometer at 25±0.1 ℃, and the M_η was calculated by the following **equation (3-1)**[187]:

$$[\eta]=3.72\times10^{-2}\,[M_\eta]^{0.77} \qquad \textbf{(3-1)}$$

To understand the crystallinity structure of spruce cellulose after hydrolysis, wide-angle X-ray diffraction (WAXD) measurements were carried out using an X-ray diffractometer (Ultimate IV, Rigaku, Japan) in symmetric reflection mode. The diffracted intensity of Cu K*a* radiation (average λ is 0.1542 nm) at 40 kV and 44 mA was recorded in the 2θ range of 4°-40°. The original spruce cellulose and the hydrolyzed samples were cut into powders and dried in a vacuum oven at 60 ℃ for 24 h before the measurements. The crystallinity index χ_c (%) was calculated using the following **equation (3-2)**:

$$\chi_c = \int_0^\infty S^2 I_c(s)ds \,/\, \int_0^\infty S^2 I(s)ds \qquad \textbf{(3-2)}$$

Where S is the magnitude of the reciprocal-lattice vector and is given by $S=(2\sin\theta)/\lambda$, θ is one half of the scattering angle, λ is the wavelength of the X-ray, $I(s)$ is the intensity of the coherent X-ray scattering from both the crystalline and amorphous region, while $I_c(s)$ is only the intensity of the crystalline region from the samples. The lateral dimensions of the raw spruce pulp and the hydrolyzed cellulose samples were calculated by using Scherrer's equation[188]:

$$D_{(hkl)}=K\lambda/(\beta\cos\theta) \qquad \textbf{(3-3)}$$

Where λ is the X-ray wavelength, 2θ is the angle between incident and diffracted rays, β is the half bandwidth of (hkl) diffraction peak in radians, and K is a constant with a value of 0.94.

3.2.4 Cellulose solubility test

Solubility of the hydrolyzed cellulose in NaOH/urea aqueous solution was measured as follows: 96 g of 7% NaOH/12% urea aqueous solution was precooled to -12.6 ℃. Subsequently, 4.0 g of hydrolyzed cellulose was added into the precooled solution with mechanical stirring at 2,000 rpm for 3 min to obtain stable cellulose suspensions, which were then centrifuged at 8,000 rpm for 10 min at 5 ℃ to separate the insoluble, but well dispersed cellulose. The precipitate was rinsed with diluted H_2SO_4 (1 M), distilled water and acetone, respectively. Finally, the dispersed cellulose was dried to constant weight at 60 ℃. The solubility of the hydrolyzed cellulose was calculated according to the **equation (3-4)**:

$$S_a=(W_0-W_i)/W_0\times 100 \qquad \textbf{(3-4)}$$

Where W_0 is the mass of the original cellulose, W_i is the mass of the residue and S_a is the solubility index.

3.2.5 Gelation behavior study

The thermal-induced gelation behavior of cellulose suspensions was investigated by recording the storage modulus (G') and loss modulus (G'') as a function of temperature (T) using a dynamic shear method. A DHR-3 rheometer (TA Instrumens, DE, USA) with a parallel plate geometry (plate diameter 40 mm) was employed. Hydrolyzed cellulose/NaOH/urea suspension (4 $^{w}/_{w}$%) was centrifuged at 4,000 rpm for 10 min at 5 ℃ to remove bubbles and then directly introduced onto the plate. To avoid dehydration during the rheological measurements, a layer of silicon oil was covered around the exposed surface of the suspension. The measurements were carried out from 20 to 50 ℃ at an angular frequency of 1.0 Hz with a heating ramp of 2 ℃/min. The value of strain

amplitude was set as 10%, which was within a linear viscoelastic region. By noting the temperature at which $G' = G''$, the profile could provide evidence of the gel point and gelation behavior[189].

3.2.6 Preparation of cellulose gels

Thermally induced cellulose gels were prepared as described by Wang and Chen (2011)[186]. Briefly, fresh bubble-free cellulose suspensions (4 $^{w}/_{w}$%) were loaded into a tube (15 mL) and heated in a water bath at 50 ℃ for 10 h. The gels were rinsed in running water for 3 days and kept in deionized water for further use. No obvious loss of cellulose was observed during rinsing. WAXD was used to determine the crystallinity index to understand the structural changes of the thermally induced cellulose gel samples.

3.2.7 Morphology of cellulose gels

A Philips XL-30 scanning electron microscopy (SEM) was employed to observe the morphology of the samples. The accelerating voltage was set at 20 kV and the working distance was 10 mm. Cellulose gels prepared by different conditions were frozen in liquid nitrogen, snapped immediately and then freeze-dried. The cross-sectional fracture surfaces of the gels were coated by a thin layer (8-10 nm) of sputtered gold under vacuum, and then were observed and photographed.

3.2.8 Swelling behavior study

The swelling ratio of thermally induced cellulose gels was measured gravimetrically in deionized water at 25 ℃. After incubated for 24 h, excess surface water was blotted with filter paper, and the weight of the water-saturated gels was recorded. The equilibrium swelling ratio (*ESR*) was calculated according to the **equation (3-5)**:

$$ESR = (W_s - W_d)/ W_d \qquad \textbf{(3-5)}$$

Where W_s is the weight of the swollen gel at 25 ℃ and W_d is the dry weight of the gel.

3.2.9 Mechanical analysis

The mechanical properties of the cellulose gels were measured using an Instron 5967 Testing Machine (Instron Corp., MA, USA). The gels had a cylindrical shape of 11 mm in diameter and 10 mm in height, and were kept in deionized water at 25 ℃ for 24 h before determining their mechanical properties. Gels were compressed twice to 50% of their original height in air at room temperature at a rate of 1 mm/min. The compressive stress vs. strain was recorded and all measurements were repeated at least five times.

3.2.10 Statistical analysis

Experimental results were represented as the mean of five batches ± SD. Statistical evaluation was carried out by analysis of variance (ANOVA) followed by multiple-comparison tests using Duncan's multiple-range test at the 95% confidence level. All of the analyses were conducted using SAS statistical software (SAS Institute, Inc., Cary, NC) with a probability of $p < 0.05$ considered to be significant.

3.3 Results and discussion

3.3.1 Cellulose hydrolysis

The idea of acid-catalyzed hydrolysis of cellulose into fermentable sugars in order to develop cost-efficient replacement for fossil fuels has come into being since the two oil crises in the 20th century[190]. However, in this study, complete hydrolysis of cellulose into sugars was not desirable. Instead, partial acid degradation of spruce cellulose under mild conditions was necessary to enable its subsequent dissolution in an environmentally "green" NaOH/urea aqueous solution. This permitted suitable molecular structure characteristics of the cellulose products with desirable functionalities. For this purpose, the reaction conditions, such as acid type, acid concentration,

hydrolysis time and temperature, were of interest. In this study, diluted sulfuric acid was selected due to its low cost[191] and high efficiency[192, 193]. Moreover, in order to reduce energy consumption for potential industrial applications, the reaction temperature was strictly controlled at 30 ℃. Herein, the effects of acid concentration and hydrolysis time on spruce cellulose structure were investigated.

It has been proposed that the acid-catalyzed hydrolysis of cellulose could follow three steps: protonation of glycosidic oxygen or pyranic oxygen, formation of the carbocation, and regeneration of H_3O^+ species and cleavage of glucosidic bonds[190]. In this study, the mild conditions were not strong enough to hydrolyze spruce cellulose into mono-/di-/oligo-saccharides, but may disrupt the more accessible amorphous regions and cut the linear chains, resulting in changes in molecular parameters and physicochemical properties.

3.3.2 Molecular weight and crystallinity

Table 3-1 shows the viscosity-average molecular weight (M_η) of the hydrolyzed spruce cellulose. The M_η values were distinctly reduced when increasing the acid concentration or hydrolysis time, comparing with the untreated samples ($M_\eta = 40\times10^4$ Da). For example, the M_η of 10%-6-Cellulose was 18.6×10^4 Da, which decreased to 10.6×10^4 Da when the acid concentration increased to 20 $^{w}/_{w}$% at the same hydrolysis time. A similar decrease could also be observed for the samples hydrolyzed for 12 h and 24 h, of which the M_η decreased from 18.6 to 15.2 and 10.6 $\times10^4$ Da, respectively. The M_η of 20%-6-Cellulose was the same as that of 10%-24-Cellulose, which implies that both acid concentration and hydrolysis time played important roles in reducing cellulose molecular weight. For 20%-24-Cellulose, the M_η was largely reduced from original 40×10^4 Da to 5.8×10^4 Da. This suggests that the molecular structure of spruce cellulose may undergo dramatic changes when treated at higher acid concentrations for a longer period of time.

This may facilitate the development of cellulose-solvent interactions so as to improve the dissolution of spruce cellulose in NaOH/urea aqueous solutions.

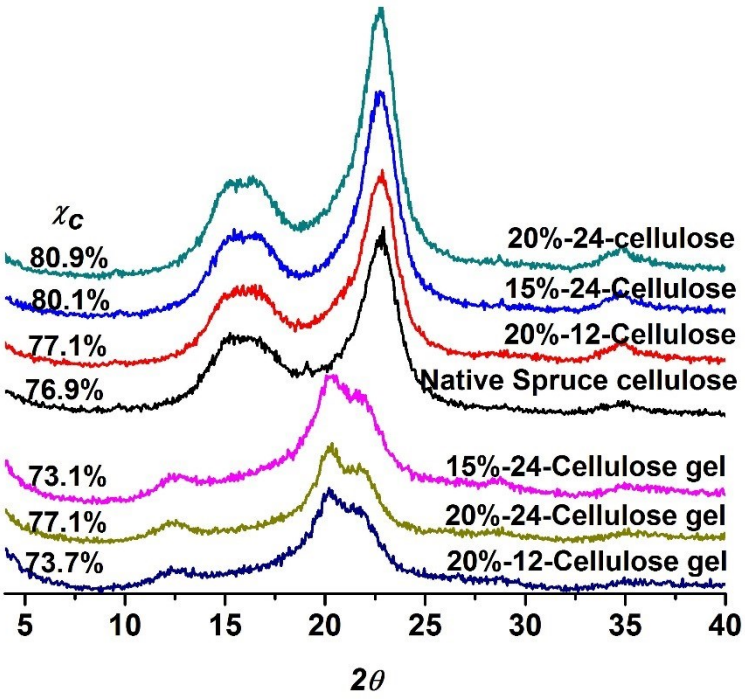

Figure 3- 1 Wide angle X-ray diffraction of native/hydrolyzed/regenerated spruce cellulose.

The crystallinity index χ_c can be another factor that impacts the dissolution of cellulose in NaOH/urea solution[12]. **Fig. 3-1** shows the WAXD pattern of the native and hydrolyzed spruce cellulose with the calculated crystallinity index χ_c listed on the left. All these samples exhibited the same diffraction peaks at 2θ=14.9°, 16.7°, and 22.7°, which are assigned to the ($1\bar{1}0$), (110) and (200) planes of cellulose I_β[194]. It indicated that the crystalline structure of spruce cellulose remained after the treatment.

The χ_c values of native and hydrolyzed spruce cellulose were compared to reveal the effect of acid treatment on cellulose structure. The native sample had a χ_c value of 76.9%, which was much

higher than that of Sitka spruce cellulose[195]. There were two possible reasons for this increase: first, the production process of bleached kraft pulp might result in the rise of crystallinity; second, some of the conformationally disordered chains are located close enough to the corresponding lattice points and are in approximately the right axial and rotational orientations to contribute to the crystalline part of the WAXS pattern even though they differ conformationally[195]. However, compared with that of the native spruce cellulose, the χ_c value was seldom changed after 12 h of treatment in 20% acid solution, while the M_η decreased from 40×10^4 Da to 9.0×10^4 Da. These results show that the acid hydrolysis under mild conditions led mainly to the breakage of cellulose molecular chains. Even the χ_c values of 15%-24-Cellulose and 20%-24-Cellulose only slightly increased to 80.1% and 80.9%, respectively, because of the removal of amorphous regions under long time hydrolysis. At the same time, the lateral dimensions of cellulose didn't obviously change after the acid hydrolysis. Therefore, the hydrolyzed spruce cellulose exhibited a similar crystalline structure after treating with diluted acid, and the crystallinity index is not likely to be a key factor to influence wood cellulose dissolution.

3.3.3 Solubility of hydrolyzed spruce cellulose

The solubility index (S_a) of hydrolyzed spruce cellulose in NaOH/urea aqueous solution is listed in **Table 3-1**. The original spruce cellulose could not be dispersed in the solvent, but all hydrolyzed samples formed a stable and homogenous suspension in NaOH/urea aqueous solution. After hydrolysis in 10% acid solution for just 6 h, nearly half of the spruce cellulose was dissolved, while the remainder was uniformly dispersed as swollen fibers. It indicates that the acid treatment, even at mild conditions, resulted in the decrease of cellulose molecular weight. This largely promoted the penetration of solvent molecules and thus the solvent-cellulose interactions. The S_a increased from 44.0% to 76.2% when the acid concentration increased from 10% to 20%. When the acid

concentration remained at 10%, 63.5% of cellulose was dissolved when the hydrolysis time was prolonged to 24 h. More than 85% hydrolyzed spruce cellulose was soluble when the molecular weight was lower than 7.0×10^4 Da, and the S_a value increased to 92.5% for 20%-24-Cellulose at the molecular weight of 5.8×10^4 Da. Cotton linters with a molecular weight lower than 11.4×10^4 Da can be completely dissolved in the NaOH/urea aqueous solution at -12.6 ℃ as reported by Cai and Zhang (2005)[19], whereas the hydrolyzed spruce cellulose (20%-6-Cellulose) with the M_η of 10.6×10^4 Da exhibited a S_a of 76.2%. This could be due to the relatively higher crystallinity of hydrolyzed spruce cellulose (>76.9%), since the crystallinity of cotton linters with a molecular weight between 4.8×10^4 to 11.1×10^4 Da was in the range of 67~72%[12]. Therefore, the suspension of hydrolyzed spruce cellulose in NaOH/urea aqueous solution consisted of dissolved cellulose and dispersed cellulose fibers was successfully prepared. This suspension was stable and could be stored at 4℃ for at least 3 months without separated layers or aggregation.

3.3.4 Gelation behavior of hydrolyzed cellulose/NaOH/urea/water suspensions

The gelation behaviors of hydrolyzed spruce cellulose in 7% NaOH/12% urea aqueous solutions were investigated to evaluate the potential applications of the cellulose suspensions. In this study, the crossover point of storage modulus (G') and loss modulus (G'') was considered as the indicator of gel point. Since the gel point determined by this method was frequency-dependent, a frequency of 1 Hz was used to ensure the linearity of viscoelasticity for all sample measurements.

To understand gelation behavior of spruce cellulose hydrolyzed at different acid conditions, the evolution of G' and G'' as a function of temperature was recorded for 10%-12-Cellulose, 15%-12-Cellulose and 20%-12-Cellulose suspensions. As showed in **Fig. 3-2a**, the rheological behavior of 10%-12-Cellulose was overall distinct from other two suspensions. The G' curve was above the G'' curve during the whole process, indicating a solid-like behavior. For 15%-12-Cellulose and 20%-

12-Cellulose, the G'' value was higher than G' value at the initial stage, suggesting that these two suspensions behaved like viscous liquid at lower temperatures. These different rheological behaviors may be closely related to cellulose molecular weight resulting from hydrolysis by various acid concentrations. When compared at the same hydrolysis time, spruce cellulose hydrolyzed by stronger sulfuric acid showed lower molecular weight (**Table 3-1**). The suspensions of cellulose with larger molecular weight (10%-12-Cellulose) exhibited more elasticity due to a lower relaxation capacity and easy entanglement of the longer chains[196]. Whereas the 15%-12-Cellulose and 20%-12-Cellulose suspensions were more viscous liquid-like because of a reduced molecular weight and increased S_a. The clear plateaus of G' curve of all three suspensions appeared at the lower temperatures indicated the aggregation of cellulose chains[196]. As the temperature elevated, their G' value increased quickly, and the crossover points were observed at 32.5 ℃ and 36.0 ℃ for 15%-12-Cellulose and 20%-12-Cellulose, respectively, suggesting the dynamic transitions of sol-gel process. It was reported that the possible forms of hydrogen bonds in the Cellulose/NaOH/urea/water system were as follows: intra- and intermolecular hydrogen bonding between hydroxyl groups of cellulose; hydrogen bonding between hydroxyl groups of cellulose and solvent molecules (NaOH hydrate, urea hydrate and free water); and hydrogen bonding and electrostatic interaction between the solvent molecules[19, 32]. Elevation of temperature led to the weakened hydrogen bond strength between cellulose and solvent molecules, whereas the intra- and intermolecular hydrogen bonds of cellulose tended to increase as a result of its strong self-association tendency[32]. Therefore, the structure of inclusion complexes (IC) was destroyed and physical entanglements occurred between the cellulose backbones, which is called "thermal-induced phase separation processing" [20, 197]. The gelling temperature of hydrolyzed cellulose suspensions rose with the increase of S_a values, which suggests that the uniformly dispersed

swollen cellulose fibers "bridged" and facilitated the crosslinking of cellulose molecules. This is like the effects observed with cellulose nanocrystals that reinforced all cellulose gels[186]. **Fig. 3-2b** shows the effect of hydrolysis time on the rheological behaviors of cellulose suspensions. Similarly, 15%-6-cellulose suspension with a S_a value of 55.5% behaved more like a solid, which did not display any crossover point in the temperature range; while 15%-12-Cellulose and 15%-24-Cellulose suspensions exhibited the dynamic sol-gel transitions and had gel points of 32.5 ℃ and 43.0 ℃, respectively. Likewise, the rising gel point observed for samples treated with longer period of hydrolysis was due to the higher hydrolysis degree of spruce cellulose, leading to smaller molecular weight and shorter chains with higher relaxation capacity and less entanglement at lower temperatures[196].

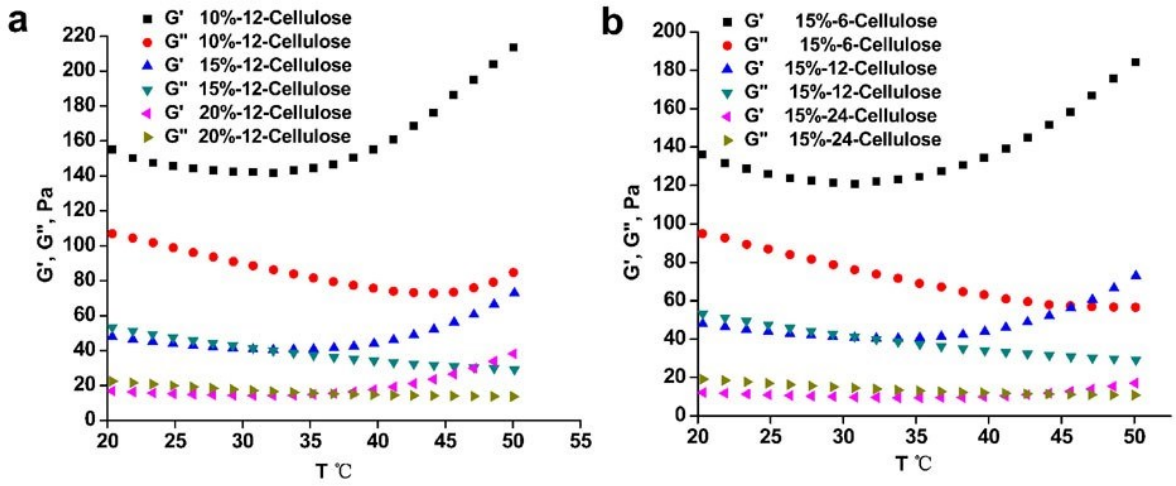

Figure 3- 2 Temperature dependence of storage modulus (G′) and loss modulus (G″) of cellulose suspensions with a heating rate of 2 ℃/min at a frequency of 1 Hz.

3.3.5 Structure of thermal-induced spruce cellulose gels

All spruce cellulose suspensions formed thermal-induced gels after heating at 50 ℃ for 10 h. As shown in **Fig. 3-3**, the network structure of these gels varied with different hydrolysis conditions. Specifically, the 15%-6-Cellulose gel obtained from a relatively mild hydrolysis condition exhibited thinner wall. With an increase of hydrolysis degree, a denser crosslinking structure was observed in the 15%-24-Cellulose gel, suggesting more interactions were developed. The 20%-12-Cellulose gel had a uniform and well-established network structure, and the wall became denser in 20%-24-Cellulose gel. During the gelation, the interactions were rebuilt among the cellulose chains, with the dissolved cellulose crosslinked to form 3D network and the dispersed swollen cellulose fibers serving as fillers in the gel matrix. According to the data in **Table 3-1**, 15%-6-Cellulose with a molecular weight of 16.9×10^4 Da had a solubility of 55.5%, while the S_a of 15%-24-Cellulose, which had a molecular weight of 7.0×10^4 Da, was 86.2%. Comparing these two samples, 15%-6-Cellulose had less dissolved cellulose to form the gel network but more dispersed fillers, resulting in the thin wall structure formed by the joined swollen cellulose fibers. For the 15%-24-Cellulose, more hydrolyzed cellulose was dissolved so as to increase connections in the thermally induced gel. Therefore, by altering the hydrolysis conditions, the ratio of "matrix" and "filler" in hydrolyzed spruce cellulose gels could be adjusted. Accordingly, a denser structure was observed in 20%-12-Cellulose gel due to a well-balanced ratio of "matrix" and "filler". When the hydrolysis time was further increased, 20%-24-Cellulose exhibited a S_a of 92.5%, where most cellulose was dissolved and then crosslinked to form a dense structure. Interestingly, it was difficult to distinguish the undissolved cellulose fibers or large aggregates on the cross-section of gels, which was a direct evidence that hydrolyzed spruce cellulose suspensions were stable and the swollen cellulose fibers were uniformly dispersed. Moreover, no obvious irregular shrinkage took

place when these spruce cellulose gels were immersed and regenerated in a water bath, indicating that the gels with "matrix-filler" structures had a better stability than the thermally induced cotton linter gels.

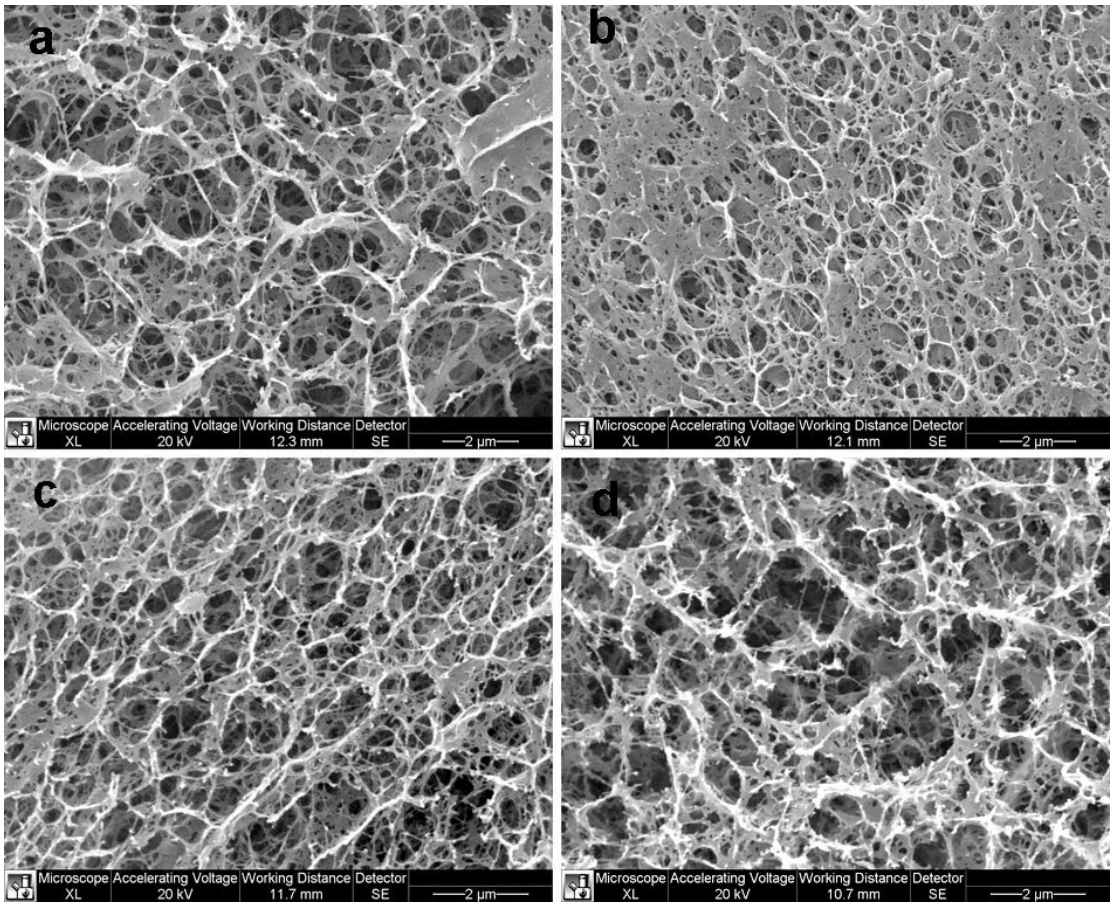

Figure 3- 3 SEM images of thermal-induced spruce cellulose gels: (a) 15%-6-Cellulose gel; (b) 15%-24-Cellulose gel; (c) 20%-12-Cellulose gel; and (d) 20%-24-Cellulose gel.

The χ_c of hydrolyzed spruce cellulose gels was also investigated (as shown in **Fig. 3-1**). The diffraction peaks at 2θ=12.1°, 19.8°, and 22.2° are assigned to the ($1\bar{1}0$), (110) and (200) planes, which are typical peaks of cellulose II, suggesting a transformation from cellulose I to cellulose II

during the gelation[183]. Similarly, the lateral dimensions of regenerated cellulose were not obviously affected by the different hydrolysis conditions. It was noteworthy that, unlike the cellulose nanocrystals reinforced all cellulose materials made of cotton linter[109], no typical peaks of cellulose I were observed in spruce cellulose gels. It suggests that, with acid hydrolysis, the solvent molecules could easily penetrate into spruce cellulose, leading to the dissolution of cellulose with relatively lower molecular weight. At the same time, most highly crystallined structures were likely broken and dispersed as swollen fibers, which were covered by the crosslinked cellulose "matrix" during gelation.

3.3.6 Swelling behavior

Fig. 3-4 shows the equilibrium swelling ratio (ESR) of hydrolyzed spruce cellulose gels. These ESR values of all gels were higher than 15.0, which were superior to the cotton linter gel with an ESR of 9.88[186]. This was because of the "matrix-filler" structure of hydrolyzed spruce cellulose gels, where undissolved cellulose fibers provided extra support to the gel network and enabled the formation of more interspaces to hold water. The ESR values of hydrolyzed spruce cellulose gels also depended on the acid hydrolysis conditions, where ESR increased with higher acid concentration and prolonged hydrolysis time. The hydrolyzed cellulose prepared at relatively harsh conditions exhibited lower molecular weight and improved solubility, which endowed the cellulose matrix the increased relaxation capacity to hold more water. However, the ESR of the 20%-24-Cellulose gel decreased compared to that of the 15%-24-Cellulose gel. It was probably due to less "filler" content in the 20%-24-Cellulose gel inadequate to support the highly porous structure.

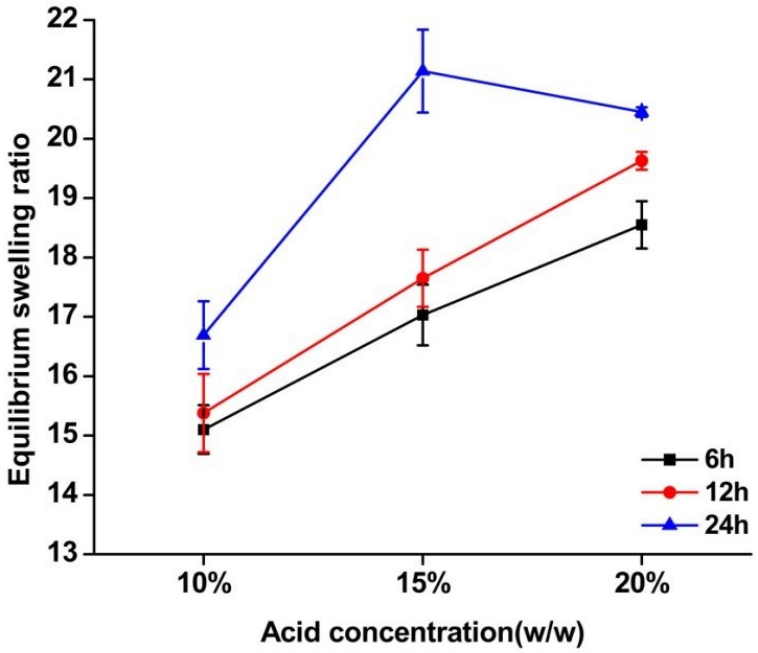

Figure 3- 4 Equilibrium swelling ratios of thermal-induced spruce cellulose gels.

3.3.7 Mechanical properties

Mechanical performance of the thermally induced spruce cellulose gels was investigated under compression mode. Typical stress-strain curves are shown in **Fig. 3-5**. All gels behaved in a non-Hookean mode, like rubbers, in the deformation range of 0~50%. According to the theory of rubber elasticity, the relationship of stress-deformation could be mathematically modeled by the simplified Mooney-Rivlin equation[198, 199]:

$$\sigma=G(\lambda-\lambda^{-2}) \qquad \textbf{(3-6)}$$

Where σ is the stress defined as the force per cross-sectional area of the cylindrical samples and λ is the deformation ratio equal to L/L_0 in which L and L_0 are the deformed length and the original length of the gels, respectively. In a plot of stress vs. $-(\lambda-\lambda^{-2})$ (**Fig. 3-6**), the simulation of the data showed very straight lines in the deformation range of 0~50% (R^2=0.992~0.999, **Table 3-2**) and

the slopes of these lines were used to calculate the compressive modulus of the gels (**Table 3-2**). Generally, the compressive stress of hydrolyzed spruce cellulose gels increased with higher acid concentration and prolonged hydrolysis time, indicating that a sufficient content of dissolved cellulose was necessary to join the dispersed cellulose fibers and establish a strong gel network. The compressive modulus of the 20%-12-Cellulose gel was 354.2 kPa, much greater than that of other gels, which were less than 15 kPa. This was due to its balanced "matrix-filler" ratio, where enough cellulose fibers reinforce the network and contribute to the stiffness of the gels, and an adequate amount of dissolved cellulose crosslinked with each other via hydrogen bonds to form the gel matrix. Therefore, a uniform porous structure of the 20%-12-Cellulose gel was formed as revealed by SEM image. However, the 20%-24-Cellulose gel exhibited the lowest compressive stress, because it only contained 7.5% of undissolved cellulose as the fillers. **Fig. 3-5d** also shows a successive compression of the 20%-12-Cellulose gel for 2 cycles. The highest compressive stress was not obviously decreased in the second round, suggesting the spruce cellulose gels were elastic and could be recompressed without losing their elasticity. This thermal-induced spruce cellulose gel exhibited similar modulus compared to those of bacterial cellulose scaffold and PLA-PEO-PLA hydrogels[200, 201]. This research demonstrates how these gels have both controllable mechanical strength and good flexibility, and may have significant potential to be used in cartilage engineering.

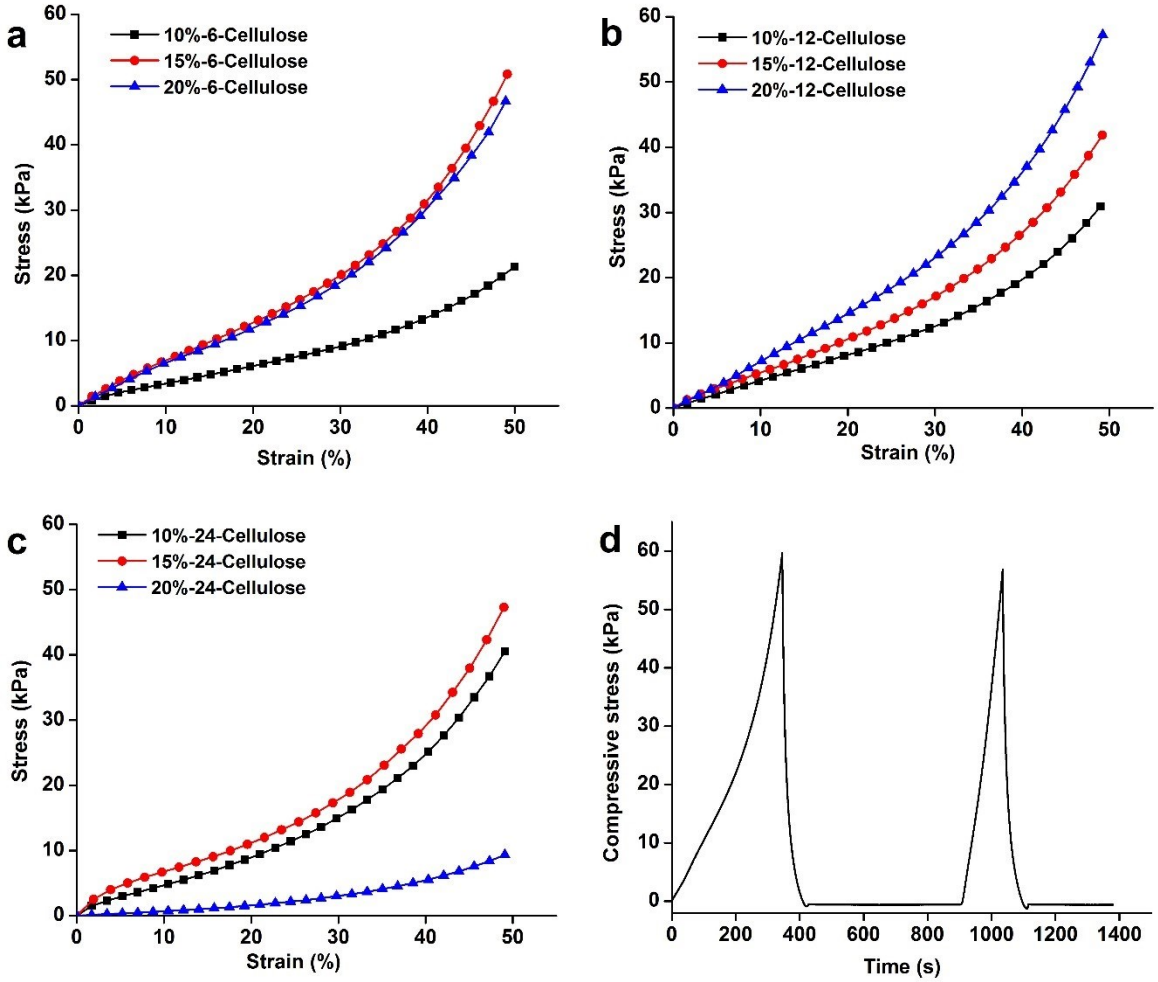

Figure 3- 5 Stress-strain curves of thermal-induced spruce cellulose gels: (a) cellulose hydrolyzed for 6 h; (b) cellulose hydrolyzed for 12 h; and(c) cellulose hydrolyzed for 24 h. (d) compressive-stress vs. time during two cycles of compression of 20%-12-Cellulose gel.

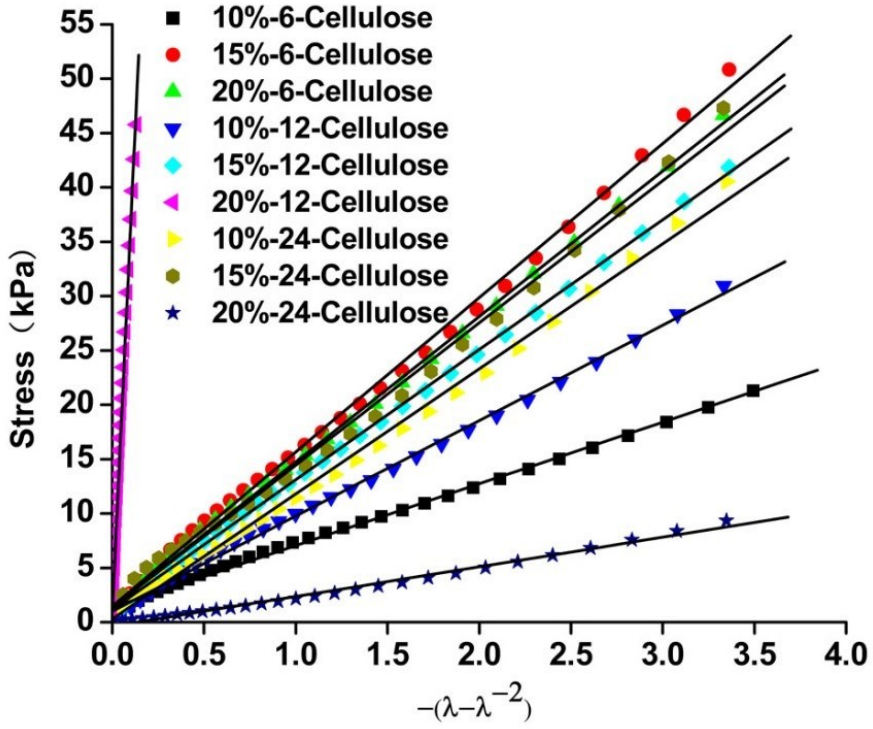

Figure 3- 6 Stress vs. deformation function for thermal-induced spruce cellulose gels, showing very good linear correlation.

Table 3- 2 Compressive modulus and R^2 of thermal-induced spruce cellulose gels.

Samples	Compressive Modulus (kPa)	R^2
10%-6-Cellulose	5.7	0.996
15%-6-Cellulose	14.2	0.997
20%-6-Cellulose	13.4	0.998
10%-12-Cellulose	8.9	0.998
15%-12-Cellulose	12.0	0.999
20%-12-Cellulose	354.2	0.995
10%-24-Cellulose	11.5	0.997
15%-24-Cellulose	13.1	0.994
20%-24-Cellulose	2.7	0.992

3.4 Conclusions

Wood-based cellulose was hydrolyzed by diluted sulfuric acids with various hydrolysis times at 30 ℃. By this mild treatment, the long molecular chains of spruce cellulose were cleaved, and then dispersed to form stable suspensions in an environmentally "green" NaOH/urea aqueous solution. The relationship between the molecular weight and solubility of hydrolyzed cellulose was revealed. Solvent molecules penetrated into spruce cellulose, leading to the dissolution of cellulose with low molecular weight and the dispersion of undissolved cellulose fibers. The resultant spruce cellulose suspensions showed good gelling properties when the temperature was increased. These thermal-induced cellulose gels exhibited interconnected porous morphology, good flexibility and a "matrix-filler" structure. The dissolved cellulose crosslinked upon heating and regenerated in water to form the gel matrix and the dispersed swollen cellulose fibers acted as fillers to support the gel network. The gel properties largely depended on the ratio of "matrix" and "filler". By altering the acid hydrolysis conditions, the 20%-12-Cellulose gel with a balanced "matrix-filler" content, possessed a uniform structure, the highest compression stress and a good swelling ratio. This study has demonstrated an efficient method of dissolution of wood cellulose in an eco-friendly solution from which to prepare cellulose gel targeted toward biomedical materials. This has provided new opportunities to facilitate the industrial utilization of wood-based cellulose.

Chapter 4 - Enhanced emulsifying properties of wood-based cellulose nanocrystals as Pickering emulsion stabilizer*

4.1 Introduction

Pickering emulsions stabilized by solid particles have advantages of being extremely stable and require less particle stabilizers compared to other traditional surfactants[38, 202]. The "surfactant-free" character also makes them attractive, particularly for food, cosmetic and pharmaceutical applications where surfactants may have adverse effects or may be preserved as undesirable by the consumer[38, 203, 204]. In addition, there is a shift toward studying Pickering emulsions agents of biological origin since these solid colloids are usually biocompatible, biodegradable, and environmentally friendly[36, 38, 205]. Solid colloids can form an effective steric and electrostatic shield at the oil-water interface, which prevents the emulsion droplets from coalescence so as to improve emulsion stability[204].

Cellulose has both good biodegradability and biocompatibility and is the most abundant renewable polymer resource available with an annual production of 1.5×10^{12} tons/year[2]. Recently, hydrophobilized microfibrillated cellulose and cellulose nanocrystals solid particles have been used to stabilize Pickering emulsions[39, 41]. However, these cellulose materials are apt to aggregate in aqueous medium, due to either their enhanced hydrophobic interactions with microfibrillated cellulose[39], or due to the weakened electrostatic repulsions between the cellulose nanocrystals hydrolyzed by hydrochloride acid[41]. Thus it is difficult to keep them stable as well dispersed colloids for long periods. More recently, highly homogeneous, and electrostatically stable oxidized

* A version of this chapter has been published: Xiaoyu Gong, Yixiang Wang, Lingyun Chen, "Enhanced emulsifying properties of wood-based cellulose nanocrystals as Pickering emulsion stabilizer" in *Carbohydrate polymers*, 2017, 169: 295-303.

cellulose nanocrystals (O-CNCs) were obtained by consecutive oxidation to introduce carboxyl groups onto the surface of oxidized cellulose nanocrystals. These oxidized cellulose nanocrystals have similar dimensions to cellulose nanocrystals prepared by acid hydrolysis, but have a larger charge density, and thus are mostly homogeneous and electrostatically stable in aqueous medium[29]. Their size and rod-like morphology make them suitable to be adsorbed to the oil-water interface, making them potential Pickering emulsion stabilizer[42-44]. However, oxidized cellulose nanocrystals have limited interfacial activity due to their hydrophilic nature, and they need modification to increase their amphipathy as emulsion stabilizers. Recent strategies are mainly chemical modifications, such as butylamination of dialdehyde cellulose nanocrystals, free radical polymerization of N,N-(Dimethylamino)ethyl methacrylate (DMAEMA) on the surface of cellulose nanocrystals, or esterification of cellulose nanocrystals with lauroyl chloride (C12)[204, 206, 207]. However, physical modifications of cellulose nanocrystals, which are attractive due to the chemical-free concept, are much less reported. Herein, we employed the method of physical adsorption of cation on the surface of oxidized wood cellulose nanocrystals, so as to increase their amphipathy and expand their application as Pickering emulsion stabilizer.

In the present study, we used wood pulp as the starting material to prepare wood-based oxidized cellulose nanocrystals. Then these oxidized cellulose nanocrystals were modified using phenyltrimethylammonium chloride to introduce phenyl groups serving as the hydrophobic domains to enhance their interfacial properties. Afterwards, the feasibility of the modified oxidized cellulose nanocrystals (m-O-CNCs) as a Pickering emulsion stabilizer was investigated in comparison to Tween-20 as a conventional surfactant.

4.2 Materials and methods

4.2.1 Materials

Spruce cellulose (bleached kraft pulp) was a gift from Alberta-Pacific Forest Industries Inc. (AB, Canada). Its viscosity-average molecular weight (M_η) was determined with an Ubbelohde viscometer in LiOH/urea aqueous solution at 25±0.1 ℃ and calculated to be 4 $\times 10^5$ Da^2. Styrene was purchased from Sigma-Aldrich Canada Ltd. (Oakville, ON, Canada) and was purified by repeated washing with 5 $^{w}/_{w}$% NaOH aqueous solution and then with deionized water until the washings were neutral. After drying with anhydrous Na_2SO_4 for 1 h, styrene was distilled under reduced pressure and stored in the dark at 4 ℃[208]. All the other chemicals were purchased from Sigma-Aldrich Canada Ltd. (Oakville, ON, Canada) and used as received.

4.2.2 Oxidized cellulose nanocrystal preparation

Three steps of consecutive oxidation were carried out to obtain well-dispersed oxidized cellulose nanocrystal suspension according to the method of Yang with some refinements[29]. Milled spruce pulp (<0.8 mm, 20 g) was wetted in deionized water followed by addition of $NaIO_4$/NaCl aqueous solution ($NaIO_4$ 13.32 g, NaCl 78 g, total volume 1332 mL). The mixture was kept in a light-proof beaker and stirred at 350 rpm at room temperature for 36 h. Ethylene glycol (30 mL) was then added to quench the residual periodate. The oxidized pulp was washed and suspended in deionized water (1,000 mL) followed by addition of $NaClO_2$ (14.24 g), NaCl (58.40 g), and H_2O_2 (13.20 g) under stirring at 350 rpm for 24 h (pH maintained at 5). Ethanol was then used to precipitate the oxidized cellulose followed by thorough washing with water/ethanol solution (50:50, $^{v}/_{v}$) and then with acetone. The chlorite-oxidized cellulose was dried in a fume hood (yield=81.5%). The chlorite-oxidized cellulose (5 g), TEMPO (0.008 g), $NaClO_2$ (5.65 g), and phosphate buffer (450 mL, pH 6.8) were added into a three-necked flask followed by continuous

heating and stirring at 250 rpm until 50 ℃. NaClO (1.25 mL in 50 mL of phosphate buffer) was then added and the mixture was stirred at 500 rpm at 60 ℃ for 48 h. The mixture was then dialyzed against deionized water and further freeze dried (final yield=79%).

4.2.3 Surface modification of oxidized cellulose nanocrystals

Surface modification of oxidized cellulose nanocrystals was carried out according to the method of Salajková with some modifications[209]. The oxidized cellulose nanocrystals were dispersed in deionized water at a concentration of 0.1 $^{w}/_{w}$% with continuous stirring overnight and the pH adjusted to 10 afterward. Phenyltrimethylammonium chloride solution (PTAC, 0.1 $^{w}/_{w}$%) was then prepared in deionized water at 60 ℃ followed by dropwise addition of the above oxidized cellulose nanocrystal suspension at feed ratios of 2:1, 1:1, and 1:2 ($^{v}/_{v}$), respectively. The mixture was then stirred at 60 ℃ for 3 h and further stirred at room temperature (23 ℃) overnight. Finally, the mixture was dialyzed against deionized water until pH was neutral. The samples were freeze dried and kept at 4 ℃ for further use. With the increasing feed ratio of PTAC/O-CNCs, samples were denoted as m-O-CNCs-1, m-O-CNCs-2, and m-O-CNCs-3, respectively.

4.2.4 Pickering Emulsion preparation

For all the Pickering emulsions, the aqueous phase was prepared by dispersing the modified oxidized cellulose nanocrystals into deionized water at various concentrations (0.5 g/L to 5.0 g/L), forming stable and transparent suspensions. Then, 0.75 mL of hexadecane was added into 1.75 mL of modified oxidized cellulose nanocrystal suspension, followed by sonication with a probe-type sonifier for 20 s to form a Pickering emulsion[41]. To protect the samples from heating, a pulse function was used (pulse on, 3.0 s; pulse off, 3.0 s; Power, 2 W/mL). The emulsions prepared from hexadecane/O-CNC aqueous suspensions were used as controls and emulsions stabilized by Tween-20 under the same conditions were used for comparison.

4.2.5 Characterizations of modified oxidized cellulose nanocrystals

To study the structure of modified oxidized cellulose nanocrystals, Fourier transform infrared (FTIR) spectra of phenyltrimethylammonium chloride, oxidized cellulose nanocrystals, and m-O-CNCs-2 were recorded on a Nicolet 6700 spectrophotometer (Thermo Fisher Scientific Inc., MA, USA). The samples were prepared into KBr-disks. Spectra were recorded as the average of 128 scans at 4 cm^{-1} resolution and 25 ℃, using KBr as blank. The content of phenyltrimethylammonium chloride on the surface of modified oxidized cellulose nanocrystals was determined based on estimation of the nitrogen content (N%) measured by a Leco C/N determinator (TruSpec CN, USA). Samples were dried at 80 ℃ for 24 h before test.

The zeta potential of oxidized cellulose nanocrystals and modified oxidized cellulose nanocrystals was measured by dynamic light scattering using a Zetasizer Nano-ZS ZEN3600 (Malvern Instruments Ltd, UK). Oxidized cellulose nanocrystals and modified oxidized cellulose nanocrystals were dispersed in deionized water (1 mg/mL) to form transparent suspensions. All measurements were carried out at 25 ℃ in triplicates.

The morphologies of oxidized cellulose nanocrystals and modified oxidized cellulose nanocrystals were observed by transmission electron microscopy (TEM, Morgagni 268, Philips-FEI, Hillsboro, USA) at an accelerating voltage of 80 kV. Nanoparticles were negatively stained with 2 $^{w}/_{v}$% sodium phosphotungstate (pH 7.4). One drop of the nanoparticle sample (1 mg/mL) was added to a carbon-coated copper grid and kept still for 3 min. Then, a drop of sodium phosphotungstate was added to the top of the nanoparticle droplet on the grid. Excess liquid was blotted from the grid, and then samples were air dried at room temperature. The dimensions of oxidized cellulose nanocrystals and modified oxidized cellulose nanocrystals were measured via

image analysis using the ImageJ image-visualization software developed by the National Institute of Health[210].

4.2.6 Characterizations of Pickering emulsions

The size of the modified oxidized cellulose nanocrystal stabilized Pickering emulsions was characterized by the laser light scattering using a Mastersizer 2000 instrument (Malvern, USA). All measurements were carried out at room temperature in triplicate. For optical microscopic observation, 20 μL of the emulsions prepared from hexadecane/m-O-CNC aqueous suspensions were diluted by 1 mL of deionized water and dispersed well by vortex. Then a drop of the diluted emulsion was placed on a glass slide and capped with a cover slip. Samples were all observed using a ZEISS PrimoVert microscope (Carl Zeiss Microscopy GmbH, Göttingen, Germany).

Due to hexadecane volatility, the emulsions tended to collapse during the drying process[211]. In order to confirm the presence of modified oxidized cellulose nanocrystals at the oil-water interface, a solid interphase was needed[41] for scanning electron microscopy (SEM) observation. Since modified oxidized cellulose nanocrystals showed the same ability to stabilize styrene/water emulsion, and hexadecane and styrene have similar surface tension (27 mN/m and 32 mN/m, respectively), m-O-CNCs-2 stabilized styrene/water Pickering emulsion (1 mg/mL) was prepared and solidified by polymerization[40, 212]. Specifically, 0.2 mL of purified styrene-AIBN mixture (100:1, $^{w}/_{w}$) was added into 1.8 mL of m-O-CNCs-2 aqueous suspension (1.0 g/L) and the dissolved oxygen in the mixture was removed with nitrogen for 10 min, followed by sonication using a probe-type sonifier for 20 s (pulse on, 3.0 s; pulse off, 3.0 s; Power, 2 W/mL). Then, the emulsion was deoxygenated with nitrogen for 10 min and polymerized at 50 ℃ in a water bath without stirring overnight. The solid beads were separated by centrifugation and were freeze dried.

The dried sample was coated with platinum (2 nm thickness) and visualized on a Hitachi S-4800 Field Emission Gun SEM (Hitachi High-Technologies Canada, Inc. Ontario, Canada) at 5.0 kV.

To check if the obtained Pickering emulsions were able to resist deformation and coalescence, dispersed phase volume fraction was tested which is defined as the volume of oil incorporated in the emulsion divided by the volume of emulsion after centrifugation[40, 41]. Samples were prepared from 0.75 mL hexadecane and 1.75 mL aqueous phase with various m-O-CNCs-2 concentrations. The m-O-CNCs-2 stabilized Pickering emulsions were then centrifuged at 4,000×g for 2 min. The thickness of the hexadecane separated from the emulsion was measured with a digital caliper. The dispersed phase volume fraction (DPVF) was calculated by $(H_{org} - H_{sep})\ /H_e$, where H_{org} is the original height of oil phase before preparation of the emulsion, H_{sep} is the height of oil separated from the emulsion after centrifugation, and H_e is the height of emulsion after centrifugation. For comparison, the DPVF of Tween-20 stabilized emulsions was also evaluated.

To further verify if the stability of oxidized cellulose nanocrystals were enhanced by surface modification, the centrifugation stability of the emulsions stabilized by oxidized cellulose nanocrystals and modified oxidized cellulose nanocrystals were evaluated. The emulsions were centrifuged at 4,000×g for 2 min and the photographs of the emulsion tubes before and after centrifugation were taken by a digital camera. To further evaluate the thermal stability of the modified oxidized cellulose nanocrystal stabilized Pickering emulsions, the samples were placed in an incubator at 80 ℃ for 48 h. The emulsion size was monitored by a Mastersizer 2000 instrument (Malvern, USA). The emulsions stabilized by Tween-20 (1.0 g/L Tween-20) were used for comparison.

4.2.7 Statistical analysis

Emulsions prepared from three separated batches will be analyzed for their properties. Experimental results were represented as the mean of three batches ± SD. Statistical evaluation was carried out by analysis of variance (ANOVA) followed by multiple-comparison tests using Duncan's multiple-range test. All of the analyses were conducted using SAS statistical software (SAS Institute, Inc., Cary, NC) with a probability of $p < 0.05$ considered to be significant.

4.3 Results and discussion

4.3.1 Preparation of oxidized cellulose nanocrystals and modified oxidized cellulose nanocrystals

As shown in **Fig. 4-1**, it was expected that periodate could selectively oxidize C2, C3-hydroxyl groups of the glucose unit into 2, 3-dialdehyde units, which could be further converted to carboxyl groups by chlorite oxidation. To obtain highly stable and well-dispersed oxidized cellulose nanocrystal suspensions, the primary hydroxyl group (C6-hydroxyl group) of chlorite-oxidized cellulose can be further oxidized to carboxyl groups[29]. The surface modification of oxidized cellulose nanocrystals could then be carried out to facilitate the adsorption of the solid colloids at the water-oil interface. Phenyltrimethylammonium chloride was proposed in this study that could readily interact with the negatively charged oxidized cellulose nanocrystal surface and partially screen the negative charge. Phenyltrimethylammonium chloride is a strong ammonium base and permanently charged in aqueous medium[213]. Therefore, pH may not impact its interaction with the modified cellulose nanocrystal. Additionally, the phenyl group can provide a hydrophobic domain to better adsorb at the interface.

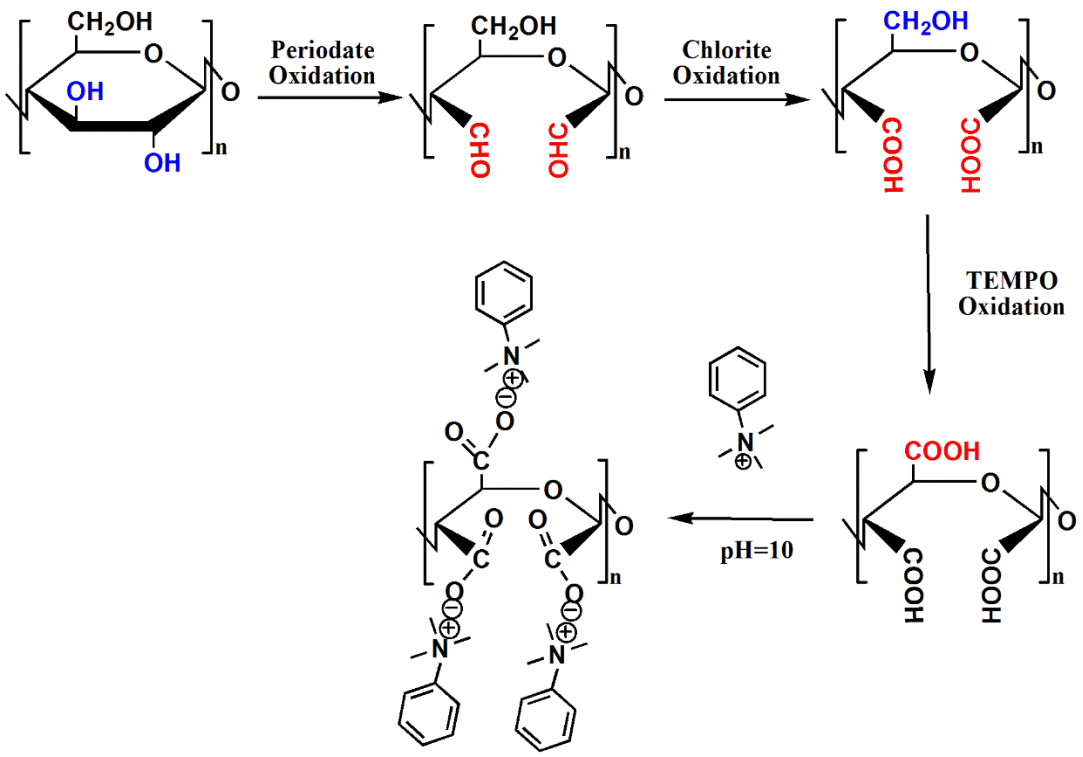

Figure 4- 1 Reaction scheme of the cellulose nanocrystal oxidation and the surface modification of O-CNCs.

The prepared oxidized cellulose nanocrystals were readily dispersed in deionized water, forming a transparent and stable suspension owing to the strong electrostatic repulsion among oxidized cellulose nanocrystals. FT-IR spectroscopy was used to examine the structure of oxidized cellulose nanocrystals and modified oxidized cellulose nanocrystals. As shown in **Fig. 4-2**, oxidized cellulose nanocrystals had characteristic peaks at 1620 cm^{-1} (-COO^- asymmetric vibration band), 1425 cm^{-1} (-COO- symmetric vibration band), and an intensive band at 1050 cm^{-1} (vibration of pyranose ring ether band on cellulose), which indicated the successful oxidation of hydroxyl groups of cellulose into carboxyl groups[29, 209]. The peaks in the spectrum of free phenyltrimethylammonium chloride were assigned to the stretching vibrations of phenyl group at 1594 cm^{-1}, 1500 cm^{-1}, 1474 cm^{-1}, 1462 cm^{-1}, and the ammonium group at 1300 cm^{-1}(C-N)[214]. There

were some weak peaks in the wavenumbers ranging from 2000 cm^{-1} to 1650 cm^{-1}, which were attributed to -C-H (out of the phenyl ring) and -C=C- (in plane deforming vibration in the phenyl ring). Comparing the spectrum of m-O-CNCs-2 with those of oxidized cellulose nanocrystals and phenyltrimethylammonium chloride, the new peak of m-O-CNCs-2 could be observed at 1500 cm^{-1} (stretching vibration of the phenyl ring), demonstrating phenyl group had been successfully introduced at the oxidized cellulose nanocrystal surface by electrostatic interaction between oxidized cellulose nanocrystals and phenyltrimethylammonium cation.

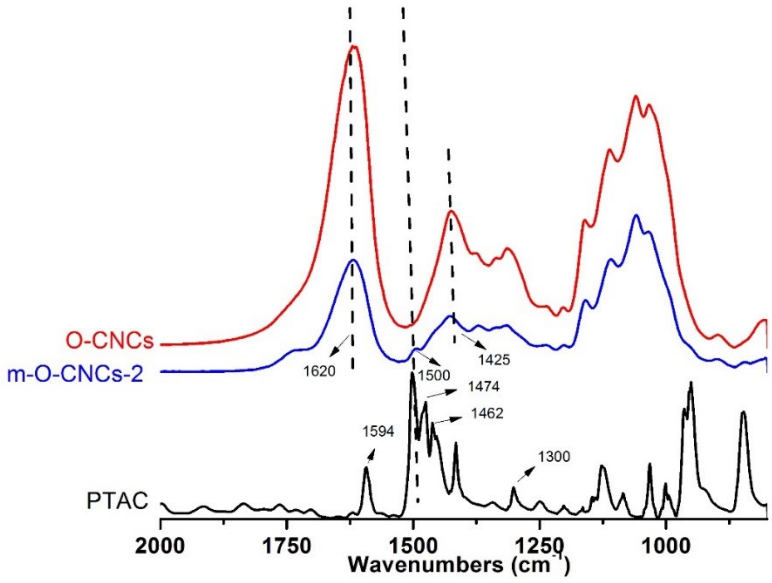

Figure 4- 2 FITR spectra of the phenyltrimethylammonium chloride (PTAC), O-CNCs and m-O-CNCs-2.

The content of phenyltrimethylammonium (CP%) adsorbed on modified oxidized cellulose nanocrystal surface was measured based on estimation of nitrogen content (N%) by elementary

analysis. As shown in **Table 4-1**, the nitrogen content of oxidized cellulose nanocrystals was zero, while in modified oxidized cellulose nanocrystals, it increased from 0.97% to 1.93% as the feed ratio of PTAC/O-CNCs increased. The content of phenyltrimethylammonium (CP) on the surface of modified oxidized cellulose nanocrystals was calculated to be 9.42% in m-O-CNCs-1, 15.36% in m-O-CNCs-2, and 18.77% in m-O-CNCs-3, respectively (see calculation in **Appendix**). It was noted that larger feed ratio of PTAC/O-CNCs leads to higher content of phenyltrimethylammonium introduced onto the surface of oxidized cellulose nanocrystals. When the feed ratio increased from 0.5 to 1, the CP on the surface of modified oxidized cellulose nanocrystals increased by 5.94%, whereas it increased by 3.41% when feed ratio of PTAC/O-CNCs increased from 1 to 2. Since the carboxyl group on the surface of oxidized cellulose nanocrystals was limited, the phenyltrimethylammonium cation could be easily adsorbed onto the surface of oxidized cellulose nanocrystals when PTAC/O-CNCs was low. As the feed ratio increased, on one hand, the carboxyl group available has been reduced; on the other hand, the previously adsorbed phenyltrimethylammonium has screened partial surface charge, which weakened the adsorption of phenyltrimethylammonium. Therefore, the increase of CP has been slowed down with increasing feed ratio.

The zeta-potentials of the oxidized cellulose nanocrystal suspension (1 mg/mL) and modified oxidized cellulose nanocrystal suspensions (1 mg/mL) were tested and the results were shown in **Table 4-1**, oxidized cellulose nanocrystals had a zeta-potential of -57.7 mV, whereas the modified oxidized cellulose nanocrystals had a zeta-potential ranging from -31.8 mV to -37.1 mV. Oxidized cellulose nanocrystals had a relatively greater absolute value of zeta-potential with strong electrostatic interactions between the nanocrystals, resulting in a transparent and well-dispersed suspension. Compared with oxidized cellulose nanocrystals, modified oxidized cellulose

nanocrystals had relatively lower absolute values of zeta-potential, due to the adsorption of the phenyltrimethylammonium on the surface, partially screening the surface charge. However, the suspensions of modified oxidized cellulose nanocrystals were stable without any visible aggregation for 1 month as observed by microscopy. Additionally, the absolute values of zeta potential of modified oxidized cellulose nanocrystals decreased from 37.1 to 31.8 when the content of phenyltrimethylammonium increased from 9.42% to 18.77%, since the greater negative charge on the surface of oxidized cellulose nanocrystals was neutralized with an increasing amount of phenyltrimethylammonium groups.

Table 4- 1 Zeta-potential, nitrogen content and phenyltrimethylammonium content of oxidized cellulose nanocrystals and modified oxidized cellulose nanocrystals.

Samples	N%	CP%	Zeta-potential (mV)
m-O-CNCs-3	1.93±0.001	18.77±0.01	-31.8±1.1
m-O-CNCs-2	1.58±0.04	15.36±0.41	-32.8±0.7
m-O-CNCs-1	0.97±0.002	9.42±0.03	-37.1±0.8
O-CNCs	0	N/A	-57.7±0.3

CP: content of phenyltrimethylammonium

TEM images showed that the oxidized cellulose nanocrystals were homogenously distributed in the aqueous suspension (**Fig. 4-3a**). This was different from cotton and bacterial cellulose nanocrystals prepared from hydrochloric acid hydrolysis, which still showed a tendency to aggregate due to relatively lower surface charge[40]. As observed from **Fig. 4-3a**, all the oxidized cellulose nanocrystals were similar in shape with narrowly distributed length and width. Detailed

analysis of the TEM images using the "Image J" software confirmed that they had an average length of 123±16 nm and width of 6±3 nm (n=100). After surface modification of oxidized cellulose nanocrystals by phenyltrimethylammonium chloride, the crystalline particles were still homogeneous and stable in aqueous medium. As observed from **Figs. 4-3b-d,** the m-O-CNCs-1 had an average length of 148±18 nm, and width of 6±4 nm (n=50), the m-O-CNCs-2 had an average length of 153±21 nm and width of 8±3 nm (n=50), and the m-O-CNCs-3 had an average length of 164±24 nm, and width of 9±3 nm (n=50), respectively. The size of three modified oxidized cellulose nanocrystals showed no significant difference. Compared with the oxidized cellulose nanocrystals, the modified oxidized cellulose nanocrystals showed a slight increase in size after surface modification. It has been proposed that shorter cellulose nanocrystals are able to reach the oil-water interface faster to attach at the interface and promote the formation of individual droplets. Whereas the larger sized ones need longer time to reach the oil-water interface, and tend to be entangled with each other in the continuous phase, leading to the droplet coalesces and formation of large emulsions[40]. Therefore, m-O-CNCs-3 and m-CNCs-2 stabilized Pickering emulsions might have relatively larger size when compared with those prepared from m-O-CNCs-1.

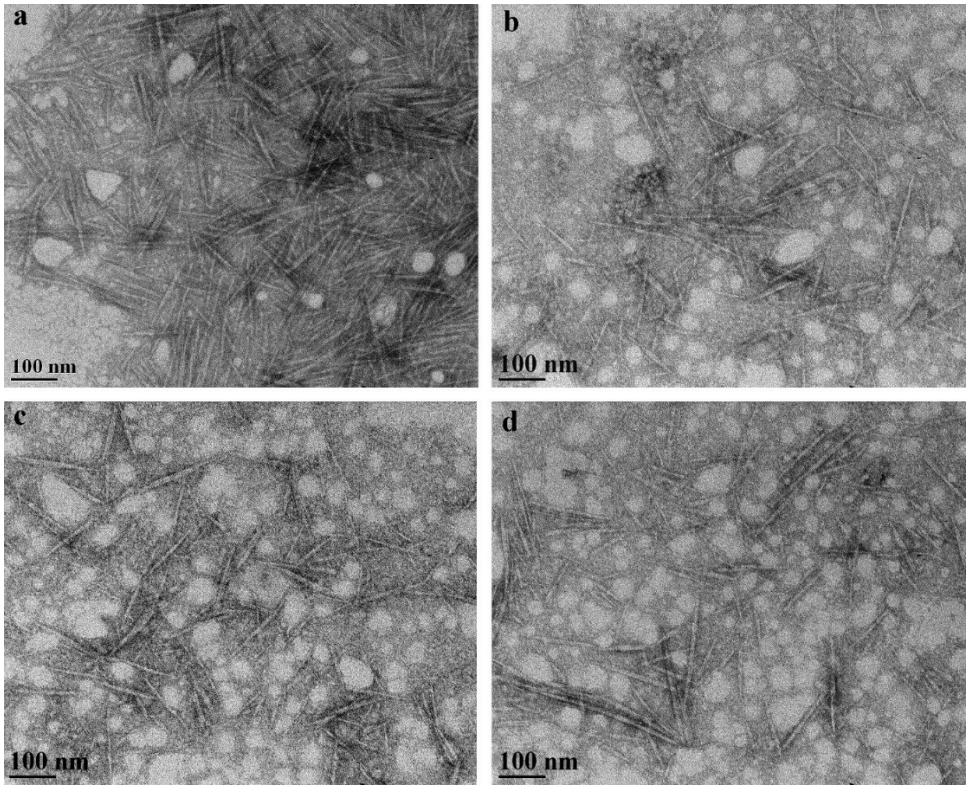

Figure 4- 3 TEM image of O-CNCs (a); TEM image of m-O-CNCs-1 (b); TEM image of m-O-CNCs-2 (c); TEM image of m-O-CNCs-3 (d).

4.3.2 Pickering emulsion preparation

It was noted that obvious phase separation occurred in oxidized cellulose nanocrystal stabilized emulsions at oxidized cellulose nanocrystal concentration of 0.5 g/L to 4.0 g/L, therefore, the oxidized cellulose nanocrystal data were not included in **Fig. 4-4**. The impact of modified oxidized cellulose nanocrystal concentration on emulsion size was studied and shown in **Fig. 4-4a**. For each sample, the emulsion size was sharply decreased with the increase of modified oxidized cellulose nanocrystal concentration (0.5 g/L to 3.0 g/L) until a plateau value of around 2.4 μm reached in the concentration range from 3.0 g/L to 5.0 g/L. For the Pickering emulsions, the interfacial tension was lowered with the increase of the modified oxidized cellulose nanocrystal concentrations in the aqueous phase until the plateau value. Their size was set initially by the particle concentration until

a size limit is reached after which an excess of particles may occur in the continuous phase[215]. The size limitation was less than that in Capron's work, in which they used bacterial cellulose nanocrystals (BCN) to prepare hexadecane/water Pickering emulsions and found the size limitation was 4.2 μm[41]. It has been reported that the size limitation is influenced by the surface chemistry of the particles, as well as the size and flexibility of the solid colloids[41]. In our current research, modified oxidized cellulose nanocrystals were much smaller (around 150-160 nm) compared to BCN of 855 nm in length. The smaller sized modified oxidized cellulose nanocrystals were able to reach the oil-water interface faster to attach at the interface, forming individual small emulsion droplets. Whereas the larger sized BCNs need longer time to approach the oil-water interface, and tend to be entangled with each other in the continuous phase, leading to droplet coalesces and formation of larger emulsions[40]. In addition, stabilizers of different sizes may behave differently at the oil-water interface, such as their range of coverage and packing pattern, leading to the various sizes of Pickering emulsions[42, 43].

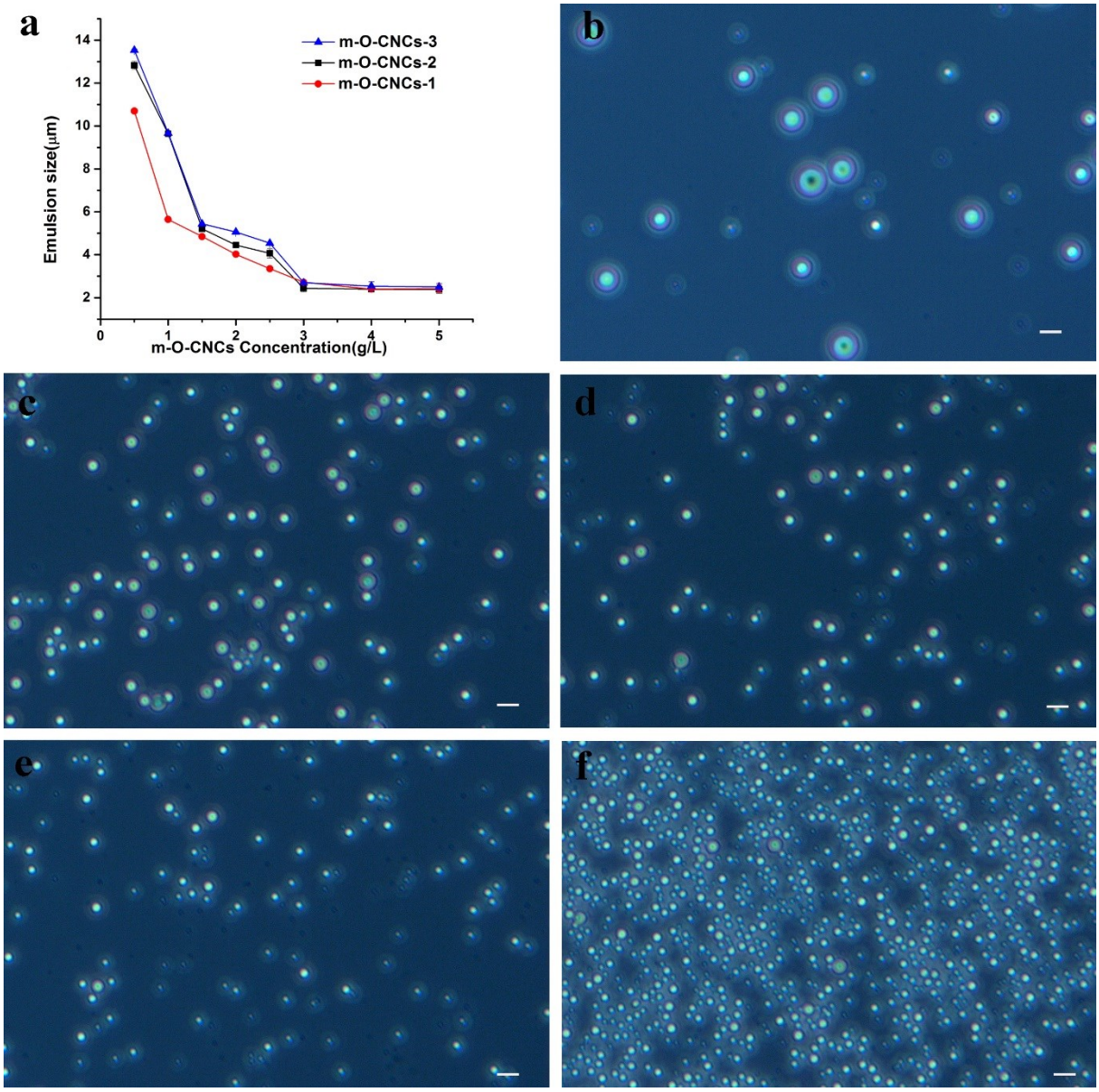

Figure 4- 4 The emulsion size stabilized by m-O-CNCs of different concentration (a); optic microscopic images of the hexadecane/water Pickering emulsions stabilized by m-O-CNCs-2 at various concentrations. (b) 0.5 g/L (c) 1.0 g/L(d) 2.0 g/L (e)4.0 g/L (f) 5.0 g/L. Scale bar: 10 μm.

Additionally, the impact of phenyltrimethylammonium chloride content in modified oxidized cellulose nanocrystals on emulsion size was studied. As shown in **Fig. 4-4a**, when the

concentration of modified oxidized cellulose nanocrystals was lower than 3.0 g/L, the sizes of the Pickering emulsions stabilized by m-O-CNCs-2 and m-O-CNCs-3 were not significantly different. However, they were larger than those stabilized by m-O-CNCs-1. As determined by elementary analysis in **Table 4-1**, the content of PTAC in modified oxidized cellulose nanocrystals followed an order: m-O-CNCs-3 (18.77%) > m-O-CNCs-2 (15.36%) > m-O-CNCs-1 (9.42%). And their zeta potential tests showed an increase from -37.1 to -31.8 mV when the PTAC content increased from 9.42% to 18.77%. It is likely the relatively weaker electrostatic repulsion and stronger hydrophobic interactions were due to introduction of the phenyl group on the oxidized cellulose nanocrystal surface, resulting in droplet coalescence, leading to an increased emulsion size. When the concentration of modified oxidized cellulose nanocrystals was greater than 3.0 g/L, the size of the Pickering emulsions approached a plateau value of 2.4 μm. As reported by Frelichowska and Midmore in their work on silica-stabilized Pickering emulsions, the plateau in this current research may also be due to the limit of the emulsification process, in which the energy of sonication was unable to break the oil droplet down to a smaller size[216, 217].

The emulsions were also visualized by optical microscopy. The images of m-O-CNCs-2 stabilized Pickering emulsions were shown in **Figs. 4-4b-f**, while those of m-O-CNCs-1 and m-O-CNCs-3 stabilized Pickering emulsions were shown in **Figs. S1-S2**, in which they were similar in size and morphology. In **Figs. 4-4b-f**, at a lesser m-O-CNC-2 concentration (0.5 g/L, **Fig. 4-4b**), large droplets formed in the emulsion. With an increase of m-O-CNC-2 concentration, the emulsion size decreased sharply, and the emulsions were homogeneous without any bulk aggregates formed (**Figs. 4-4c-f)**.This was different from those stabilized by the bacterial cellulose nanocrystals (BCNs), where more aggregated clusters with non-homogeneously distributed droplets formed when the cellulose nanocrystal concentration increased from 2.0 g/L to 5.0 g/L[40].

This may have been caused by the different size of cellulose used. As suggested by Kalashnikova[40], the shorter cellulose nanocrystals at the oil-water interface may have promoted the formation of individual droplets in the emulsions, whereas longer nanocrystals led to networking systems with aggregated clusters.

To observe the localization of modified oxidized cellulose nanocrystals at the O/W interface, the morphology of the polystyrene beads covered with m-O-CNCs-2 was shown in **Fig. 4-5**. Here it was shown that there were some large polystyrene beads (~700 nm) and some small beads (~140 nm). As reported by Kalashnikova, the smaller beads cannot be avoided due to the artifactual outgrowths formed during styrene polymerization[41]. On the large beads, the interface was homogeneously covered by m-O-CNCs-2. Even though cellulose nanocrystals are rigid rod-like particles[128], the modified oxidized cellulose nanocrystals here showed some flexibility to bend along the oil-water interface[40, 41]. This could be caused by two reasons: (a) the surface tension required to form the Pickering emulsion was greater enough to force the modified oxidized cellulose nanocrystals to align on the surface without desorption[41], (b) the modified cellulose nanocrystals were partially inserted in the oil phase and were bended due to the polymerization and solidification. More investigations are still required to understand how the bending occurred. Hereby, we could only conclude that the modified oxidized cellulose nanocrystals were deformed to some degree to be better adsorbed at the water/oil interface.

Although emulsion droplets stabilized by m-O-CNCs-1 were smaller than those stabilized by m-O-CNCs-2 and m-O-CNCs-3 at lower concentrations, phase separation was observed for the Pickering emulsions stabilized by m-O-CNCs-1 at the concentration of 0.5-1.0 g/L, whereas m-O-CNCs-2, and m-O-CNCs-3 stabilized emulsions showed no obvious phase separation at the concentrations of 0.5-5.0 g/L. As reported by Binks and Dickinson, the free energy ΔG_d of

spontaneous desorption of the solid colloids is influenced by the contact angle, interfacial tension, and particle size[38, 177]. Apart from the interfacial tension and particle size, the most important factor controlling the free energy is the contact angle. Since m-O-CNCs-2 and m-O-CNCs-3 had relatively higher content of phenyl groups, the balance of hydrophobic interaction and electrostatic repulsion could impact the contact angle and endow them with better stability. Thus, the m-O-CNCs-2 sample was selected for the next steps of research.

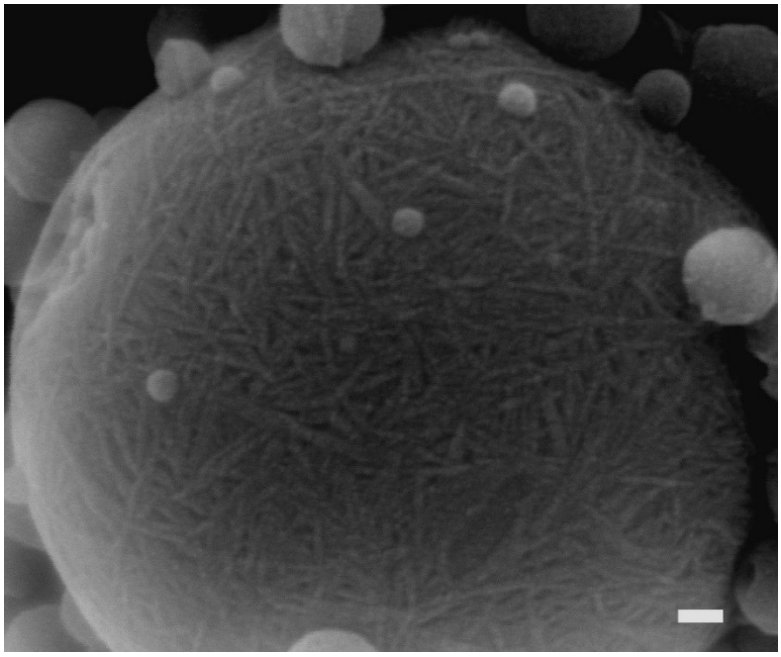

Figure 4- 5 Surface morphology of the m-O-CNCs-2 stabilized Pickering emulsion, Scale bar: 50 nm.

4.3.3 Pickering emulsion stability

As shown in **Fig. 4-6**, the dispersed phase volume fraction (DPVF) of the emulsions increased when the concentrations of their stabilizers increased. At greater concentrations of m-O-CNCs-2 and Tween-20, their DPVFs tended to reach a plateau value of around 0.7, which is close to the

theoretical value of 0.74 for monodispersed spheres under close packing conditions[218]. However, to reach this plateau value, the Pickering emulsion only needed a relatively small concentration of m-O-CNC-2 (~1.5 g/L), but Tween-20 stabilized emulsion needed much more stabilizer of about 20 g/L. This means that we can use much less stabilizer to prepare emulsions when modified oxidized cellulose nanocrystals is used.

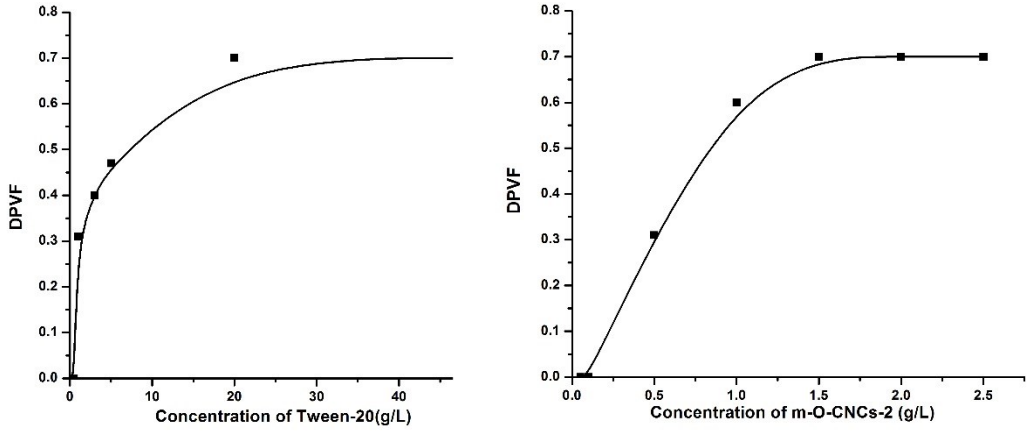

Figure 4- 6 Comparison of the dispersed phase volume fraction (DPVF) between Tween-20 stabilized emulsions and m-O-CNCs-2 stabilized Pickering emulsion.

To verify if the emulsion stability was enhanced by surface modification, oxidized cellulose nanocrystals was also used to prepared emulsions for comparison. When centrifuged at 4,000×*g* for 2 min, obvious phase separation was observed for Pickering emulsions stabilized by oxidized cellulose nanocrystals (**Fig. 4-7b**). Due to their hydrophilic nature, a large portion of the particles still remained in the aqueous phase rather than adsorbed at the oil-water interface, limiting their emulsifying property to stabilize the Pickering emulsion[177]. **Figs. 4-7c** and **d** are pictures of hexadecane/water Pickering emulsions stabilized by m-O-CNCs-2 (0.5-5.0 g/L) before (**c**) and

after (**d**) centrifugation at 4,000×*g*. The emulsions were stable when the m-O-CNC-2 concentration was in the range of 0.5-5.0 g/L, which means that m-O-CNCs-2 stabilized Pickering emulsions were resistant against deformation and coalescence, and these Pickering emulsions were stable during processing. It was observed that phase separation occurred in m-O-CNCs-1 stabilized Pickering emulsions when m-O-CNCs-1 was at low concentrations (0.5-1.0 g/L), whereas the m-O-CNCs-3 stabilized Pickering emulsions were stable without obvious phase separation in the m-O-CNCs-3 concentration of 0.5-5.0 g/L.

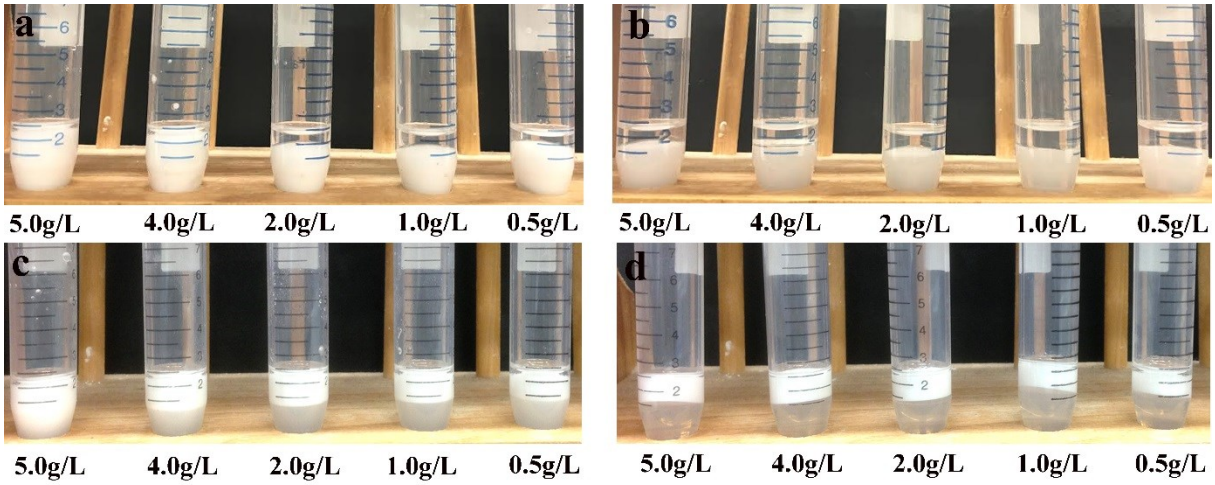

Figure 4- 7 (a-b) Wood-based O-CNC stabilized emulsions before (a) and after (b) centrifugation at 4,000×*g*; (c-d) m-O-CNCs stabilized emulsions before (c) and after (d) centrifugation at 4,000×*g*.

To evaluate the thermal stability of the prepared Pickering emulsions, Tween-20 stabilized emulsion (1.0 g/L Tween-20) and modified oxidized cellulose nanocrystal stabilized Pickering emulsion (1.0 g/L modified oxidized cellulose nanocrystals) were placed in an incubator at 80 ℃. It is accepted that an emulsion can be considered stable as long as no coalescence occurs, which

means the size should not significantly change during the storage time[41]. Therefore, the size of the emulsions was monitored by mastersizer. Since obvious phase separation occurred in oxidized cellulose nanocrystal stabilized emulsions at oxidized cellulose nanocrystal concentration of 0.5 g/L to 4.0 g/L, the oxidized cellulose nanocrystal data were not included in **Fig. 4-8**. As shown in **Fig. 4-8**, modified oxidized cellulose nanocrystal stabilized Pickering emulsions, in some degree, showed coalescence at 80 ℃ in 48 h, in which the size of m-O-CNCs-1 stabilized emulsion increased from 5.64 to 15.22 μm, the size of m-O-CNCs-2 stabilized emulsion increased from 9.64 to 17.5 μm, and the size of m-O-CNCs-3 stabilized emulsion increased from 9.67 to 19.91 μm. However, those size changes were much less than that of Tween 20 stabilized emulsions (size changed from 5.67 to 52.47 μm). This indicates modified oxidized cellulose nanocrystal stabilized Pickering emulsions were more stable against heat. According to Dickinson and Binks, removing solid colloids from the interface needs significant energy and the solid colloids are considered irreversibly adsorbed at the oil-water interface, rather than the reversible balance of adsorption/desorption of traditional surfactants such as Tween[38, 177]. Therefore, modified oxidized cellulose nanocrystal stabilized Pickering emulsions had better thermal stability compared with Tween-20 stabilized emulsions. The evolution of the size of emulsions set for 48 h, during which time no obvious mass loss of hexadecane could be noticed. Due to the volatility of hexadecane at high temperatures, greater monitoring times were not possible.

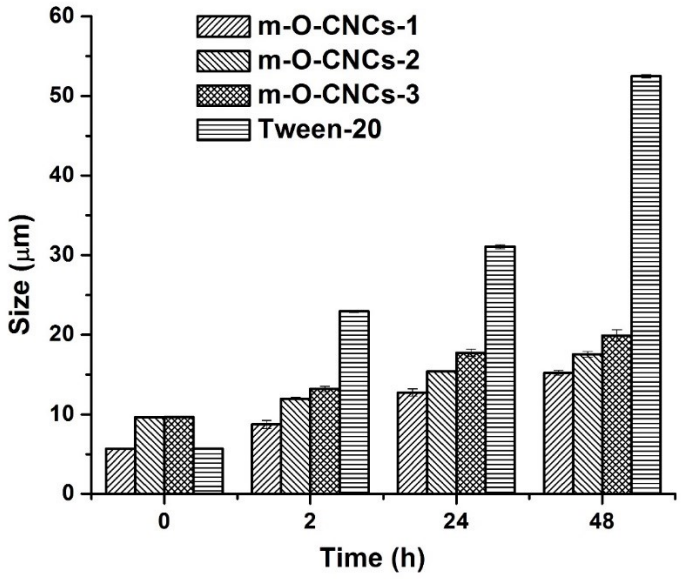

Figure 4- 8 The size evolution of Tween-20 stabilized emulsion and m-O-CNCs stabilized Pickering emulsion at 80 ℃.

4.4 Conclusions

Homogeneous and electrostatically stable oxidized cellulose nanocrystals were obtained from wood pulp. Surface modification was successfully carried out on these oxidized cellulose nanocrystals using phenyltrimethylammonium chloride to create hydrophobic domains comprised of phenyl groups. When employed as solid colloids to stabilize an oil-in-water Pickering emulsion, modified oxidized cellulose nanocrystals showed a dispersed phase volume fraction (DPVF) of 0.7 at around 1.5 g/L, whereas tween-20 needed a 13-fold greater concentration (around 20 g/L) to have a similar DPVR value. Thus, a smaller quantity of modified oxidized cellulose nanocrystals was required to act as a Pickering emulsion agent compared to a traditional surfactant. In addition, the emulsion size is adjustable by modulating the concentration of modified oxidized cellulose

nanocrystals, and the resulting emulsions have good stability against centrifugation and thermal treatment. Thus, these modified oxidized cellulose nanocrystals could be used as efficient stabilizers for emulsion products. This identified property may allow potential applications of modified oxidized cellulose nanocrystals in household cleaning products, cosmetic/body care products, and pharmaceutical formula.

Chapter 5 - Robust and highly compressible aerogels based on cellulose nanocrystals percolated networks supported by crosslinked PVA matrix*

5.1 Introduction

Compressible aerogels have been of increasingly important for the high demand of next generation of products, such as super absorbents[45, 46], electrode substrate for batteries and supercapacitors[47, 48], catalyst supports[49], and chemical and biological sensors[50, 51] etc. Many of these applications require the aerogel materials to be strong yet compressible and capable of reversible deformation under large strain[52]. Traditional aerogels are mostly fabricated from silica materials featured with large porosity (up to 99.8%), low density (4-500 mg/cm^3), and large surface area (100-1000 m^2/g)[53, 54]. There are considerable studies on silica-based aerogels for various applications, including thermal and acoustic insulator[55, 56], optical applications[57], batteries[58, 59] and capacitor electrodes[60, 61], nuclear waste storage[62] and catalysis[63] etc. However, the traditional silica-based aerogels usually suffer from fragility, and they are too brittle to meet the mechanical robustness as compressive materials[64].

Recently, aerogels prepared from Poly(vinyl alcohol)(PVA) have drawn attention since they are generally less brittle, more flexible, and easy-processable[65], in addition to their excellent merits such as cost-effectiveness, biocompatibility, and biodegradability[66-68]. However, PVA aerogels alone don't have adequate mechanical strength and compressibility to be used as compressible

*A version of this chapter is considered to be published: Xiaoyu Gong, Yao Huang, Jingqi Yang, Guangyu Liu, Weijuan Huang, Yixiang Wang, Lingyun Chen, "Robust and highly compressible aerogels based on cellulose nanocrystals percolated networks supported by crosslinked PVA matrix".

materials. Incorporating carbon nanotubes or graphene into the PVA aerogels as reinforcing agents has led to compressible aerogels with good mechanical strength [53, 69, 70]. However, those carbon-based materials are not readily available for large-scale applications[64] due to the high cost and complicated procedures.

Cellulose materials, the most abundant renewable natural polymer (annual production of 1.5×10^{12} tons/year[2]), could be an alternative for carbon nanotubes and graphene materials to prepare the mechanically strong yet highly compressive PVA aerogels, owing to their readily availability, low cost, good mechanical properties and low density. So far, cellulose nanofibers (CNFs) have been incorporated with PVA to form the PVA/CNFs aerogels[71]. However, these aerogels were not elastic enough and deformed permanently when the compression strain was higher than 20%[71]. Cellulose nanocrystals (CNCs), on the other hand, are highly ordered rod-like nanoparticles, and they are generally considered as effective fillers in aerogels to reinforce networks[72], due to their intrinsic rigidity and excellent mechanical strength (elastic modulus~100-200 GPa[22]). Hence, there are considerable studies on the reinforcement of the mechanical strength of PVA aerogels with cellulose nanocrystals. However, even though these CNCs/PVA aerogels showed significantly improved mechanical strength, they have poor compressibility.

Canada has a forest area of 396,940,350 hectares, however wood cellulose is still mainly used for paper-making and lumbering. Research effort is required to develop their value-added applications. In the current study, mechanically strong yet highly compressible aerogels were fabricated by combining PVA and wood-based cellulose nanocrystals. First, homogeneous and hydrocolloidally stable cellulose nanocrystals were prepared by sulfuric acid hydrolysis. The hydrocolloidal stability and the morphology of the obtained cellulose nanocrystals were characterized. Then the crosslinked CNCs/PVA aerogels were fabricated by adding low amount

of PVA into cellulose nanocrystal network which were further crosslinked by epichlorohydrin (ECH). The aerogel microstructures and the polymer interactions in the matrices were characterized, and the aerogel mechanical properties were evaluated. Furthermore, the aerogel formation mechanism and the role of each component contributing to the compressibility were discussed.

5.2 Materials and methods

5.2.1 Materials

Spruce cellulose (bleached kraft pulp) was a gift from Alberta-Pacific Forest Industries Inc. (AB, Canada). Its viscosity-average molecular weight (M_η) was determined with an Ubbelohde viscometer in LiOH/urea aqueous solution at 25±0.1 ℃ and calculated to be 4 $\times 10^5$ Da [2]. PVA (99+% hydrolyzed) was purchased from Sigma-Aldrich Canada Ltd with an average molecular weight of 1.3×10^5 Da. Epichlorohydrin (ECH) and all other chemicals were purchased from Sigma-Aldrich Canada Ltd. (Oakville, ON, Canada) and used as received.

5.2.2 Cellulose nanocrystal preparation

The preparation of cellulose nanocrystals was carried out according to the method of Shopsowitz with some modifications[219]. Spruce cellulose (bleached commercial kraft pulp) was milled to pass through a 0.75 mm screen in a Retsch mill (ZM200, Germany) to obtain the uniform fibers. 20 g of the milled cellulose fibers were added into a round-bottom flask, following by the addition of 400 mL of sulfuric acid (64 $^{w}/_{w}$%). Then the mixture was vigorously stirred at 45 ℃ for 30 min, and the hydrolysis was quenched by dilution with large amount of deionized water (~3000 mL). The mixture was stored at room temperature to settle overnight. The clear upper layer was then disregarded, and the remaining cloudy layer was washed with deionized water by centrifugation

(17,700 *g* × 10 min / round) until the sample was not separated into two layers. The sample was then dialyzed against deionized water until pH remained constant in the dialysis tubes (MWCO 3.5-5kD). The sample was then sonicated at 80 KHz/100 power for 30 min, followed by centrifugation at 17,700 *g* × 5 min. The upper supernatant was then collected as stock samples and quantified by freeze drying of a small volume of the sample. To prepare cellulose nanocrystal suspensions with various concentrations (0.5 $^{w}/_{w}$%, 1.0 $^{w}/_{w}$%, and 2.0 $^{w}/_{w}$%), the stock cellulose nanocrystal suspension was diluted by adding desired amount of deionized water. The obtained suspensions were stored at 4 ℃ for further use.

5.2.3 Crosslinked CNCs/PVA aerogel preparation

For preparation of the crosslinked CNCs/PVA aerogels, a desired amount of PVA was added into 5 mL of cellulose nanocrystal suspension in a vial under vigorous stirring at 90 ℃ for 3 h until PVA was completely dissolved. Then the mixture pH was adjusted to 10 by 0.1 M NaOH aqueous solution, and 0.1 mL of ECH was added dropwise into the vial in 5 min, followed by a vortex mixing for 1 min. The crosslinking reaction was subsequently carried out at 60 ℃ for 24 h and then the sample was molded in a 12-welled plate and freeze-dried. As per in **Table 5-1**, the samples were coded as Aerogel-1 to Aerogel-5 with the concentration of cellulose nanocrystal suspensions varying from 0.5 to 2.0 w/w%, and the mass of PVA from 0.01 g to 0.1 g. Aerogel-6 was prepared only with cellulose nanocrystals and PVA without addition of ECH. Samples without addition of cellulose nanocrystals or PVA were also prepared for comparison.

Table 5- 1 Sample codes and reaction conditions to prepare the aerogels.

Sample code	CNCs volume	CNCs concentration	Mass of PVA	Volume of ECH
	mL	$^{w}/_{w}$%	g	mL
Aerogel-1	5	1	0.01	0.1
Aerogel-2	5	1	0.05	0.1
Aerogel-3	5	1	0.1	0.1
Aerogel-4	5	2	0.05	0.1
Aerogel-5	5	0.5	0.05	0.1
Aerogel-6	5	1	0.05	0

5.2.4 Characterizations of cellulose nanocrystals

The zeta potential of cellulose nanocrystal suspensions was measured by dynamic light scattering using a Zetasizer Nano-ZS ZEN3600 (Malvern Instruments Ltd, UK). To study the hydrocolloidal stability, the obtained cellulose nanocrystals were suspended in NaCl solution at various concentrations (0 to 200 mM) and the cellulose nanocrystal concentration was fixed at 1 mg/mL. Zeta potentials of cellulose nanocrystals (1 mg/mL) as a function of NaCl concentration were measured to study the hydrocolloidal stability. All measurements were carried out at 25 ℃ in triplicates.

The morphology of cellulose nanocrystals was observed by transmission electrical microscopy (TEM, Morgagni 268, Philips-FEI, Hillsboro, USA) at an accelerating voltage of 80 kV. Cellulose nanocrystals were negatively stained with 2 $^{w}/_{v}$% sodium phosphotungstate (pH 7.4). One drop of the cellulose nanocrystal sample (1 mg/mL) was added to a carbon-coated copper grid and kept still for 3 min. Then, a drop of sodium phosphotungstate was added to the top of the cellulose nanocrystal droplet on the grid. Excess liquid was blotted from the grid, and then the sample was air dried at room temperature. The dimensions of cellulose nanocrystals were measured via image

analysis using the ImageJ image-visualization software developed by the National Institute of Health[210].

5.2.5 Characterizations of aerogels

Fourier Transform Infrared Spectroscopy: Fourier transform infrared (FTIR) spectra of the pristine materials cellulose nanocrystals and PVA, Aerogel-2, and Aerogel-6 were recorded on a Nicolet 6700 spectrophotometer (Thermo Fisher Scientific Inc., MA, USA). The samples were prepared into KBr-disks. Spectra were recorded as the average of 128 scans at 4 cm^{-1} resolution and 25 °C, using KBr as blank.

Morphology and Nanostructure: The morphology of crosslinked CNCs/PVA aerogels were characterized by scanning electrical microscopy (SEM). The dried samples were coated with gold (3 nm thickness) and visualized on a Hitachi S-4800 Field Emission Gun SEM (Hitachi High-Technologies Canada, Inc. Ontario, Canada) at 1.0 kV. Meanwhile, ECH-crosslinked PVA gel, and Aerogel-6 without addition of ECH were also prepared and observed for comparison.

Crystallinity: cellulose nanocrystals, PVA, Aerogel-2, Aerogel-4, and Aerogel-5 were studied for the crystallinity using the wide-angle X-ray diffraction measure (WAXD) on an X-ray diffractometer (Ultimate IV, Rigaku, Japan) in symmetric reflection mode. The diffracted intensity of Cu K_α radiation (λ=0.1542 nm) at 40 kV and 44 mA was recorded in the 2θ range of 4°-40° with a scanning rate of $1° \cdot min^{-1}$. Samples were all cut into powders and dried in a vacuum oven at 60 °C for 24 h before the measurements.

Mechanical Properties: The mechanical properties of the crosslinked CNCs/PVA aerogels were characterized using an Instron 5967 Testing Machine (Instron Corp., Norwood, MA, USA) at cyclic compressive mode. Samples were compressed ten times to 50% of their original height in air at room temperature at a rate of 3 mm/min. The compressive stress-time and compressive stress-

strain response were recorded, and all measurements were repeated at least three times. Meanwhile, ECH-crosslinked PVA gel, and Aerogel-6 without addition of ECH were also prepared for comparison.

5.2.6 Statistical analysis

Samples prepared from three separated batches were analyzed for their properties. Experimental results were represented as the mean of three batches ± SD. Statistical evaluation was carried out by analysis of variance (ANOVA) followed by multiple-comparison tests using Duncan's multiple-range test. All the analyses were conducted using SAS statistical software (SAS Institute, Inc., Cary, NC) with a probability of $p < 0.05$ considered to be significant.

5.3 Results and discussion

5.3.1 Preparation of homogeneous/hydrocolloidally stable cellulose nanocrystals

The release of cellulose nanocrystals from bulk cellulose fibers usually involves the acid-catalyzed disintegration process, in which the small acid molecules diffuse into the amorphous regions of cellulose fibers and cut off the glycosidic bonds. Even though various acids such as the sulfuric, hydrochloric, phosphoric and hydrobromic acids have been used to disintegrate cellulose fibers and release the highly crystalline cellulose nanocrystals, sulfuric acid is the most extensively used reagent. It reacts with the hydroxyl groups of cellulose fibers via an esterification process to form charged sulfate ester groups, which are randomly distributed along the crystals and form a negatively electrostatic layer covering the surface of the prepared cellulose nanocrystals to promote their dispersion in water.

Figs. 5-1a-c presents the cellulose nanocrystals in deionized water with various concentrations (2.0 -0.5 $^{w}/_{w}$%). As observed, cellulose nanocrystal suspensions were homogeneous without

obvious aggregation for up to 24 months due to the strong electrostatic repulsion between the individual cellulose nanocrystals that kept them apart from each other. The hydrocolloidal stability of the obtained cellulose nanocrystals was also studied by measuring the zeta potential value, which has been widely used to predict the colloidal stability of nanoparticle suspensions with various electrolyte concentrations[220]. As shown in **Fig. 5-1d**, without addition of the electrolyte, the cellulose nanocrystals had a zeta potential of -55.03±0.76 mV. With the increase of NaCl concentration, the absolute value of zeta potentials of cellulose nanocrystals was decreased due to the adsorption of Na^+ counterion on the negatively charged cellulose nanocrystal surface. It is widely accepted the hydrocolloids with zeta potential value higher than +30 mV or lower than -30 mV are considered to be hydrocolloidally stable[221]. In this study, the zeta potential of the cellulose nanocrystal suspensions was lower than -30 mV when the sodium chloride concentration was lower than 30 mM, suggesting the obtained cellulose nanocrystal suspensions were hydrocolloidally stable at low electrolyte concentrations.

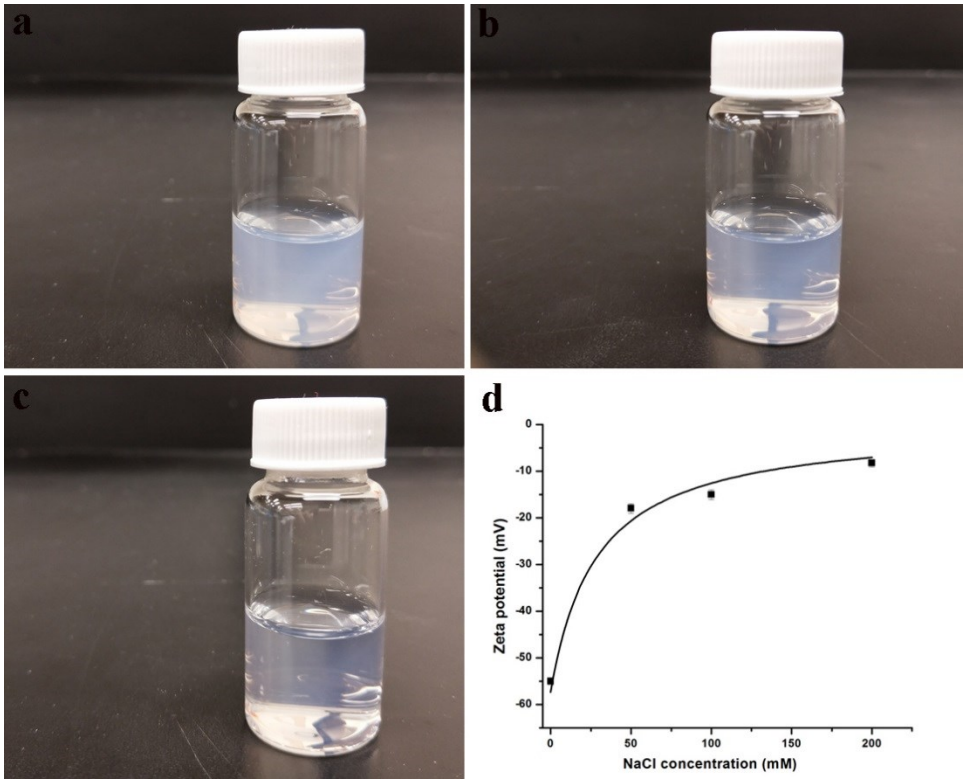

Figure 5- 1 (a-c) Cellulose nanocrystal suspensions in deionized water with various concentrations: (a) 2.0 $^{w}/_{w}$%, (b) 1.0 $^{w}/_{w}$%, and (c)0.5 $^{w}/_{w}$%, respectively. (d) Zeta potentials of cellulose nanocrystals (1mg/mL) in water as a function of NaCl concentration.

The prepared cellulose nanocrystals were observed under the transmission electronic microscopy (TEM). As shown in **Fig. 5-2**, cellulose nanocrystals were homogenously distributed in the aqueous suspension and they were similar in shape with narrow distribution of the length and width. Detailed analysis of the TEM images using the "Image J" software indicated that the obtained cellulose nanocrystals had an average length of 177±34 nm and width of 9±4 nm (n=50). It is noticed that the obtained cellulose nanocrystals could be well dispersed in deionized water without obvious aggregation for more than 24 months, showing good hydrocolloidal stability. In this study, the cellulose nanocrystal sample was further separated by centrifugation at 17,700 *g* ×

5 min and the upper supernatant with good hydrocolloidal stability was collected as stock cellulose nanocrystal suspension after the typical sulfuric acid hydrolysis, centrifugation, dialysis, and sonification. It was expected that the hydrocolloidally stable cellulose nanocrystals could be more homogeneously distributed in the aqueous PVA solution, and then embedded evenly in the PVA matrix after crosslinking and freeze-drying.

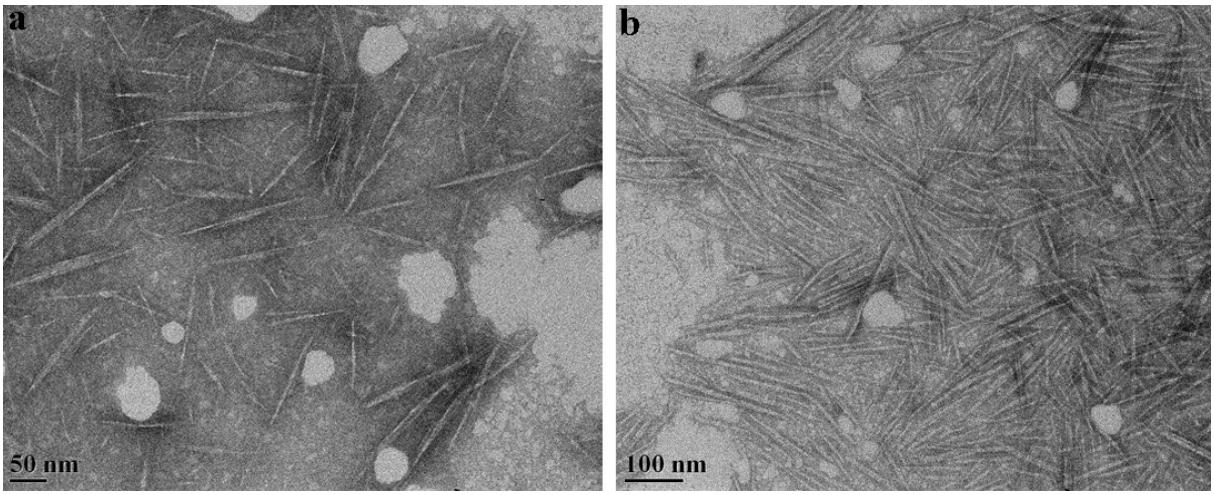

Figure 5- 2 TEM image of cellulose nanocrystals at different magnifications.

5.3.2 Molecular structure of the crosslinked CNCs/PVA aerogel

To study the molecular interactions of the crosslinked CNCs/PVA aerogels, FT-IR spectroscopy was performed on Aerogel-2, with comparison to the spectra of pristine cellulose nanocrystals, PVA, and Aerogel-6 prepared with cellulose nanocrystals and PVA without addition of ECH. As shown in **Fig. 5-3**, cellulose nanocrystals had characteristic absorbances at 3340 cm^{-1} (-O-H stretching), 2896 cm^{-1} (-CH- symmetric stretching), and 1050 cm^{-1} (vibration of pyranose ring ether). PVA had featured peaks at 3450 cm^{-1} (-O-H stretching), 2920 cm^{-1} ($-CH_2-$ symmetric stretching), and 2890 cm^{-1} (-CH- symmetric stretching). It was noted the absorbance band of -OH

stretching of cellulose nanocrystals was sharp and at a relatively lower wavenumber, while that of PVA was broad and at a higher wavenumber. This was due to the different hydrogen bond patterns in PVA and cellulose nanocrystals[222]. In cellulose nanocrystals, intermolecular hydrogen bonds were dominant, whereas both intra-/intermolecular hydrogen bonds were involved in PVA. Compared to the spectrum of PVA, -O-H vibration of Aerogel-6 shifted to a lower wavenumber at 3360 cm^{-1}, indicating the formation of hydrogen bonding between cellulose nanocrystals and PVA matrix, likely -OH groups on the surface of cellulose nanocrystals interacting with adjacent -OH groups in the PVA molecule[222]. When crosslinked by ECH, the absorbance band of -O-H stretching in Aerogel-2 was still narrowed and sharpened without significant changes in shape and intensity, compared to that of Aerogel-6, suggesting further chemical crosslinking did not change the hydrogen bonding that occurred between cellulose nanocrystals and PVA. Since cellulose nanocrystals are rigid rod-like crystals composting of bundles of cellulose molecules, most of the hydroxyl groups on the cellulose molecules are buried in the crystals[112]. Additionally, the ECH-crosslinking of the hydroxyl groups on cellulose nanocrystals has never been reported. Therefore, it was assumed that ECH-crosslinking would not occur between PVA and cellulose nanocrystals or between cellulose nanocrystals themselves. It was noteworthy the intensity of the $-CH_2-$ stretching (2920 cm^{-1}) increased in Aerogel-2 when compared to that of PVA and Aerogel-6. This was due to the introduction of more $-CH_2-$ into the aerogel in the crosslinking process. Moreover, a new peak was observed at 1200 cm^{-1}, which was ascribed to the C-O-C stretching due to the chemical crosslinking by ECH. It has been reported that PVA can be crosslinked by ECH under alkaline condition[223]. Hereby, it is proposed that the hydrocolloidally stable cellulose nanocrystals were firstly homogeneously distributed in the aqueous PVA solution. When the samples were crosslinked and freeze-dried, cellulose nanocrystals interacted with each other, and also strongly

interacted with PVA matrix via hydrogen bonding. Meanwhile, the PVA matrix was further crosslinked by ECH, leading to the crosslinked CNCs/PVA aerogels.

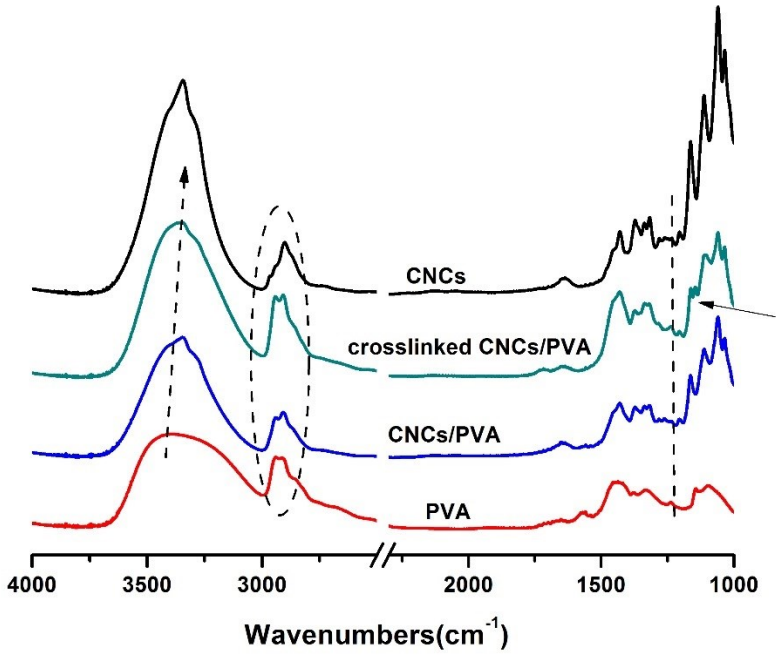

Figure 5- 3 FITR spectra of cellulose nanocrystals, PVA, Aerogel-6 and Aerogel-2.

5.3.3 Crystallinity study

The Wide-angle x-ray diffraction pattern (WAXD) of the Aerogel-4, Aerogel-2, and Aerogel-5 were studied as a function of cellulose nanocrystal concentration. As shown in **Fig. 5-4**, the pristine PVA sample showed a strong peak at 2θ=20°, which was assigned to the crystalline structure resulting from the strong intermolecular hydrogen bonding between PVA chains[224, 225]. Pure cellulose nanocrystals exhibited the characteristic diffraction peak at 2θ=22.6°, ascribing to the

(200) plane of cellulose I_β[224]. In the spectrum, the well-defined peaks of cellulose nanocrystals at 2θ=14.9° and 16.7°, which were ascribed to the $(1\bar{1}0)$ and (110) planes of cellulose I_β, overlapped with each other in the WAXD pattern. When PVA was added and chemically crosslinked by ECH, these two featured peaks in the crosslinked CNCs/PVA aerogels were separated. This was probably due to the change of the cellulose nanocrystal crystallization when it formed strong intermolecular hydrogen bonding with PVA in the aerogel networks[225]. Moreover, the peaks of cellulose I_β became more pronounced with the increase of cellulose nanocrystals in the crosslinked CNCs/PVA aerogels, whereas the characteristic peak of PVA became weaker, indicating a reduction in the degree of crystallinity of PVA and an increment in the degree of crystallinity of cellulose nanocrystals in the aerogels[226]. This suggested the addition of cellulose nanocrystals affected the formation of the PVA crystals in the cross-linked CNCs/PVA aerogels due to the strong intermolecular hydrogen bonding between cellulose nanocrystals and PVA chains[224]. Therefore, the crosslinked CNCs/PVA aerogels could have significant reinforcement in mechanical strength when compared to PVA samples. Additionally, it was noteworthy that the intensities of the characteristic peaks of cellulose nanocrystals in the crosslinked CNCs/PVA aerogels were much weaker than that of the pristine cellulose nanocrystals, suggesting cellulose nanocrystals were well embedded in the PVA matrix[224].

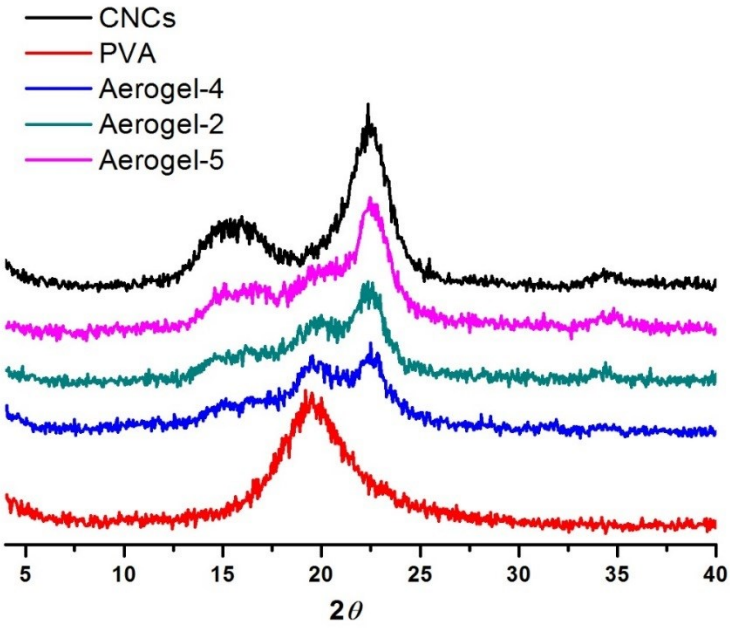

Figure 5- 4 WAXD spectrum of CNCs, PVA, and Aerogel-2, Aerogel-4, and Aerogel-5.

5.3.4 Morphology study

The microstructure of aerogels usually reveals the underlying features that have a significant influence on the properties of the prepared products. To further understand the formation of the crosslinked CNCs/PVA aerogels, the morphology of the samples was studied by SEM observation.

The effect of cellulose nanocrystals on the morphology of the crosslinked CNCs/PVA aerogels

ECH-crosslinked PVA gel was prepared from 0.05 g PVA and 0.1 mL of ECH in 5 mL of deionized water without addition of cellulose nanocrystals (**Fig. 5-5a**), whereas Aerogel-4, Aerogel-2, and Aerogel-5 were prepared from 0.05 g PVA, 0.1 mL of ECH and 5 mL of cellulose

nanocrystal aqueous suspension with various concentrations (0.5, 1.0 and 2.0 $^{w}/_{w}$%) (**Figs. 5-5b-f**). Different morphologies were observed with or without addition of cellulose nanocrystals. When cellulose nanocrystals were not added, ECH-crosslinked PVA gel showed a dense irregular filament structure (**arrow in Fig. 5-5a**). This was different from those of the PVA gels prepared by physical crosslinking or glutaraldehyde-crosslinking[28-30], which typically showed 3D interconnected and continuous porous networks[28,29]. Even though large amount of PVA (up to 80 $^{w}/_{w}$%) was used in those physically crosslinked sponge or glutaraldehyde-crosslinked gels, the porous networks usually had relatively thin walls with weak mechanical strength. In this study, even with small amount of PVA (1.0 $^{w}/_{w}$%), the ECH-crosslinked PVA gel was still strong enough without significant shrinkage after freeze-drying. This can be explained by the synergistic effect of the hydrogen bonding and chemical crosslinking by ECH between PVA chains.

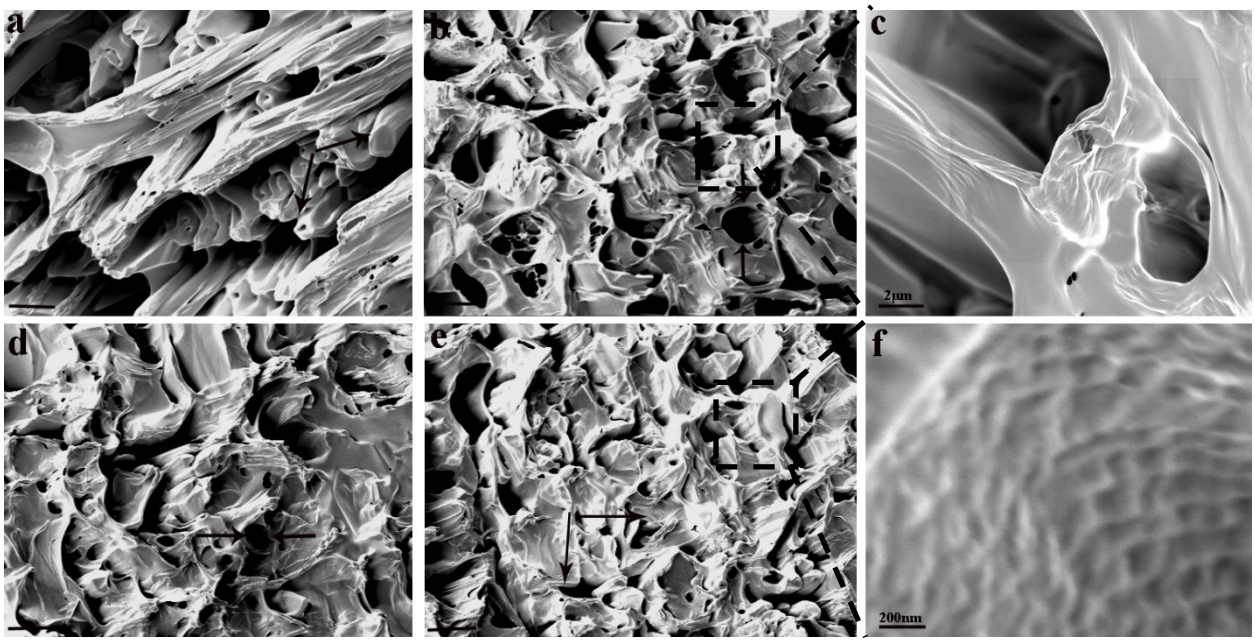

Figure 5- 5 SEM images of the ECH-crosslinked PVA (a), Aerogel-4 (b), Aerogel-4 at higher magnification(c), Aerogel-2(d), Aerogel-5 (e), Aerogel-5 at higher magnification. Scale bar for a,b,d,e: 30 μm.

Addition of cellulose nanocrystals significantly changed the morphology of the crosslinked aerogels. As shown in **Figs. 5-5b, d, e**, The Aerogel-4, Aerogel-2, and Aerogel-5 showed 3D interconnected porous networks with some macrospores embedded in (**arrows in Figs. 5-5b, d, e**). Unlike the filament structure in ECH-crosslinked PVA gel, these aerogels formed a porous yet dense structure, which has never been reported for PVA gels in previous studies. However, the dense walls remained in the porous CNCs/PVA networks that maintained the physical structure of the aerogels during the freeze-drying process. With increase of the cellulose nanocrystal concentration, less macrospores were observed in the aerogels and the pore size became smaller. Such morphology formation was driven by the phase separation when ice crystals formed and demixed from the crosslinked polymer molecules, leaving behind a porous structure upon water removal[31]. The size of ice crystals decreased with the increasing number of cellulose nanocrystals that occupied more space in the mixture and removal of these ice crystals resulted in smaller macrospores in the crosslinked CNCs/PVA aerogels[72]. **Figs. 5-5c, f** were the SEM images of the aerogels at higher magnification, in which the aerogels were highly porous (**Fig. 5-5c**). It was noteworthy that cellulose nanocrystals were percolated with each other and formed an interpenetrated network that embedded in the PVA matrix (**arrow in Fig. 5-5f**). This observation was in accordance with the FTIR and WAXD result, suggesting that cellulose nanocrystals formed percolated network and then strongly interacted with the PVA matrix via hydrogen bonding. Meanwhile, the PVA matrix was crosslinked by ECH, leading to the porous networks with strong and dense walls.

The effect of ECH on the morphology of the crosslinked CNCs/PVA aerogels

The morphology of Aerogel-2 and Aerogel-6 prepared with or without addition of ECH was presented in the SEM images in **Fig. 5-6**. The Aerogel-6 without ECH showed a 3D interconnected

network with considerable number of macrospores. These pores were relatively uniform in morphology and size. Aerogel-6 had pore size lower than 10 μm with thin pore walls. However, when ECH was applied, Aerogel-2 formed a 3D interconnected network with much larger pore size and significantly increased wall thickness when compared with its counterpart. CNCs/PVA nanocomposite has been fabricated based on strong hydrogen bonding between cellulose nanocrystals and PVA chains. Different from previous works, ECH was selected to further react with the hydroxyl groups on PVA molecules[223]. In addition to the hydrogen bonding between cellulose nanocrystals and PVA chains, the covalent bonds between the matrix molecules enabled stronger pore connections in the aerogels, resulting in a highly interconnected and dense 3D network.

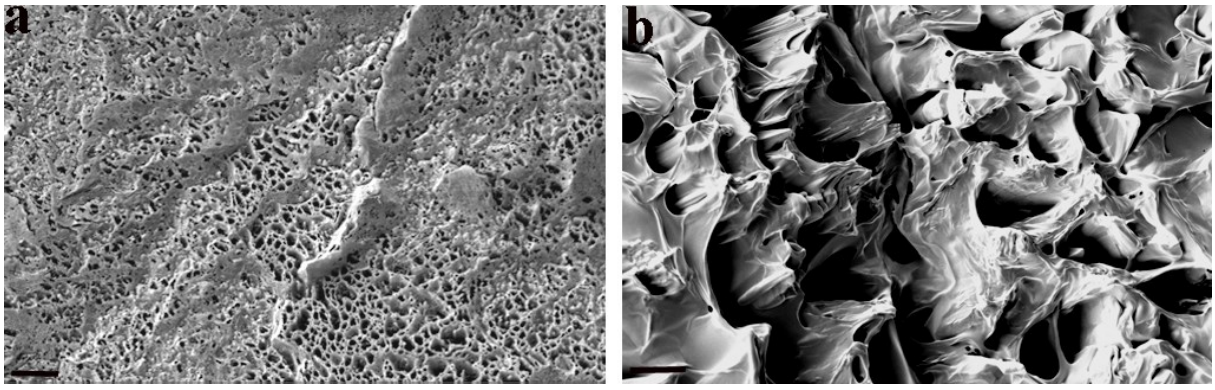

Figure 5- 6 SEM images of the cross-section of Aerogel-6 (a) and Aerogel-2(b). Scale bar: 10 μm.

The effect of PVA on the morphology of the crosslinked CNCs/PVA aerogels

To demonstrate the role of PVA in the formation of the crosslinked CNCs/PVA aerogels, the morphology of Aerogel-1 and Aerogel-3 were shown in the SEM images (**Fig. 5-7**). Even though

the two samples were prepared with the same amount of cellulose nanocrystals and crosslinker under the same protocol, their morphologies were significantly different due to the different amount of PVA used. A spider-web pattern appeared in Aerogel-1 prepared with 0.01 g of PVA, whereas a continuous and interconnected/denser network was observed in Aerogel-3. Comparing the morphology of these two samples, it was obvious that PVA worked as a matrix material to form the 3D interconnected continuous network. As shown in **Fig. S3**, cellulose nanocrystals could not form strong structure, even with addition of ECH. After being freeze-dried, the sample collapsed with significantly decreased volume and it was too weak to be compressed. Even though ECH has been widely reported for the fabrication of bulk cellulose gels[33, 227, 228], it has never been achieved for the chemical crosslinking of cellulose nanocrystals. This could be explained by the limited reactive hydroxyl groups on the surface of cellulose nanocrystals, since most of the hydroxyl groups were buried in the crystals. Hereby in this study, the aerogels were strategically designed by dispersing hydrocolloidally stable cellulose nanocrystals homogeneously in the aqueous PVA solution. This has led to new cellulose nanocrystals-based aerogels formed from a percolated cellulose nanocrystal network via hydrogen bonding with the help of the PVA matrix by strong hydrogen bonding between cellulose nanocrystals and PVA. Furthermore, the PVA matrix was further crosslinked by ECH to form strong and dense microstructures.

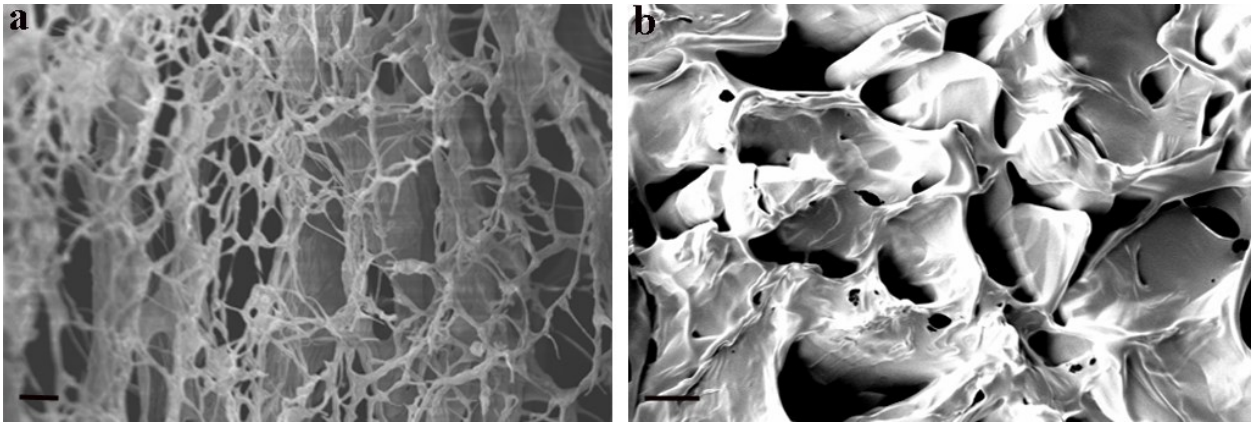

Figure 5- 7 SEM images of the Aerogel-1 and Aerogel-3 with increase of PVA content. Scale bar: 10 μm.

5.3.5 Mechanical properties of the crosslinked CNCs/PVA aerogels

The crosslinked CNCs/PVA aerogels were compressed under the Instron Testing machine at the strain of 50%, and their compressive modulus was investigated as a function of the cellulose nanocrystal concentration (0.5, 1.0 and 2.0 $^{w}/_{w}$%). As shown in **Fig. 5-8**, the compressive modulus of Aerogel-4 was 49.9±5.2 KPa with the addition of 0.5 $^{w}/_{w}$% of cellulose nanocrystals. It increased to 92.9±4.6 KPa for Aerogel-2 and 200.9±8.0 KPa for Aerogel-5 when the concentration of cellulose nanocrystals was increased to 1.0 and 2.0 $^{w}/_{w}$%. It has been reported the compressive modulus of pure PVA aerogels (5 mL, 10 $^{w}/_{w}$%) was only 17 KPa, and addition of large amount of cellulose nanofiber (up to 16 $^{w}/_{w}$%) increased the compressive modulus of PVA/CNF aerogel to 150 KPa[229]. In this study, only small amount of cellulose nanocrystals (0.5-2.0 $^{w}/_{w}$%) can significantly increase the compressive modulus of the crosslinked CNCs/PVA aerogels. This excellent reinforcing effect of cellulose materials was ascribed to a mechanical percolation phenomenon[33].

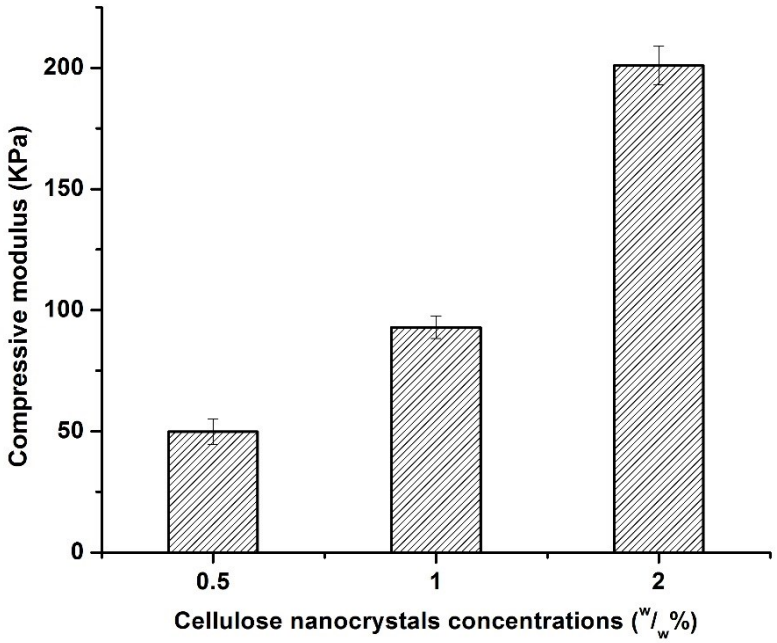

Figure 5- 8 Compressive modulus of the Aerogel-4, Aerogel-2, and Aerogel-5 as a function of the cellulose nanocrystal concentrations.

The compressibility of Aerogel-2 was tested on an Instron Testing Machine at cyclic compressive mode. As shown in **Fig. 5-9a,** the compressive stress of Aerogel-2 after ten cyclic compressions remained almost the same without a discernible variation compared to the original value. Thus, the unique structure of these aerogels allowed a large deformation without obvious fracture or collapse. **Fig. 5-9b** displayed the stress-strain response of the Aerogel-2 at maximum strain of 50% during ten cyclic compressions. The compressive stress-strain behavior of Aerogel-2 was typical of an open-cell aerogel[230]. The stress-strain curves of the crosslinked CNCs/PVA aerogels showed two distinct deformation regimes typically observed in open-cell aerogels[231], namely an initial Hookean region during which the stress increased linearly at low strain (<35%),

and a densification regime for strain >35% with a steep increase in stress[52]. Hence, hysteresis loops appeared in the loading-unloading cycles, due to the mechanical energy dissipation[232]. Furthermore, the stress remained above zero until the strain = 0, suggesting the aerogel rapidly and completely got recovered to its original status. **Fig. 5-9c** showed the compression images of the Aerogel-2 at maximum strain of 50% during the loading-unloading cycle. The sample stayed intact without obvious crack or volume shrink after the compression. Even though a large deformation could be observed during the compression, the Aerogel-2 showed excellent shape recovery to its original status. This observation further indicated the outstanding mechanical strength and robustness of the crosslinked CNCs/PVA aerogels.

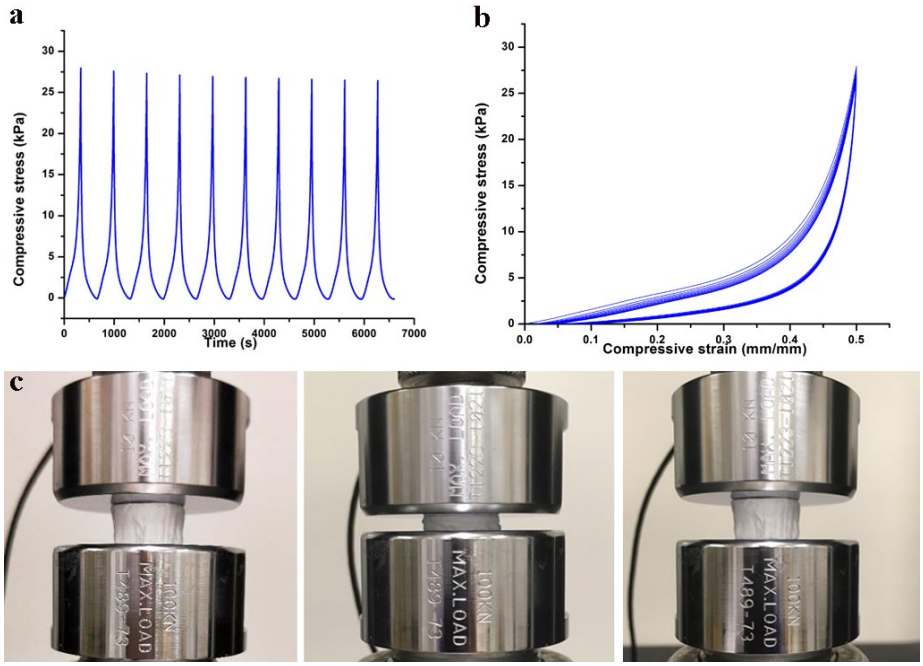

Figure 5- 9 Compressibility of the Aerogel-2: (a) Compressive stress versus time during ten cycles of compression of Aerogel-2; (b) stress-strain response of the Aerogel-2 for ten cycles; (c) compression images of the Aerogel-2.

For comparison, ECH-crosslinked PVA gel was obtained by substitution of cellulose nanocrystal suspension with only deionized water during the preparation process. As shown in **Fig. S4**, ECH-crosslinked PVA gel and Aerogel-6 could not get completely recovered when compressed. The matrix with CNCs/ECH was not studied due to its poor mechanical strength after freeze drying, resulting in weak solid that are not compressible (**Fig. S3**). The compressive performance of the crosslinked CNCs/PVA aerogels is superior to silica aerogels which are typically fragile, brittle, and can not be cyclically compressed[64]. Compared with the compressible PVA/carbon nanotubes or PVA/graphene aerogels[53, 69, 70], the aerogel developed in this work can be easily prepared and readily available due to the sustainability of cellulose nanocrystals and its lower cost, thus can be suitable for large-scale application.

5.3.6 Mechanism of the compressibility

Fig. 5-10 demonstrated the proposed mechanisms of the compressibility of our the crosslinked CNCs/PVA aerogels. The high compressibility of the crosslinked CNCs/PVA aerogels developed in this research can be attributed to their unique structures. The aerogel network was significantly reinforced by cellulose nanocrystals due to the mechanical percolation phenomenon, and the excellent compressibility of the crosslinked CNCs/PVA aerogels could be derived from their strong, dense, and porous microstructures. Additionally, it has been widely accepted that cellulose nanocrystals have excellent mechanical properties, and they cannot be easily deformed, either in the longitude or transverse axis. However, Yang and Cranston indicated cellulose nanocrystals could have some flexibility in shape-recoverable aerogels[65]. Recent studies further revealed that cellulose nanocrystals and bacterial cellulose showed flexibility to bend along the oil-water interface in Pickering emulsions[41, 233]. Therefore, the cellulose nanocrystals on the one hand increased the mechanical strength of the crosslinked CNCs/PVA aerogels by mechanical

percolation, and on the other hand helped the crosslinked aerogels to get completely recovered to its original status with cellulose nanocrystals bended and bounced back at cyclic compressive mode. PVA and ECH are also important for the formation of the unique structure of the crosslinked CNCs/PVA aerogels. PVA worked as a matrix material to form the 3D interconnected continuous network by hydrogen bonding and chemical crosslinking. It attached on the surface of cellulose nanocrystals and provided abundant hydroxyl groups for ECH-crosslinking.

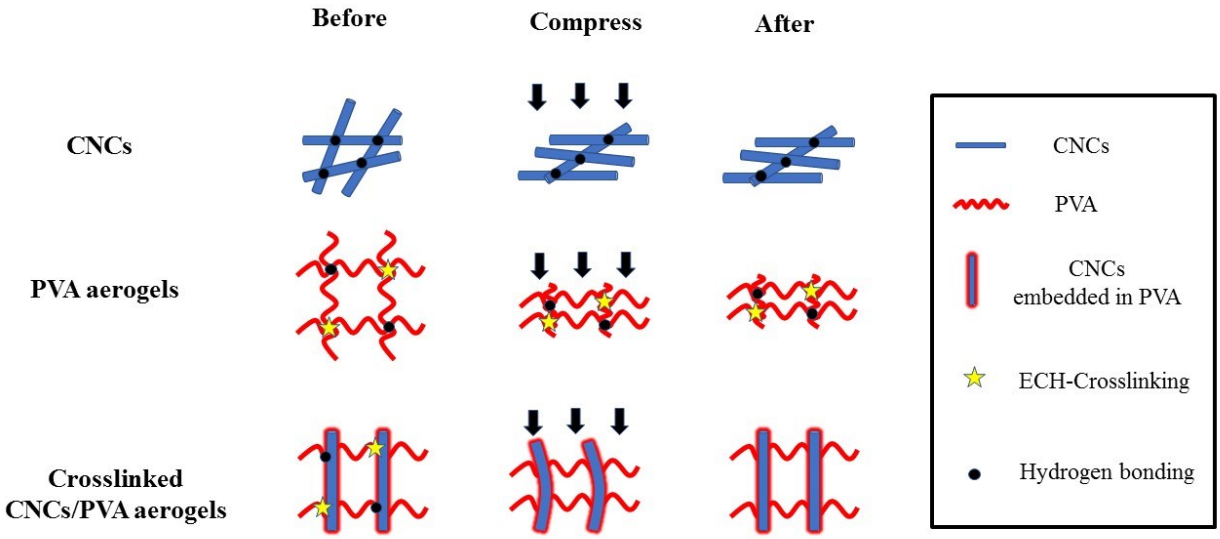

Figure 5- 10 Representation of each component's role in compressible CNCs/PVA aerogels formation.

5.4 Conclusions

Cellulose nanocrystals could not form strong gel, even with addition of ECH (**Fig. S3**). When the freeze-dried cellulose nanocrystals and CNCs/ECH matrices were compressed, their structures were destroyed. It has been widely reported that the foams and gels prepared with PVA are not compressible, even after crosslinking by physical or chemical approaches. Hereby, the compressive aerogels were strategically designed by dispersing hydrocolloidally stable cellulose nanocrystals homogeneously in the aqueous PVA solution and then crosslinked by ECH. This has led to new cellulose nanocrystals-based aerogels formed from a percolated cellulose nanocrystal network via hydrogen bonding with the help of the crosslinked PVA matrix. The crosslinked CNCs/PVA aerogels showed porous yet dense microstructures and could be cyclically compressed for ten times without significant variation in mechanical performances, showing better compressibility than the PVA/CNFs aerogels. The role of each component in the compressive aerogel was further investigated. It was proposed that the cellulose nanocrystals on the one hand increased the mechanical strength of the aerogels by mechanical percolation, and on the other hand helped the crosslinked aerogels to get completely recovered to its original status with cellulose nanocrystals bended and bounced back at cyclic compressive mode. PVA worked as a matrix material to form the 3D interconnected continuous network by hydrogen bonding and chemical crosslinking, while ECH chemically crosslinked with the hydroxyl groups on PVA, resulting in the formation of the porous yet dense microstructures of the compressible CNCs/PVA aerogels. With the outstanding mechanical strength/robustness, and convenient preparation method using sustainable cellulose nanocrystals, the crosslinked CNCs/PVA aerogels are novel compressive materials for many potential applications such as super absorbents, compressible supercapacitors, and energy-absorbing devices etc.

Chapter 6 - Highly porous, hydrophobic, and compressible cellulose nanocrystals/PVA aerogels as recyclable absorbents for oil-water separation*

6.1 Introduction

Oil and fuel spill at sea from petroleum industry or oil tankers/ship sinking occur frequently in recent years[234]. For example, the explosion of Deepwater Horizon oil rig in 2010 released 210 million gallons of oil into the Gulf of Mexico, which is the largest accidental marine oil spill in the history[64, 235]. The industrial discharge of oily wastewater and organic solvents also causes severe environmental issues. In spite of the tremendous efforts to control the pollution, the oil spill and organic solvent discharge can be devastating, due to the short-term of life threatening to thousands of species, and the long-term irrecoverable damage to the aquatic ecosystems. Currently, three categories of strategies have been widely accepted for oil/organic solvent cleanup (i) collecting oil/organic solvent from water surface by absorbents; (ii) dispersing oil/organic solvent using effective dispersants to accelerate the natural degradation process; (iii) and burning oil/organic solvent *in situ*[64, 236-238]. Among all these approaches, extracting oil/organic solvent by some absorbents is the most promising way due to its convenience, high efficiency, low cost, and secondary pollution prevention.

Traditional oil/organic solvent absorption materials include mineral products (zeolites[239]), natural materials (wool fibers[240], kapok fibers[241]), and synthetic materials (polystyrene fibers[242], rubber[243]). The mineral products and natural materials usually show the drawbacks of poor

*A version of this chapter is considered to be published: Xiaoyu Gong, Yixiang Wang, Hongbo Zeng, Mirko Betti, Lingyun Chen, "Highly porous, hydrophobic, and compressible PVA/cellulose nanocrystals aerogels as recyclable absorbents for oil-water separation".

buoyancy, low absorption capacity, and poor recyclability. As for the currently used synthetic polymers, they are generally not environmentally compatible, and their influence on the marine and ecological system is not clear yet[3]. On the other hand, current studies mainly focus on the efficient cleanup of oil/organic solvent, and significant progress has been made to improve the absorption capacity of the absorbents. However, very few studies have addressed the recycle and reuse of the oil/organic solvent spill. Given the growing efforts for energy conservation, it would be ideal the oil/organic solvent spill, once collected by the absorbents, can be further recycled and reused. Squeezing oil/organic solvent from absorbent is an efficient, energy saving and convenient approach for oil/organic solvent recovery. To achieve this recycle method, high performance absorbent materials are still required which should have high absorption capacity, oil/water selectivity and compressibility, as well as environmental friendliness.

Compressible aerogels are promising materials for oil/organic solvent cleanup and recovery, due to their excellent compressibility, large porosity (up to 99.8%), low density (4-500 mg/cm^3), and large surface area (100-1000 m^2/g)[53, 54]. However, the traditional silica aerogels usually suffer from fragility, and they are too brittle to meet the mechanical robustness as compressive materials[64]. Recently, aerogels fabricated from Poly(vinyl alcohol)(PVA) have attracted interest because they are less brittle, more flexible, and easy-processable[65], in addition to their excellent merits such as cost-effectiveness, biocompatibility, and biodegradability[66-68]. However, PVA aerogels are neither mechanically strong nor highly compressible. More recently, PVA aerogels reinforced by carbon nanotubes and graphene materials with good mechanical strength and high compressibility have been reported[53, 69, 70]. Nevertheless, those carbon-based materials are not readily available for large-scale applications due to the high cost of raw materials[64]. Cellulose materials, as the most abundant renewable natural polymer (annual production of 1.5×10^{12} tons/year[2]), are potential

candidates to replace the carbon nanotubes and graphene materials for the preparation of compressive aerogels, due to their renewability, outstanding mechanical properties, low density, and biocompatibility[233]. Some nanocellulose materials including cellulose nanofibers (CNFs) and cellulose nanocrystals (CNCs) have been incorporated with PVA to form aerogels[71, 244]. However, the PVA/CNFs aerogels did not show adequate elasticity and deformed permanently when the compression strain was higher than 20%[71]. Cellulose nanocrystals have excellent mechanical strength (elastic modulus~100-200 GPa[22]), and they are generally considered as excellent nano-reinforcement to fabricate materials of high mechanical performances[72]. However, even though the CNCs/PVA aerogels show significantly improved mechanical property, they have poor compressibility.

In our recent work, a highly compressible CNCs/PVA aerogel was fabricated from a percolated cellulose nanocrystal network via hydrogen bonding with the help of the PVA matrix. The compressibility study demonstrated the excellent shape recovery of the cross-linked CNCs/PVA aerogels which could be cyclically compressed for 10 times without significant variation in mechanical strength. It is of our interest to explore the aerogel application for oil/organic solvent spill cleanup and recovery. In the present study, the CNCs/PVA aerogels were further modified by methyltrichlorosilane (MTCS) through thermal chemical vapor deposition (CVD) to enhance the surface hydrophobicity. The molecular structure, density, porosity, morphology, contact angle, and mechanical properties of the obtained aerogels were systematically characterized, and their oil/organic solvent absorption capacity and oil-water separation efficiency were studied. In addition, the recyclability of the aerogels was evaluated by cyclic compression and rinsing.

6.2 Materials and methods

6.2.1 Materials

Cellulose nanocrystals were obtained by sulfuric acid hydrolysis according to our previous work. The rod-like cellulose nanocrystals had an average length of 177±34 nm and width of 9±4 nm (n=50) and could be homogenously dispersed in deionized water without obvious aggregation for more than 24 months. The zeta potential of cellulose nanocrystal suspension was -55.03±0.76 mV in deionized water. PVA (99+% hydrolyzed) was purchased from Sigma-Aldrich Canada Ltd with an average molecular weight of 1.3×10^5 Da. Methyltrichlorosilane, epichlorohydrin (ECH) and all other chemicals were purchased from Sigma-Aldrich Canada Ltd. (Oakville, ON, Canada) and used as received.

6.2.2 CNCs/PVA aerogel preparation

Desired amounts of PVA (0.01-0.1 g) were added into 5 mL of the cellulose nanocrystal suspension (1.0 $^{w}/_{w}$%) in a vial under vigorous stirring at 90 ℃ for 3h until PVA was completely dissolved. The pH of the suspension was adjusted to 10 by 0.1 M NaOH. ECH (0.1 mL) was then added dropwise into the vial within 5 min followed by vortex mixing for 1 min. The mixture was reacted at 60 ℃ for 24h and then the sample was molded in a 12-welled plate and frozen with liquid nitrogen followed by lyophilization. The freeze-dried samples were kept in a desiccator with drying reagent at room temperature for further use.

6.2.3 Silanization of the CNCs/PVA aerogels

The thermal chemical vapor deposition (CVD) technique was employed to hydrophobilize the CNCs/PVA aerogels. An open vial with saturated solution of K_2CO_3 was placed in a desiccator overnight to maintain the relative humidity (43%). Another open vial containing 1 mL of methyltrichlorosilane was also placed in the same desiccator with CNCs/PVA aerogels. The

desiccator was then tightly sealed and placed in an incubator at 50 ℃ for 24h (**Fig. 6-1**). The silanized aerogels were then kept in a vacuum oven at 50 ℃ for 24h to remove the residual silane and the by-product (HCl). AS denoted in **Table 6-1**, samples were coded as Aerogel-1, Aerogel-2, Aerogel-3, Aerogel-4, with respect to the increased amount of PVA from 0.01 g to 0.1 g. These obtained samples were stored in a desiccator with drying reagent at room temperature for further use.

Table 6- 1 Sample codes and reaction conditions to prepare the aerogels.

Sample code	Volume of CNCs (mL)	CNC concentration ($^{w}/_{w}$%)	Mass of PVA (g)	Volume of ECH (mL)	Silanized
Aerogel-1	5	1.0	0.01	0.1	Y
Aerogel-2	5	1.0	0.03	0.1	Y
Aerogel-3	5	1.0	0.05	0.1	Y
Aerogel-4	5	1.0	0.1	0.1	Y

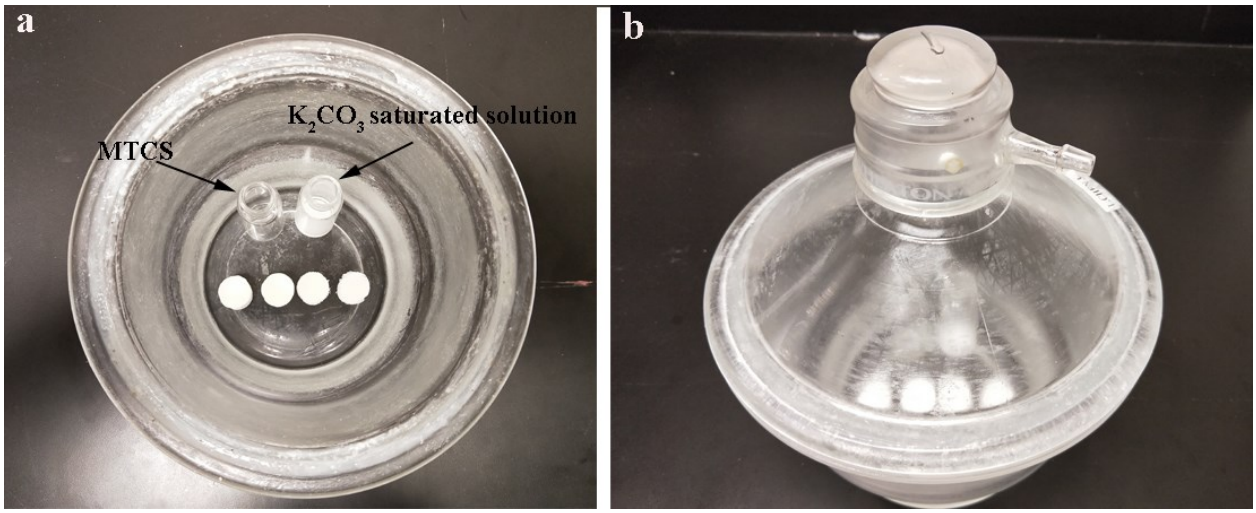

Figure 6- 1 The reaction device with samples in it (a-b).

6.2.4 Characterizations

Fourier transform infrared (FTIR) spectroscopy: Fourier transform infrared (FTIR) spectra of the Aerogel-1 to Aerogel-4, as well as the pristine materials cellulose nanocrystals and PVA, were recorded on a Nicolet 6700 spectrophotometer (Thermo Fisher Scientific Inc., MA, USA). The samples were prepared into KBr-disks. Spectra were recorded as the average of 128 scans at 4 cm^{-1} resolution and 25 ℃, using KBr as blank.

Density and porosity: The radius and height of the Aerogel-1 to Aerogel-4 were measured by a digital caliper. The apparent volumetric mass density of the aerogels was calculated using the **equation (6-1)**:

$$\rho = m/V \qquad \textbf{(6-1)}$$

where m and V are the mass (*g*) and volume (cm^3) of the aerogels, respectively.

Since a small amount of ECH and methyltrichlorosilane was used for the crosslinking and silanization of the CNCs/PVA aerogels, and the crosslinker ECH and methyltrichlorosilane are volatile, only cellulose nanocrystals and PVA were considered to simplify the porosity calculation. The porosity (*P, %*) of the aerogels was calculated according to **equation (6-2)**, where V (cm^3) is the volume of the aerogels, m_c (*g*) and m_p (*g*) represent the weight of cellulose nanocrystals and PVA, respectively. ρ_c is the density of the cellulose nanocrystals (1.59 g/cm^3)[54], and ρ_p is the density of PVA (1.29 g/cm^3)

$$P = (V - m_c/\rho_c - m_p/\rho_p)/V \qquad \textbf{(6-2)}$$

Morphology and nanostructure: The morphology of Aerogel-1 to Aerogel-4 was visualized by scanning electrical microscopy (SEM). The dried samples were coated with gold (3nm thickness) and visualized on a Hitachi S-4800 Field Emission Gun SEM (Hitachi High-Technologies Canada, Inc. Ontario, Canada) at 1.0 kV.

Contact angle measurements: The water contact angles of Aerogel-1, 2, 3, and 4 were measured by a contact angle goniometer (KRUSS DSA 10, Germany) using the sessile drop method at room temperature. Each sample was fixed on a microscope slide by double-faced adhesive tape to prevent the movement of the flat surface during wetting. Water droplets (3 μL) were then placed on the surface of the sample, followed by the images taken and analyzed by the goniometer. The contact angle of all aerogels was measured based on the shape of the sessile drop. The test for each aerogel was repeated for at least three samples with three tests for each sample.

Mechanical properties: The mechanical properties of Aerogel-2 and Aerogel-4 were measured using an Instron 5967 Testing Machine (Instron Corp., Norwood, MA, USA). Samples of Aerogel-2 were compressed to 20%, 40%, and 60% of their original height in air at room temperature at a rate of 3 mm/min. The compressive stress-strain curves were recorded accordingly. To investigate the compressibility of the aerogels, Aerogel-2 and Aerogel-4 were compressed and characterized at cyclic compressive mode. Samples were compressed 50 times to 60% of their original height in air at room temperature at a rate of 3 mm/min. The compressive stress-strain response and compressive stress-time during 50 cycles were recorded. The measurement for each aerogel was repeated for at least three samples.

6.2.5 Oil/organic solvent-water separation performance

Oil/organic solvent-water separation: 5 mL of oil-red-colored chloroform was dripped into 60 mL of deionized water in a petri dish followed by slight shaking to disperse the red-colored chloroform into smaller droplets. Aerogel-2 was used to absorb the oil- red-colored chloroform. The similar protocol was used for treatment of other oils and organic solvents including chloroform, hexane, acetone, ethanol, DMSO, mineral oil, pump oil (hydraulic oil), and canola oil.

Table 6- 2 Source, density and viscosity of the oil/organic solvents.

Oil/organic solvents	Source	Density	Viscosity
Chloroform	Fisher Chemical	1.480 g/cm^3	0.56 mPa/s at 20 ℃
Hexane	Fisher Chemical	0.659 g/cm^3	0.31 mPa/s at 20 ℃
Acetone	Fisher Chemical	0.790 g/cm^3	0.32 mPa/s at 20 ℃
Ethanol	AFNS Store	0.789 g/cm^3	1.2 mPa/s at 20 ℃
DMSO	Sigma-Aldrich	1.100 g/mL	2.0 mPa/s at 20 ℃
Mineral Oil, Heavy	Fisher Chemical	0.830 g/mL	Saybolt viscosity >162
Pump Oil (hydraulic oil)	Exxon Mobil DTE 26	0.881 g/mL	ISO Viscosity Grade: 68
Canola oil	Local retailor (Costco)	0.920 g/mL	N.A.

Oil/organic solvent absorption capacities: To study the liquid absorption capacity (AC) of the aerogels, various oils and organic solvents, including chloroform, hexane, acetone, ethanol, DMSO, mineral oil, pump oil, and canola oil, were used. Aerogel-2 was immerged in each oil or solvent for 5 min until the absorbance reached the maximum loading. The swollen aerogel was then removed out and the surface was blotted with a filter paper to remove excess oil/solvent on its surface. The weight of the aerogel before (W_b) and after (W_a) solvent uptake was measured, and the absorption capacity was calculated according to **equation (6-3)**:

$$AC(g/g) = W_a/W_b \qquad \textbf{(6-3)}$$

Meanwhile, to compare the performance of Aerogel-1 to Aerogel-4, the absorption capacity of all samples for uptake of chloroform was measured accordingly. All the tests were repeated at least three times.

Recyclability: Two different approaches were carried out to study the recyclability of the aerogels as versatile organic solvents absorbents: (1) cyclic compression: The original weight (W_b) of the

Aerogel-2 was measured. Then Aerogel-2 was immersed in chloroform or hexane for 5 min until the absorbance reached the maximum loading. The swollen aerogel was then taken out and the surface was blotted with a filter paper to remove excess chloroform or hexane on its surface. The weight of the swollen aerogel was measured following compression between parallel glass slides to 60% of its original height to partially remove the organic solvents. The Aerogel-2 with residue was then immersed in the same solvent again and this absorption-compressing process was repeated for 10 times and the weights of the swollen aerogels in each time (W_i) were measured and the absorption capacity for each cycle was calculated by $AC(g/g) = W_i/W_b$. (2) rinsing: oil-red was used to visually indicate the rinsing effect. Aerogel-2 was immersed in the oil-red-colored chloroform for 5 min until the absorbance reached the maximum loading. The swollen sample was then rinsed with 20 mL of ethanol to remove the chloroform for several times until the sample and ethanol were both not red anymore.

6.2.6 Statistical analysis

Aerogels prepared from three separated batches were analyzed for their properties. Experimental results were represented as the mean of three batches ± SD. Statistical evaluation was carried out by analysis of variance (ANOVA) followed by multiple-comparison tests using Duncan's multiple-range test. All the analyses were conducted using SAS statistical software (SAS Institute, Inc., Cary, NC) with a probability of $p < 0.05$ considered to be significant.

6.3 Results and discussion

6.3.1 Silanization of CNCs/PVA aerogels

In our recent work, the crosslinked CNCs/PVA aerogels were successfully prepared by dispersing hydrocolloidal stable cellulose nanocrystals homogenously in the aqueous Poly(vinyl

alcohol) (PVA) solution, followed by PVA crosslinking and freeze-drying. Cellulose nanocrystals formed the percolated network with each other by hydrogen bonding, and also strongly interacted with PVA matrix. Meanwhile, the PVA matrix was cross-linked by ECH which endowed the aerogels porous structure with strong and dense walls. It was proposed that the cellulose nanocrystals on the one hand increased the mechanical strength of the aerogels by mechanical percolation, and on the other hand helped the cross-linked aerogels to get completely recovered to its original status with cellulose nanocrystals bended and bounced back at cyclic compressive mode. PVA worked as a matrix material to form the 3D interconnected continuous network by hydrogen bonding and chemical crosslinking. It was noted that only small amount of cellulose nanocrystals (0.5-2.0 $^{w}/_{w}$%) could significantly increase the compressive modulus of the crosslinked CNCs/PVA aerogel up to 200.9±8.0 KPa. Unlike the PVA/CNFs aerogels that were not elastic and deformed permanently at the compression strain of 20%[71], the crosslinked CNCs/PVA aerogels could be compressed to an strain of 50% and got completely recovered to its original status after cyclic compressions.

To fabricate hydrophobic aerogels for oil/organic solvent cleanup, thermal chemical vapor deposition (CVD) of methyltrichlorosilane was employed which is a convenient approach to modify the hydroxyl groups on the surface of aerogels (**Fig. 6-2**). It is now widely accepted that the superhydrophobic surface can be engineered by controlling the surface chemistry[71]. Silanes with hydrolysable groups, such as chloride or alkoxide, can react with water to form the intermediate silanols, which can further react with other silanols or the hydroxyl groups on the surface of solid materials and formed monolayers or silicone layers[245]. This reaction led to an interconnected and hydrophobic network of silicone coating on the surface of the aerogels[237]. Since most of the hydroxyl groups on the cellulose nanocrystals are buried in the nanocrystals[112], while

abundant hydroxyl groups on the PVA matrix are readily available for silanization, the amount of PVA was varied to modulate the CNCs/PVA aerogel surface hydrophobicity. Four aerogels, namely Aerogel-1, Aerogel-2, Aerogel-3, and Aerogel-4, were prepared with the same amount of cellulose nanocrystals and ECH, yet various amounts of PVA (0.01-0.1 g) followed by silanization.

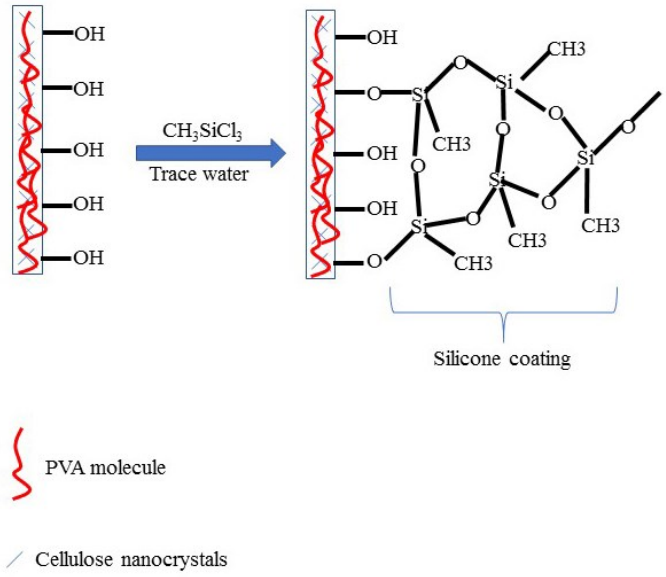

Figure 6- 2 Reaction scheme of methyltrichlorosilane with hydroxyl groups on the surface of the aerogel.

To study the chemical structure and molecular interactions of the silanized aerogels, FT-IR spectroscopy was performed on Aerogel-1 to Aerogel-4, with comparison to the spectra of pristine cellulose nanocrystals and PVA. As shown in **Fig. 6-3a**, cellulose nanocrystals had strong absorbances at 3340 cm^{-1}(-O-H stretching), 2896 cm^{-1}(-CH- symmetric stretching); and 1050 cm^{-1}(vibration of pyranose ring ether)[233]. PVA had strong peaks at 3450 cm^{-1}(-O-H stretching), 2920 cm^{-1}(-CH_2- symmetric stretching), and 2890 cm^{-1}(-CH- symmetric stretching). Compared to the spectra of cellulose nanocrystals and PVA, silanized Aerogel-4 had a sharp absorbance at 1276

cm^{-1}, which was ascribed to the asymmetric stretching of C-Si in the C-Si-O unit of the aerogel[237]. Additionally, a new peak appeared at 781 cm^{-1}, indicating the vibration of Si-O-Si in the silanized sample[237]. These new peaks in the spectrum of Aerogel-4 indicated the successfully silicone coating on the surface of Aerogel-4. **Fig. 6-3b** showed the FITR spectra of Aerogel-1, 2, 3, and 4. It was noted that the absorbance at 1276 cm^{-1} (asymmetric stretching of C-Si in the C-Si-O unit) and 781 cm^{-1} (vibration of Si-O-Si) became stronger from Aerogel-1 to Aerogel-4. With increase of the PVA content, more hydroxyl groups were available to react with intermediate silanols, thus stronger silicone coating was formed at the surface of Aerogel-4 compared to that on Aerogel-1. As a result, the Aerogel-4 with the strongest absorbance of the silicone coating could be more hydrophobic than its counterparts.

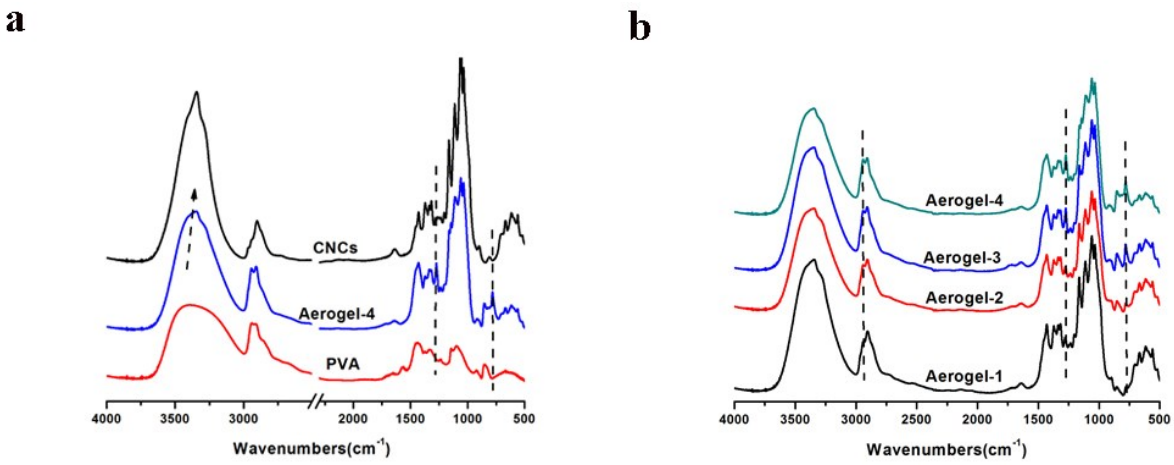

Figure 6- 3 FITR spectra of cellulose nanocrystals, PVA, and Aerogel-4 (a); FITR spectra of Aerogel-1, Aerogel-2, Aerogel-3, and Aerogel-4 (b).

The density and porosity of the prepared aerogels were calculated according to the dimensions and mass of the samples. As shown in **Table 6-2**, the volume of the samples increased as the

content of PVA increased and their densities ranged from 22.50±1.44 mg/cm^3 to 36.13±4.92 mg/cm^3, which were much lower than that of water. As for porosity, all the aerogels were highly porous with porosity ranging from 97.69±0.26% to 98.71±0.09%. Furthermore, these ultralight and highly porous aerogels were floatable on the surface of water, as displayed in **Fig. 6-4**. It could keep intact without obvious wetting by deionized water, indicating the aerogels were also highly hydrophobic.

Table 6- 3 Sample parameters.

Samples	Radius (cm)	Height (cm)	Mass (mg)	Volume (cm^3)	Density (mg/cm^3)	Porosity (%)
Aerogel-1	2.15±0.06	0.85±0.06	77.87±2.12	3.08±0.41	25.82±2.58	98.65±0.17
Aerogel-2	2.23±0.06	1.13±0.05	99.03±0.80	4.41±0.31	22.50±1.44	98.71±0.09
Aerogel-3	2.16±0.07	1.23±0.10	131.67±4.29	4.52±0.58	29.47±3.94	98.39±0.19
Aerogel-4	2.21±0.06	1.26±0.08	173.23±5.29	4.84±0.55	36.13±4.92	97.69±0.26

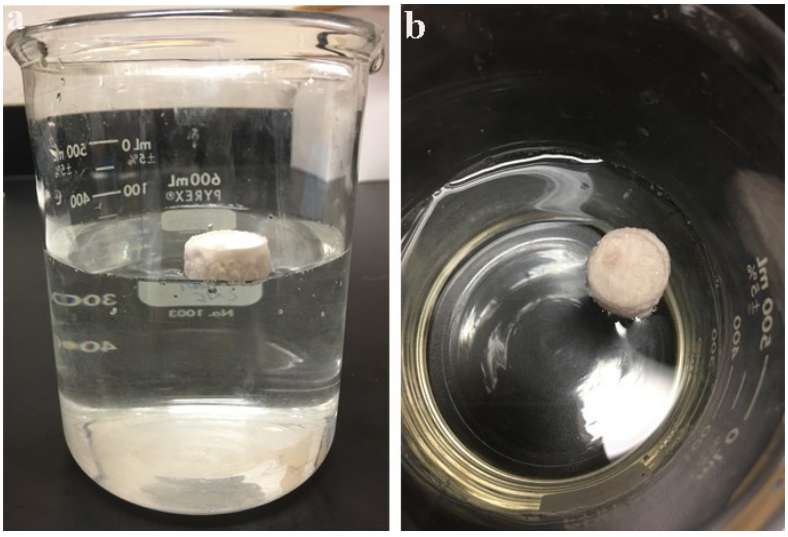

Figure 6- 4 Aerogel-3 floating on the surface of deionized water.

The structure and morphology of the aerogels were further investigated by SEM observation. **Fig. 6-5** showed the surface of the sinalized aerogels prepared with increasing amount of PVA. The aerogels had continuous and interconnected porous microstructure with pore sizes varied. It was interesting that the pore size of the aerogels decreased significantly with the increase of PVA in the samples. The pore size of Aerogel-1 ranged from around 20 μm to several hundred micrometers, several microns to 20 μm for Aerogel-2 and Aerogel-3, whereas lower than several microns for Aerogel-4. This indicates the content of PVA had a significant impact on the pore size of the obtained aerogels. As demonstrated in our previous work, cellulose nanocrystals firstly formed the percolated network with each other by hydrogen bonding, and then strongly interacted with PVA matrix. Meanwhile, the PVA crosslinked by epichlorohydrin worked as a matrix material in the aerogels. The morphology formation was driven by the phase separation when ice crystals formed and demixed from the crosslinked polymer molecules, leaving behind a porous structure upon water removal[31]. The size of ice crystals decreased with the increasing content of PVA that occupied more space. Thus removal of these ice crystals resulted in smaller macrospores in the Aerogel-4[72]. It was observed the structure of Aerogel-1 was more compact, and the pores in it collapsed to certain extend after freeze-drying, resulting in a volume shrink in the appearance and lower volume value (**Table 6-2**). Some collapse in the pores was observed for Aerogel-3 (**Fig. 6-5c**) and Aerogel-4 **(Fig. 6-5d)**, while Aerogel-2 was more porous, and the pores were interconnected without obvious collapse **(Fig. 6-5b)**. This could be due to the balanced CNCs/PVA ratio in Aerogel-2 resulted in a relatively stronger porous structure. Cellulose nanocrystals worked as a strong rod in the matrix to enable high mechanical strength and help the aerogels to get recovered when the stress was released, while PVA served as a matrix material to form the 3D interconnected continuous network. Therefore, a balanced CNCs/PVA ratio could help to obtain

aerogel with strong pore walls yet maintain its compressibility. This observation was also in accordance with the result of the porosity measurement in **Table 6-2**, in which Aerogel-2 showed the highest porosity value.

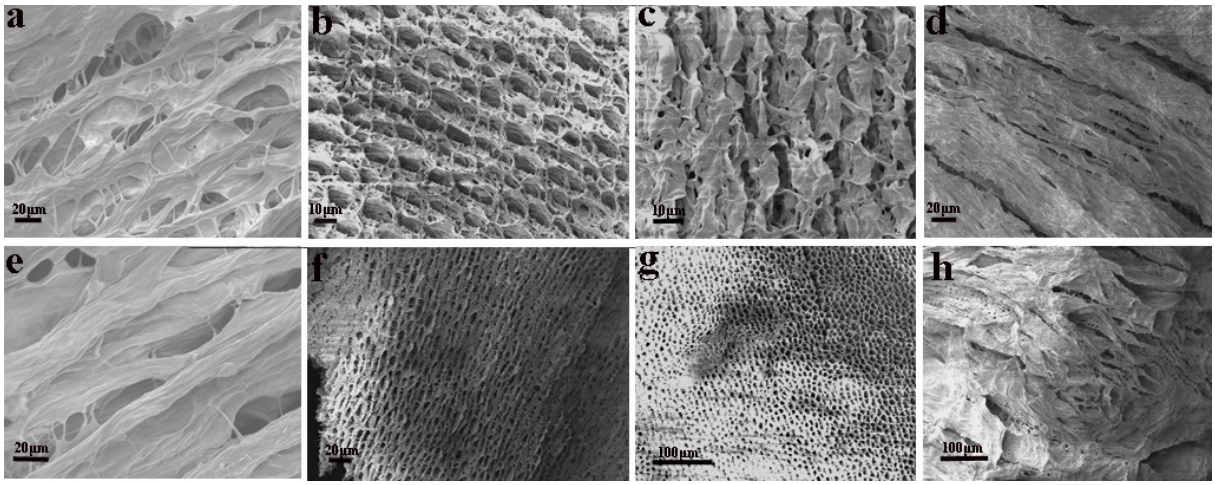

Figure 6- 5 SEM images of all samples at different magnifications: (a,e) Aerogel-1; (b,f) Aerogel-2; (c,g) Aerogel-3; (d,f) Aerogel-4.

In this study, methyltrichlorosilane was employed to modify the surface property of the prepared aerogels. As displayed in **Fig. 6-6**, water droplet could not penetrate the aerogels in 1 min, indicating the surface of the modified aerogels was hydrophobic. The hydrophobic aerogels showed high water contact angles of 95.1±0.6°, 114.9±3.4°, 128.1±1.6°, 144.5±7.8° for Aerogel-1, 2, 3, and 4, respectively. It was noted the samples prepared with higher amount of PVA had higher contact angels. This was due to the higher amount of active hydroxyl groups provided by the PVA that could react with the methyltrichlorosilane (**Fig. 6-2**) to generate more silicone coating on the surface, thus increased the hydrophobicity of the aerogel.

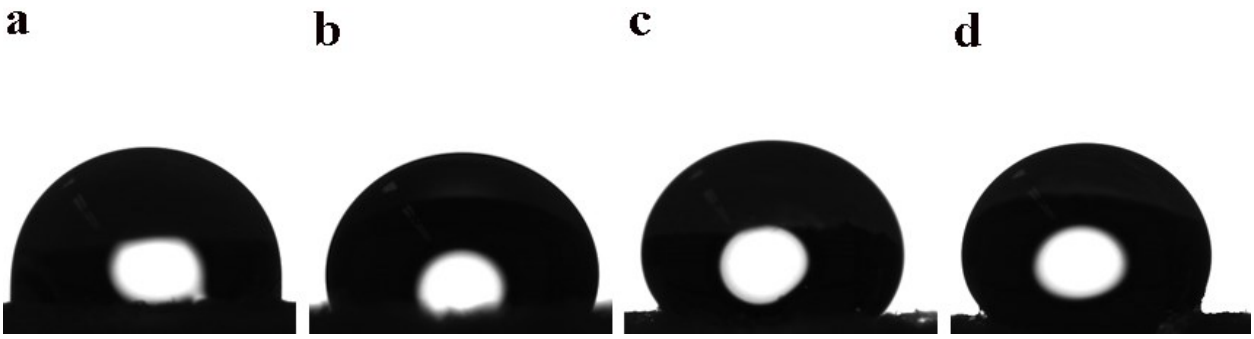

Figure 6- 6 Images of the samples contact with the water droplets and their contact angels. (a) Aerogel-1; (b) Aerogel-2; (c) Aerogel-3; (d) Aerogel-4.

Importantly, the hydrophobic aerogels were physically strong for the practical applications. When compressed in air, the mechanical performance of the obtained aerogels was superior to the traditional silica aerogels that are typically fragile, brittle, and cannot be cyclically compressed[64, 246]. PVA typically forms gels by physically repeated freeze-thawing processing or glutaraldehyde-crosslinking[66]. However, the PVA gels prepared by these physical or chemical crosslinking are not compressible either. As for cellulose nanocrystals alone, the physically crosslinked cellulose nanocrystal aerogels are too weak and usually they redisperse in liquid without a solid shape[230]. **Fig. 6-7a** presented the compressive stress-strain curves of the Aerogel-2 at various compressive strains of 20, 40, 60%. Similar to other compressible materials, hysteresis loops appeared in the loading-unloading cycles, indicating the obtained aerogels were elastic and could be compressed to large strain (20-60%) at relatively low stress (<35 KPa). **Fig. 6-7b** showed the stress-strain response of the Aerogel-2 at maximum strain of 60% during 50 cyclic compressions. The stress-strain curve displayed no significant change and the maximum stress kept stable, demonstrating the excellent cyclic compressibility of the obtained aerogels. The stress-strain curves of the aerogel showed two distinct deformation regimes that are typically observed in other open-cell aerogels[231],

namely an initial Hookean region during which the stress increases linearly at low strain (<45%), and a densification regime for strain >45% with a steep increase in stress[52]. Hence, similar to other cellular materials, hysteresis loops appeared in the loading-unloading cycles, due to the mechanical energy dissipation[232]. Furthermore, the stress remained above zero until the strain=0, suggesting the aerogel rapidly and completely got recovered to its original status, which is consistent with the observation in **Fig. 6-7a** and **Fig. 6-7c**. In dramatic contrast to the brittle nature of the traditional colloidal aerogels, the aerogels can bear a large deformation and can recover their original volume after the release of the stress. This mechanical robustness is essential for oil/organic solvent absorbing materials[45, 247].

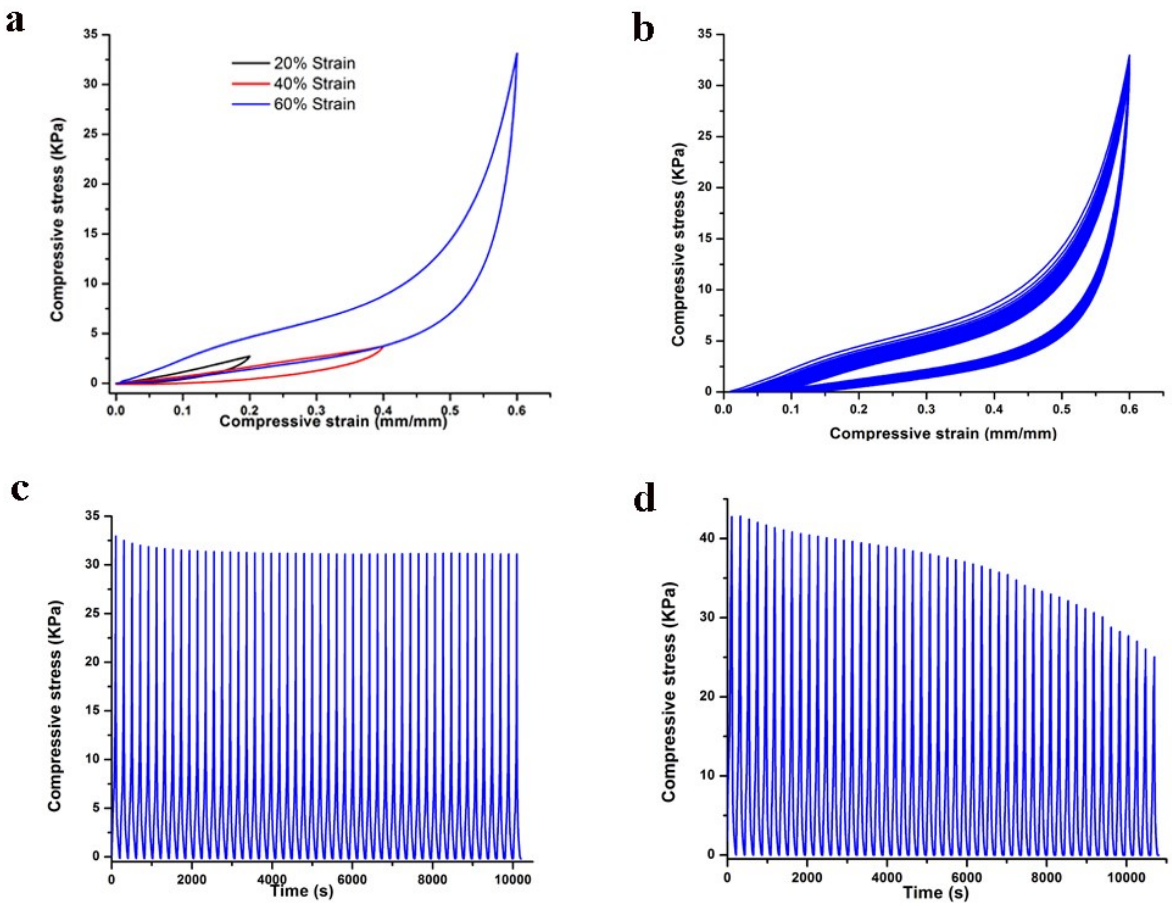

Figure 6- 7 Compressive stress-strain curves of the Aerogel-2 at different compressive strains (a); Stress-strain response of the Aerogel-2 at 60% of strain for fifty cycles (b); Compressive stress versus time during fifty cycles of compression of Aerogel-2 (c); Compressive stress versus time during fifty cycles of compression of Aerogel-4 (d).

Figs. 6-7c-d displayed the compressive stress versus time during 50 cycles of compression of Aerogel-2 (c) and Aerogel-4 (d). It was noted that the maximum compressive stress of Aerogel-2 remained almost the same without obvious decrease compared to its original value, suggesting this aerogel could allow a large deformation without obvious fracture or collapse. However, the maximum compressive stress of Aerogel-4 after 50 cyclic compression decreased from its original

value of 42.82 KPa to the final value of 25.04 KPa, indicating some compromise in function lose for Aerogel-4. Despite this, Aerogel-4 could still bear a large deformation and could be compressed cyclically.

6.3.2 Oil-water separation performance

For practical application, the obtained aerogels were applied as potential candidates for removal of various oils and organic solvents from water. Aerogel-2 was selected due to its good compressive performance. **Figs. 6-8 (a-b-d-c)** presented the process to remove the oil-red-colored chloroform from deionized water using Aerogel-2. It was noted that the oil-red-colored chloroform was completely absorbed by Aerogel-2, without any obvious residue. **Fig. 6-9a** showed the mass-based absorption capacity (AC) of Aerogel-2 in various mediums, ranging from 21.24 to 32.70 times of its original weight. There are a good number of materials with various absorption capacities to absorb oil/organic solvent, including silane-coated chitin sponge (AC: 29-58)[237], polydimethylsiloxane sponge (4-11)[248], polyurethane/polysiloxane sponge (15-25)[249], grapheme-based aerogel (28-40)[250], silane-coated polyurethane (15-25)[251], TiO_2-coated nanocellulose aerogels (20-40)[238], carbon-nanotube sponge (106-312)[252], graphene oxide-coated polyurethane sponge (80-160)[253], etc. The compressive aerogels in this study are potential for oil/organic solvent cleanup due to (i) acceptable absorption capacity to a wide range of oils/organic solvents, (ii) low cost of equipment/raw materials, and simple procedures when compared with the graphene-based materials and carbon nanotube-based materials, (iii) good biocompatibility to the environment when compared to some TiO_2-coated materials and fossil-derived materials such as polydimethylsiloxane, polyurethane.

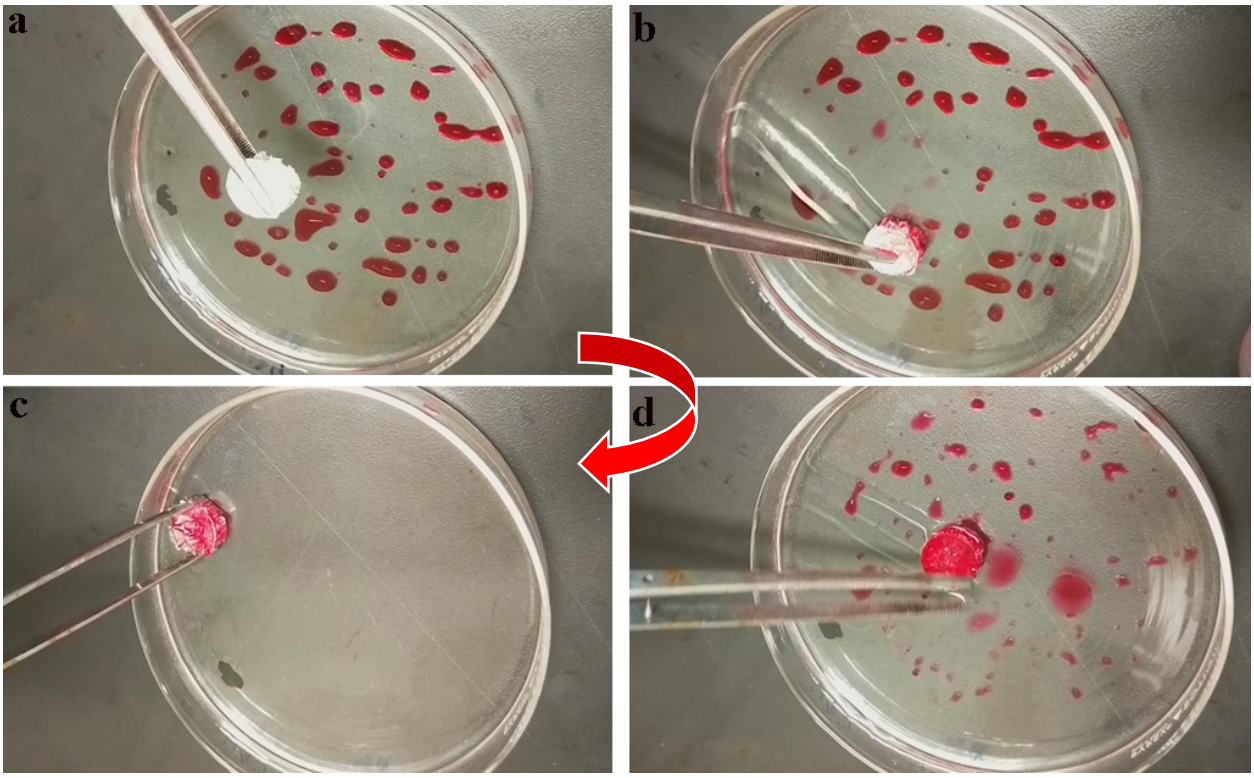

Figure 6- 8 Removal of oil-red-colored chloroform from deionized water with Aerogel-2 (a-b-d-c).

Fig. 6-9b displayed the mass-based absorption capacity of all aerogels for uptake of chloroform. The AC value was 28.91, 32.70, 29.24, 19.7 from Aerogel-1, 2, 3 and 4, respectively. It was noted that the AC value of Aerogel-2 was higher than that of its counterparts, which is due to the balanced CNCs/PVA ratio in the aerogels.

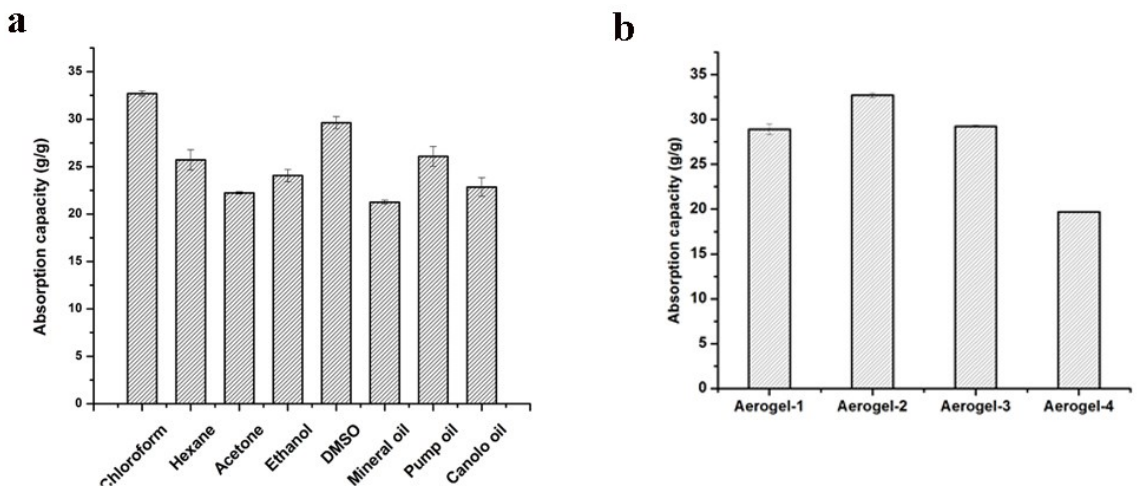

Figure 6- 9 Absorption capacity of Aerogel-2 for uptake of different oils and nonpolar solvents (a); absorption capacity of all samples for uptake of chloroform (b).

Recyclability: In this study, two approaches namely squeezing and washing, were applied to test the recyclability of the Aerogel-2. **Fig. 6-10** showed the absorption capacity of Aerogel-2 to remove chloroform or hexane by squeezing in ten cycles. The absorption capacity of the Aerogel-2 decreased as the squeezing time increased. This decreased absorption capacity for chloroform and hexane was due to the residual organic solvents in the pores of the aerogels[254]. However, even though the absorption capacity of Aerogel-2 decreased after ten cycles of compression, it can still absorb 22.40 times of hexane and 29.18 times of chloroform, respectively. As shown in **Video. S1**, Aerogel-2 was used to remove the oil-red-colored chloroform from deionized water. The aerogel was recycled by squeezing out the absorbed chloroform, during which Aerogel-2 remained intact without any visible changes in shape. After several times of squeezing, the sample could still be used to absorb chloroform, indicating the great potential to recycle these aerogels. Meanwhile, the samples could also be recycled by washing with other cheap organic solvents. **Fig. 6-11** and **Video. S2** showed the process to wash the oil-red-colored chloroform absorbed in Aerogel-2 with ethanol.

Initially, the sample was fully loaded with chloroform. After several times of washing, the chloroform diffused into the medium and the aerogel turned to its original color, indicating that the oil-red-colored chloroform had been wash out. The obtained ethanol/chloroform could be further recycled by distillation.

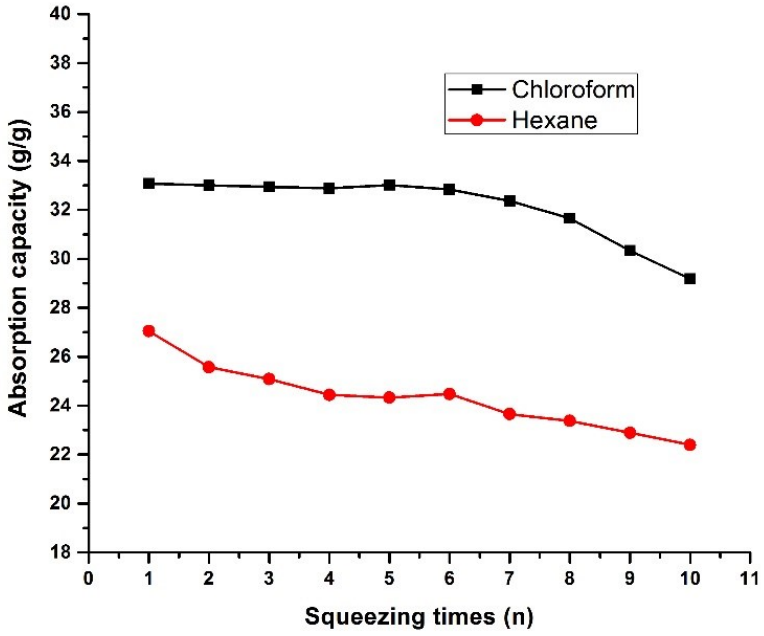

Figure 6- 10 Squeezing of Aerogel-2 to remove chloroform and hexane and it´s absorption capacity for ten cycles.

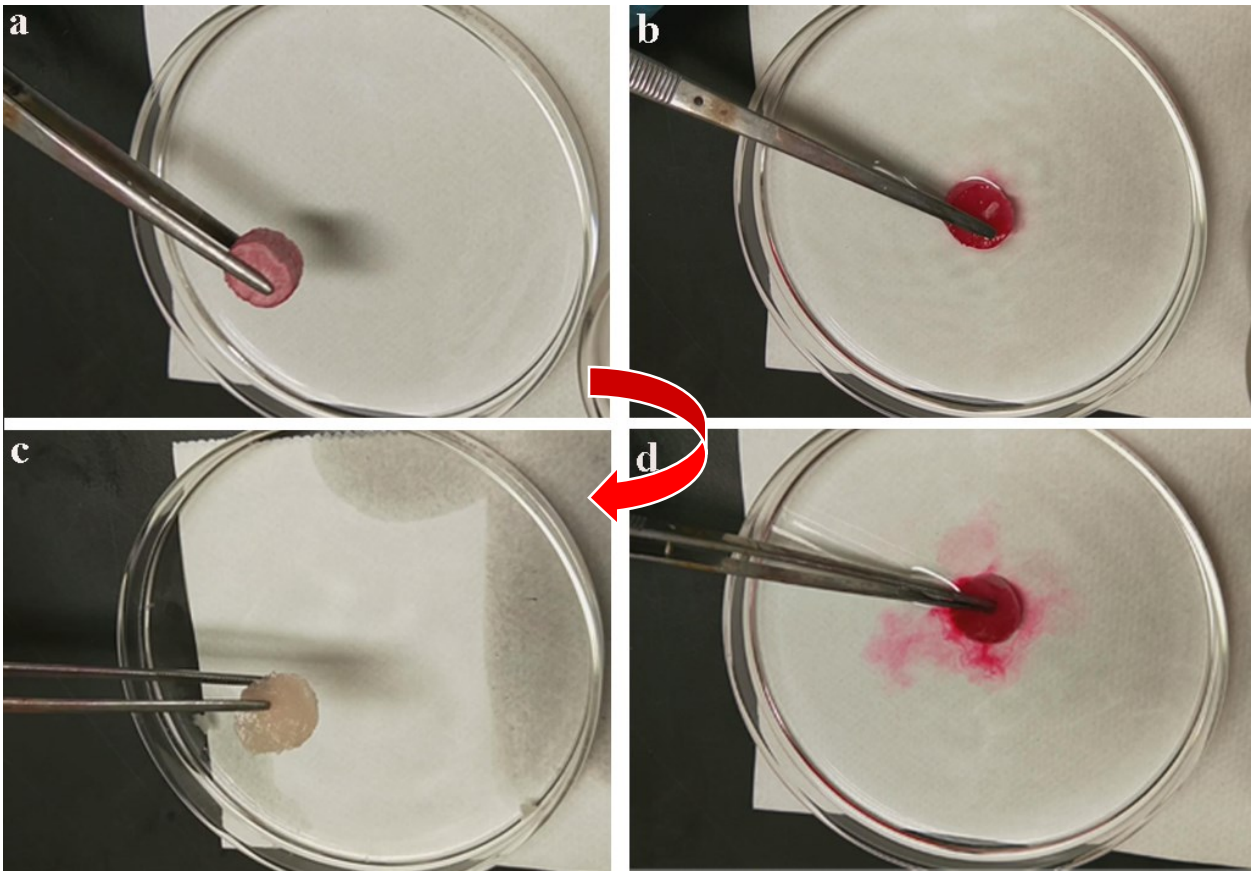

Figure 6- 11 Washing Aerogel-2 with ethanol to remove the red-oil-colored chloroform (a-b-d-c).

6.4 Conclusions

In this study, highly porous, hydrophobic, and compressible aerogels were prepared from cellulose nanocrystals with the help of the PVA, followed by thermal chemical vapor deposition of methyltrichlorosilane on the surface. The aerogels were ultralight (density: 22.50-36.13 mg/cm^3), highly porous (porosity > 97.69%), highly hydrophobic (contact angles to water droplet up to 144.5°). Further mechanical study indicated the aerogels were mechanically strong and compressible. When applied as absorbent to separate various oils and nonpolar solvents from water,

the aerogels had an absorption capacity ranging from 21.24 to 32.70 times of its original weight. Two simple approaches, including squeezing and washing, were applied to recycle the aerogels. As a result, the aerogels could be cyclically used for up to ten times without obvious decrease of absorption capacity. In addition, these aerogels are prepared from affordable and sustainable raw materials by simple procedures with good biocompatibility to the environment. Therefore, they are potential materials for the oil/organic solvent cleanup.

Chapter 7 - Summary and Conclusions

7.1 Summary

Wood fibers, as the largest source of cellulose, are abundant worldwide, especially for the countries with great forest area. However, currently, wood fibers are mainly used as the raw material for paper-making and lumbering, and only 2% with high content of cellulose pulps are used to prepare regenerated cellulose fibers, films, and some cellulose derivatives (cellulose esters and cellulose ethers). The research effort to develop wood fibers into other materials is still limited, and the huge value behind wood-based cellulose needs to be unveiled.

In this PhD program, some feasible approaches have been developed for the functionalization and applications of wood-based cellulose. Firstly, wood-based cellulose could be dissolved in the environmentally "green" and cost-effective NaOH/urea solvent system, after hydrolysis by different concentrations of sulfuric acid at various hydrolysis times. The resultant wood cellulose solution could form into hydrogels when subjected to heat treatment. These thermally induced cellulose gels also exhibited an inter-connected porous morphology, good flexibility and a "matrix-filler" structure. By altering the acid hydrolysis conditions, the 20%-12-Cellulose gel with a balanced "matrix-filler" content possessed a uniform structure, the highest compression stress and a good swelling ratio. This study has developed an efficient method of dissolution of wood cellulose in an eco-friendly solvent system from which to prepare cellulose hydrogels with adjustable properties. It has provided new opportunities to the industrial utilization of wood cellulose.

Due to the hydrophilic nature, cellulose materials are rarely applied as interfacial compounds. In the second study, homogeneous and electrostatically stable oxidized cellulose nanocrystals were prepared from wood pulp followed with surface modification using

phenyltrimethylammonium chloride to create hydrophobic domains comprised of phenyl groups. When applied to prepare oil-in-water Pickering emulsion, the modified oxidized cellulose nanocrystals showed a dispersed phase volume fraction (DPVR) of 0.7 at around 1.5 g/L, whereas tween-20 needed a 13-fold greater concentration to have a similar DPVR value, indicating a smaller quantity of modified oxidized cellulose nanocrystals was required to act as a Pickering emulsion stabilizer compared to traditional surfactant. Additionally, the size of the emulsion was adjustable by modulating the concentration of the stabilizer, and the obtained emulsions showed good mechanical/thermal stability when subjected to centrifugation or heat treatment. These modified oxidized cellulose nanocrystals could be used as efficient stabilizers for emulsion products. This identified property may allow potential applications of modified oxidized cellulose nanocrystals in household cleaning products, cosmetic/body care products, and pharmaceutical formula.

Moreover, cellulose nanocrystals showed excellent mechanical properties and potential nanoreinforcement in various nanocomposites, they could be an alternative for carbon nanotubes/graphene materials to prepare the mechanical strong yet highly compressive aerogels. In the third study, the compressive aerogels were strategically designed by dispersing hydrocolloidally stable cellulose nanocrystals homogeneously in aqueous PVA solution and then crosslinked by ECH. This has led to new cellulose nanocrystals-based aerogels formed from a percolated cellulose nanocrystal network via hydrogen bonding with the help of the crosslinked PVA matrix. As a result, the crosslinked CNCs/PVA aerogels showed porous yet dense microstructures and could be cyclically compressed for ten times without significant variation in mechanical performances. It was proposed that the cellulose nanocrystals on the one hand increased the mechanical strength of the aerogels by mechanical percolation, and on the other hand

helped the crosslinked aerogels to get completely recovered to its original status with cellulose nanocrystals bended and bounced back at cyclic compressive mode. PVA worked as a matrix material to form the 3D interconnected continuous network by hydrogen bonding and chemical crosslinking, while ECH chemically crosslinked with the hydroxyl groups on PVA, resulting in the formation of the porous yet dense microstructures. With the outstanding mechanical strength/robustness, and convenient preparation method using sustainable cellulose nanocrystals, the crosslinked CNCs/PVA aerogels are novel compressive materials for many potential applications such as super absorbents, compressible supercapacitors, and energy-absorbing devices etc.

Finally, highly porous, hydrophobic, and compressible aerogels were fabricated from cellulose nanocrystals with the help of the PVA, followed by thermal chemical vapor deposition of methyltrichlorosilane on the surface. As a result, the aerogels were ultralight (density: 22.50-36.13 mg/cm3), highly porous (porosity > 97.69%), and highly hydrophobic (contact angles to water droplet up to 144.5°). Further mechanical study showed the aerogels were mechanically strong and compressible. The aerogels were then applied as absorbent to separate various oils and nonpolar solvents from water. It showed that the aerogels had an absorption capacity ranging from 21.24 to 32.70 times of its original weight. Two simple approaches, including squeezing and washing, were applied to recycle the aerogels. As a result, the aerogels could be cyclically used for up to ten times without obvious decrease of absorption capacity. These aerogels are prepared from affordable and sustainable raw materials by simple procedures with good biocompatibility to the environment. Therefore, they are potential materials for the oil/organic solvent cleanup.

7.2 Significance of this research

During the last two decades, biomaterials have attracted increasing attention with the growing demand of environmentally green/functional products. Cellulose materials, due to their excellent merits such as abundance in nature (annual production of ~1.5×10^{12} tons), biocompatibility, biodegradability, nontoxicity, outstanding mechanical properties, low density etc., are considered as potential alternatives to replace the traditional petroleum/fossil-derived materials. Generally, cotton and wood fibers are the main source of cellulose materials. However, cotton fibers are not readily available in cold areas, whereas wood fibers, as the largest source of cellulose, are abundant worldwide, especially in the countries with great forest area. Currently, wood fibers are mainly used as the raw material for paper-making and lumbering, only 2% with high content of cellulose pulps are used to prepare regenerated cellulose fibers, films, and some cellulose derivatives (cellulose esters and cellulose ethers). Canada has a forest area of 331,285K ha, the research effort for wood fibers to develop wood cellulose-based advanced materials is still limited, and the huge value behind wood-based cellulose needs to be unveiled.

In this PhD program, the environmentally "green" and cost-effective NaOH/urea aqueous solvent was firstly applied on wood-based cellulose material. The wood-based cellulose gels were then prepared via a thermally induced gelation process. This study has demonstrated an efficient method of dissolution of wood-based cellulose in an eco-friendly solution from which to prepare cellulose gel targeted toward biomedical materials. This has provided new opportunities to facilitate the industrial utilization of wood-based cellulose.

Additionally, in this PhD program, the TEMPO-oxidized cellulose nanocrystals were firstly reported to have enhanced interfacial property for Pickering emulsion stabilization. The Pickering emulsions were prepared without addition of any traditional surfactants but only much lower

quantity of bio-based cellulose nanocrystals. When subjected to centrifugation or heat, the obtained Pickering emulsions showed good mechanical/thermal stability without obvious phase separation or significant size variation. This identified property may allow potential applications of cellulose materials in household cleaning products, cosmetic/body care products, and pharmaceutical formula.

Since cellulose nanocrystals show excellent mechanical properties and potential nanoreinforcement in various nanocomposites, they could be an alternative for carbon nanotubes/graphene materials to prepare the mechanical strong yet highly compressive aerogels. This research is the first time to investigate into the compressive CNCs/PVA aerogels. The role of each component in the aerogels was further discussed and the mechanism of compressibility was proposed. The fundamental knowledge gained in this study could help for the rational design of cellulose nanocrystals-based compressive aerogels. More importantly, the fabrication of the compressive aerogels was optimized and functionalized. The obtained absorbents were then applied for oil/organic solvent cleanup. The large-scale production of the absorbents in industry for oil/organic solvent removal is possible, due to the acceptable absorption capacity to a wide range of oils/organic solvents, low cost of equipment/raw materials, good biocompatibility to the environment, and good recyclability.

Overall, this research provides several feasible approaches for functionalization and application of wood-based cellulose materials, which could unveil the commercial benefits of wood resource in Canada.

7.3 Recommendations for future work

This research focused on the fabrication of advanced functional materials including wood-based cellulose hydrogels, wood-based Pickering emulsion stabilizer, wood-based compressive aerogels,

and wood-based oil absorbents, aiming at the functionalization and application of wood-based cellulose materials. Based on the current work, some interesting ideas that worth of further investigation are inspired as follows:

(a) The fabrication of wood-based cellulose hydrogels in the NaOH/urea aqueous solvent was successfully carried out. The obtained hydrogels showed good mechanical properties and porous structure. These current hydrogels could be further prepared into dried gels or aerogels targeted at the cleanup of pollutants in the oil sand industry. The performance of the dried gels or aerogels could be optimized by adjustment of the processing parameters including the temperature, pressure, drying time, and drying methods (air drying, vacuum drying, freeze drying, or even supercritical drying). Moreover, in order to boost the performance of the dried gels or aerogels to clean up the pollutants, pore maker such as $CaCO_3$ could also be used in the preparation process, and the effect of the pore maker on the performance of the gels could be investigated.

(b) Since cellulose materials are biocompatible, biodegradable, nontoxic, and the wood-based cellulose hydrogels prepared in this study showed good water-holding capacity and good mechanical strength, it would be worthwhile of studying the feasibility of the wood-based cellulose hydrogels as transdermal drug delivery system. Since most of the current drugs are sensitive to the harsh environment in human gastrointestinal tract, and it's challenging to avoid the first-pass effect in liver, some transdermal drug delivery systems could be developed using wood-based cellulose hydrogels as matrix. Some drugs, such as traditional Chinese medicines, nitroglycerin, could be loaded into the hydrogel matrix.

(c) In the current study, the modified oxidized wood-based cellulose nanocrystals showed enhanced emulsifying properties to stabilize Pickering emulsions with excellent mechanical/thermal stability. In order to develop emulsion products for personal care, cosmetic

and pharmaceutic industries, further safety evaluation of the products needs to be systematically studied.

(d) The CNCs/PVA aerogels with good compressibility and mechanical robustness have been fabricated in the current study. These aerogels were further optimized and developed into compressive aerogels for oil/organic solvent removal. These mechanical strong but highly compressible aerogels could be further developed into compressible supercapacitors, or energy-absorbing devices.

References

1. Rojas, O. J., Cellulose Chemistry and Properties: Fibers, Nanocelluloses and Advanced Materials Preface. Springger: 2016.

2. Gong, X. Y.; Wang, Y. X.; Tian, Z. G.; Zheng, X.; Chen, L. Y., Controlled production of spruce cellulose gels using an environmentally "green" system. *Cellulose* 2014, 21, 1667-1678.

3. Klemm, D.; Heublein, B.; Fink, H. P.; Bohn, A., Cellulose: Fascinating biopolymer and sustainable raw material. *Angew Chem Int Edit* 2005, 44, 3358-3393.

4. Shin, J. W.; Hammer, N. I.; Diken, E. G.; Johnson, M. A.; Walters, R. S.; Jaeger, T. D.; Duncan, M. A.; Christie, R. A.; Jordan, K. D., Infrared signature of structures associated with the $H^+(H_2O)(n)$ (n=6 to 27) clusters. *Science* 2004, 304, 1137-1140.

5. Eichhorn, S. J.; Baillie, C. A.; Zafeiropoulos, N.; Mwaikambo, L. Y.; Ansell, M. P.; Dufresne, A.; Entwistle, K. M.; Herrera-Franco, P. J.; Escamilla, G. C.; Groom, L.; Hughes, M.; Hill, C.; Rials, T. G.; Wild, P. M., Review: Current international research into cellulosic fibres and composites. *J Mater Sci* 2001, 36, 2107-2131.

6. Moon, R. J.; Martini, A.; Nairn, J.; Simonsen, J.; Youngblood, J., Cellulose nanomaterials review: structure, properties and nanocomposites. *Chem Soc Rev* 2011, 40, 3941-3994.

7. Liang, C. Y.; Marchessault, R. H., Infrared Spectra of Crystalline Polysaccharides .1. Hydrogen Bonds in Native Celluloses. *J Polym Sci* 1959, 37, 385-395.

8. Michell, A. J., 2nd Derivative Ft-Ir Spectra of Celluloses-I and Celluloses-Ii and Related Monosaccharides and Oligosaccharides. *Carbohyd Res* 1988, 173, 185-195.

9. Kamide, K.; Okajima, K.; Kowsaka, K.; Matsui, T., Cp Mass C-13 Nmr-Spectra of Cellulose Solids - an Explanation by the Intramolecular Hydrogen-Bond Concept. *Polym J* 1985, 17, 701-706.

10. Nishiyama, Y.; Langan, P.; Chanzy, H., Crystal structure and hydrogen-bonding system in cellulose 1 beta from synchrotron X-ray and neutron fiber diffraction. *J Am Chem Soc* 2002, 124, 9074-9082.

11. Swatloski, R. P.; Spear, S. K.; Holbrey, J. D.; Rogers, R. D., Dissolution of cellose with ionic liquids. *J Am Chem Soc* 2002, 124, 4974-4975.

12. Qi, H. S.; Chang, C. Y.; Zhang, L. N., Effects of temperature and molecular weight on dissolution of cellulose in NaOH/urea aqueous solution. *Cellulose* 2008, 15, 779-787.

13. Wendler, F.; Schulze, T.; Ciechanska, D.; Wesolowska, E.; Wawro, D.; Meister, F.; Budtova, T.; Liebner, F., Cellulose products from solutions: film, fibres and aerogels. In *The European Polysaccharide Network of Excellence (EPNOE)*, Springer: 2012; pp 153-185.

14. Rosenau, T.; Potthast, A.; Adorjan, I.; Hofinger, A.; Sixta, H.; Firgo, H.; Kosma, P., Cellulose solutions in N-methylmorpholine-N-oxide (NMMO) - degradation processes and stabilizers. *Cellulose* 2002, 9, 283-291.

15. Rosenau, T.; Potthast, A.; Sixta, H.; Kosma, P., The chemistry of side reactions and byproduct formation in the system NMMO/cellulose (Lyocell process). *Prog Polym Sci* 2001, 26, 1763-1837.

16. Zhu, S. D.; Wu, Y. X.; Chen, Q. M.; Yu, Z. N.; Wang, C. W.; Jin, S. W.; Ding, Y. G.; Wu, G., Dissolution of cellulose with ionic liquids and its application: a mini-review. *Green Chem* 2006, 8, 325-327.

17. Pinkert, A.; Marsh, K. N.; Pang, S. S.; Staiger, M. P., Ionic Liquids and Their Interaction with Cellulose. *Chem Rev* 2009, 109, 6712-6728.

18. Potthast, A.; Rosenau, T.; Buchner, R.; Roder, T.; Ebner, G.; Bruglachner, H.; Sixta, H.; Kosma, P., The cellulose solvent system N,N-dimethylacetamide/lithium chloride revisited: the effect of water on physicochemical properties and chemical stability. *Cellulose* 2002, 9, 41-53.

19. Cai, J.; Zhang, L., Rapid dissolution of cellulose in LiOH/Urea and NaOH/Urea aqueous solutions. *Macromol Biosci* 2005, 5, 539-548.

20. Cai, J.; Zhang, L.; Liu, S. L.; Liu, Y. T.; Xu, X. J.; Chen, X. M.; Chu, B.; Guo, X. L.; Xu, J.; Cheng, H.; Han, C. C.; Kuga, S., Dynamic Self-Assembly Induced Rapid Dissolution of Cellulose at Low Temperatures. *Macromolecules* 2008, 41, 9345-9351.

21. Lin, N.; Dufresne, A., Nanocellulose in biomedicine: Current status and future prospect. *Eur Polym J* 2014, 59, 302-325.

22. Mariano, M.; El Kissi, N.; Dufresne, A., Cellulose Nanocrystals and Related Nanocomposites: Review of some Properties and Challenges. *J Polym Sci Pol Phys* 2014, 52, 791-806.

23. Saito, T.; Hirota, M.; Tamura, N.; Kimura, S.; Fukuzumi, H.; Heux, L.; Isogai, A., Individualization of Nano-Sized Plant Cellulose Fibrils by Direct Surface Carboxylation Using TEMPO Catalyst under Neutral Conditions. *Biomacromolecules* 2009, 10, 1992-1996.

24. Saito, T.; Isogai, A., Ion-exchange behavior of carboxylate groups in fibrous cellulose oxidized by the TEMPO-mediated system. *Carbohyd Polym* 2005, 61, 183-190.

25. Saito, T.; Isogai, A., Introduction of aldehyde groups on surfaces of native cellulose fibers by TEMPO-mediated oxidation. *Colloid Surface A* 2006, 289, 219-225.

26. Saito, T.; Isogai, A., Wet strength improvement of TEMPO-oxidized cellulose sheets prepared with cationic polymers. *Ind Eng Chem Res* 2007, 46, 773-780.

27. Saito, T.; Kimura, S.; Nishiyama, Y.; Isogai, A., Cellulose nanofibers prepared by TEMPO-mediated oxidation of native cellulose. *Biomacromolecules* 2007, 8, 2485-2491.

28. Saito, T.; Nishiyama, Y.; Putaux, J. L.; Vignon, M.; Isogai, A., Homogeneous suspensions of individualized microfibrils from TEMPO-catalyzed oxidation of native cellulose. *Biomacromolecules* 2006, 7, 1687-1691.

29. Yang, H.; Tejado, A.; Alam, N.; Antal, M.; van de Ven, T. G. M., Films Prepared from Electrosterically Stabilized Nanocrystalline Cellulose. *Langmuir* 2012, 28, 7834-7842.

30. Van Vlierberghe, S.; Dubruel, P.; Schacht, E., Biopolymer-Based Hydrogels As Scaffolds for Tissue Engineering Applications: A Review. *Biomacromolecules* 2011, 12, 1387-1408.

31. Ullah, F.; Othman, M. B. H.; Javed, F.; Ahmad, Z.; Akil, H. M., Classification, processing and application of hydrogels: A review. *Mat Sci Eng C-Mater* 2015, 57, 414-433.

32. Cai, J.; Zhang, L., Unique gelation behavior of cellulose in NaOH/Urea aqueous solution. *Biomacromolecules* 2006, 7, 183-189.

33. Zhou, J.; Chang, C.; Zhang, R.; Zhang, L., Hydrogels prepared from unsubstituted cellulose in NaOH/Urea aqueous solution. *Macromol Biosci* 2007, 7, 804-809.

34. Chen, T.; Colver, P. J.; Bon, S. A. F., Organic-inorganic hybrid hollow spheres prepared from TiO_2-stabilized pickering emulsion polymerization. *Adv Mater* 2007, 19, 2286-2289.

35. Luo, Z. J.; Murray, B. S.; Ross, A. L.; Povey, M. J. W.; Morgan, M. R. A.; Day, A. J., Effects of pH on the ability of flavonoids to act as Pickering emulsion stabilizers. *Colloid Surface B* 2012, 92, 84-90.

36. Tzoumaki, M. V.; Moschakis, T.; Kiosseoglou, V.; Biliaderis, C. G., Oil-in-water emulsions stabilized by chitin nanocrystal particles. *Food Hydrocolloid* 2011, 25, 1521-1529.

37. Yusoff, A.; Murray, B. S., Modified starch granules as particle-stabilizers of oil-in-water emulsions. *Food Hydrocolloid* 2011, 25, 42-55.

38. Dickinson, E., Use of nanoparticles and microparticles in the formation and stabilization of food emulsions. *Trends Food Sci Tech* 2012, 24, 4-12.

39. Andresen, M.; Stenius, P., Water-in-oil emulsions stabilized by hydrophobized microfibrillated cellulose. *J Disper Sci Technol* 2007, 28, 837-844.

40. Kalashnikova, I.; Bizot, H.; Bertoncini, P.; Cathala, B.; Capron, I., Cellulosic nanorods of various aspect ratios for oil in water Pickering emulsions. *Soft Matter* 2013, 9, 952-959.

41. Kalashnikova, I.; Bizot, H.; Cathala, B.; Capron, I., New Pickering Emulsions Stabilized by Bacterial Cellulose Nanocrystals. *Langmuir* 2011, 27, 7471-7479.

42. Alargova, R. G.; Warhadpande, D. S.; Paunov, V. N.; Velev, O. D., Foam superstabilization by polymer microrods. *Langmuir* 2004, 20, 10371-10374.

43. Madivala, B.; Vandebril, S.; Fransaer, J.; Vermant, J., Exploiting particle shape in solid stabilized emulsions. *Soft Matter* 2009, 5, 1717-1727.

44. Noble, P. F.; Cayre, O. J.; Alargova, R. G.; Velev, O. D.; Paunov, V. N., Fabrication of "hairy" colloidosomes with shells of polymeric microrods. *J Am Chem Soc* 2004, 126, 8092-8093.

45. Liang, H. W.; Guan, Q. F.; Chen, L. F.; Zhu, Z.; Zhang, W. J.; Yu, S. H., Macroscopic-Scale Template Synthesis of Robust Carbonaceous Nanofiber Hydrogels and Aerogels and Their Applications. *Angew Chem Int Edit* 2012, 51, 5101-5105.

46. Gui, X. C.; Wei, J. Q.; Wang, K. L.; Cao, A. Y.; Zhu, H. W.; Jia, Y.; Shu, Q. K.; Wu, D. H., Carbon Nanotube Sponges. *Adv Mater* 2010, 22, 617-621.

47. Zhao, Y.; Liu, J.; Hu, Y.; Cheng, H. H.; Hu, C. G.; Jiang, C. C.; Jiang, L.; Cao, A. Y.; Qu, L. T., Highly Compression-Tolerant Supercapacitor Based on Polypyrrole-mediated Graphene Foam Electrodes. *Adv Mater* 2013, 25, 591-595.

48. Rolison, D. R.; Long, J. W.; Lytle, J. C.; Fischer, A. E.; Rhodes, C. P.; McEvoy, T. M.; Bourga, M. E.; Lubers, A. M., Multifunctional 3D nanoarchitectures for energy storage and conversion. *Chem Soc Rev* 2009, 38, 226-252.

49. Moreno-Castilla, C.; Maldonado-Hodar, F. J., Carbon aerogels for catalysis applications: An overview. *Carbon* 2005, 43, 455-465.

50. Zou, J. H.; Liu, J. H.; Karakoti, A. S.; Kumar, A.; Joung, D.; Li, Q. A.; Khondaker, S. I.; Seal, S.; Zhai, L., Ultralight Multiwalled Carbon Nanotube Aerogel. *Acs Nano* 2010, 4, 7293-7302.

51. Guo, F. M.; Cui, X.; Wang, K. L.; Wei, J. Q., Stretchable and compressible strain sensors based on carbon nanotube meshes. *Nanoscale* 2016, 8, 19352-19358.

52. Hu, H.; Zhao, Z. B.; Wan, W. B.; Gogotsi, Y.; Qiu, J. S., Ultralight and Highly Compressible Graphene Aerogels. *Adv Mater* 2013, 25, 2219-2223.

53. Wu, Z. Y.; Li, C.; Liang, H. W.; Chen, J. F.; Yu, S. H., Ultralight, Flexible, and Fire-Resistant Carbon Nanofiber Aerogels from Bacterial Cellulose. *Angew Chem Int Edit* 2013, 52, 2925-2929.

54. Heath, L.; Thielemans, W., Cellulose nanowhisker aerogels. *Green Chem* 2010, 12, 1448-1453.

55. Baetens, R.; Jelle, B. P.; Gustavsen, A., Aerogel insulation for building applications: A state-of-the-art review. *Energ Buildings* 2011, 43, 761-769.

56. Gronauer, M.; Fricke, J., Acoustic Properties of Microporous SiO_2-Aerogel. *Acustica* 1986, 59, 177-181.

57. Hrubesh, L. W.; Poco, J. F., Thin Aerogel Films for Optical, Thermal, Acoustic and Electronic Applications. *J Non-Cryst Solids* 1995, 188, 46-53.

58. Wang, B.; Al Abdulla, W.; Wang, D. L.; Zhao, X. S., A three-dimensional porous LiFePO4 cathode material modified with a nitrogen-doped graphene aerogel for high-power lithium ion batteries. *Energ Environ Sci* 2015, 8, 869-875.

59. Liang, H. W.; Wu, Z. Y.; Chen, L. F.; Li, C.; Yu, S. H., Bacterial cellulose derived nitrogen-doped carbon nanofiber aerogel: An efficient metal-free oxygen reduction electrocatalyst for zinc-air battery. *Nano Energy* 2015, 11, 366-376.

60. Hao, P.; Zhao, Z. H.; Leng, Y. H.; Tian, J.; Sang, Y. H.; Boughton, R. I.; Wong, C. P.; Liu, H.; Yang, B., Graphene-based nitrogen self-doped hierarchical porous carbon aerogels derived from chitosan for high performance supercapacitors. *Nano Energy* 2015, 15, 9-23.

61. Sui, Z. Y.; Meng, Y. N.; Xiao, P. W.; Zhao, Z. Q.; Wei, Z. X.; Han, B. H., Nitrogen-Doped Graphene Aerogels as Efficient Supercapacitor Electrodes and Gas Adsorbents. *Acs Appl Mater Inter* 2015, 7, 1431-1438.

62. Subrahmanyam, K. S.; Sarma, D.; Malliakas, C. D.; Polychronopoulou, K.; Riley, B. J.; Pierce, D. A.; Chun, J.; Kanatzidis, M. G., Chalcogenide Aerogels as Sorbents for Radioactive Iodine. *Chem Mater* 2015, 27, 2619-2626.

63. Du, R.; Zhang, N.; Zhu, J. H.; Wang, Y.; Xu, C. Y.; Hu, Y.; Mao, N. N.; Xu, H.; Duan, W. J.; Zhuang, L.; Qu, L. T.; Hou, Y. L.; Zhang, J., Nitrogen-Doped Carbon Nanotube Aerogels for High-Performance ORR Catalysts. *Small* 2015, 11, 3903-3908.

64. Sai, H. Z.; Fu, R.; Xing, L.; Xiang, J. H.; Li, Z. Y.; Li, F.; Zhang, T., Surface Modification of Bacterial Cellulose Aerogels' Web-like Skeleton for Oil/Water Separation. *Acs Appl Mater Inter* 2015, 7, 7373-7381.

65. Yang, X.; Cranston, E. D., Chemically Cross-Linked Cellulose Nanocrystal Aerogels with Shape Recovery and Superabsorbent Properties. *Chem Mater* 2014, 26, 6016-6025.

66. Stammen, J. A.; Williams, S.; Ku, D. N.; Guldberg, R. E., Mechanical properties of a novel PVA hydrogel in shear and unconfined compression. *Biomaterials* 2001, 22, 799-806.

67. Hou, Y.; Chen, C.; Liu, K. M.; Tu, Y.; Zhang, L.; Li, Y. B., Preparation of PVA hydrogel with high-transparence and investigations of its transparent mechanism. *Rsc Adv* 2015, 5, 24023-24030.

68. Hassan, C. M.; Peppas, N. A., Structure and morphology of freeze/thawed PVA hydrogels. *Macromolecules* 2000, 33, 2472-2479.

69. Sui, Z. Y.; Meng, Q. H.; Zhang, X. T.; Ma, R.; Cao, B., Green synthesis of carbon nanotube-graphene hybrid aerogels and their use as versatile agents for water purification. *J Mater Chem* 2012, 22, 8767-8771.

70. Kabiri, S.; Tran, D. N. H.; Altalhi, T.; Losic, D., Outstanding adsorption performance of graphene-carbon nanotube aerogels for continuous oil removal. *Carbon* 2014, 80, 523-533.

71. Zheng, Q. F.; Cai, Z. Y.; Gong, S. Q., Green synthesis of polyvinyl alcohol (PVA)-cellulose nanofibril (CNF) hybrid aerogels and their use as superabsorbents. *J Mater Chem A* 2014, 2, 3110-3118.

72. De France, K. J.; Hoare, T.; Cranston, E. D., Review of Hydrogels and Aerogels Containing Nanocellulose. *Chem Mater* 2017, 29, 4609-4631.

73. Keenan, R. J.; Reams, G. A.; Achard, F.; de Freitas, J. V.; Grainger, A.; Lindquist, E., Dynamics of global forest area: Results from the FAO Global Forest Resources Assessment 2015. *Forest Ecol Manag* 2015, 352, 9-20.

74. Fan, L.; Gharpuray, M. M.; Lee, Y., Nature of cellulosic material. In *Cellulose hydrolysis*, Springer: 1987.

75. El-Saied, H.; Basta, A. H.; Gobran, R. H., Research progress in friendly environmental technology for the production of cellulose products (bacterial cellulose and its application). *Polym-Plast Technol* 2004, 43, 797-820.

76. Klemm, D.; Schumann, D.; Kramer, F.; Hessler, N.; Hornung, M.; Schmauder, H. P.; Marsch, S., Nanocelluloses as innovative polymers in research and application. *Polysaccharides Ii* 2006, 205, 49-96.

77. Czaja, W.; Romanovicz, D.; Brown, R. M., Structural investigations of microbial cellulose produced in stationary and agitated culture. *Cellulose* 2004, 11, 403-411.

78. Wertz, J.-L.; Mercier, J. P.; Bédué, O., *Cellulose science and technology*. EPFL press: 2010.

79. Popa, V., *Polysaccharides in medicinal and pharmaceutical applications*. Smithers Rapra: 2011.

80. Krässig, H.; Schurz, J.; Steadman, R. G.; Schliefer, K.; Albrecht, W., Cellulose. *Ullmann's encyclopedia of industrial chemistry* 2000.

81. A, K. H., Cellulose: Structure Accessibility and Reactivity. Gordon and Breach Science Publishers: 1993.

82. Nevell, T. P.; Zeronian, S. H., Cellulose chemistry and its applications. 1985.

83. Davis, W.; Barry, A.; Peterson, F.; King, A., X-ray studies of reactions of cellulose in non-aqueous systems. II. Interaction of cellulose and primary amines1. *J Am Chem Soc* 1943, 65, 1294-1299.

84. Sarko, A.; Southwick, J.; Hayashi, J., Packing analysis of carbohydrates and polysaccharides. 7. Crystal structure of cellulose IIII and its relationship to other cellulose polymorphs. *Macromolecules* 1976, 9, 857-863.

85. Gardiner, E. S.; Sarko, A., Packing analysis of carbohydrates and polysaccharides. 16. The crystal structures of celluloses IVI and IVII. *Canadian journal of chemistry* 1985, 63, 173-180.

86. Kono, H.; Numata, Y.; Erata, T.; Takai, M., ^{13}C and ^{1}H resonance assignment of mercerized cellulose II by two-dimensional MAS NMR spectroscopies. *Macromolecules* 2004, 37, 5310-5316.

87. Isogai, A.; Usuda, M.; Kato, T.; Uryu, T.; Atalla, R. H., Solid-state CP/MAS carbon-13 NMR study of cellulose polymorphs. *Macromolecules* 1989, 22, 3168-3172.

88. Atalla, R. H.; Vanderhart, D. L., Native cellulose: a composite of two distinct crystalline forms. *Science* 1984, 223, 283-285.

89. Sugiyama, J.; Vuong, R.; Chanzy, H., Electron diffraction study on the two crystalline phases occurring in native cellulose from an algal cell wall. *Macromolecules* 1991, 24, 4168-4175.

90. Sugiyama, J.; Okano, T.; Yamamoto, H.; Horii, F., Transformation of Valonia Cellulose Crystals by an Alkaline Hydrothermal Treatment. *Macromolecules* 1990, 23, 3196-3198.

91. Horii, F.; Hirai, A.; Kitamaru, R., CP/MAS carbon-13 NMR spectra of the crystalline components of native celluloses. *Macromolecules* 1987, 20, 2117-2120.

92. Sugiyama, J.; Persson, J.; Chanzy, H., Combined Infrared and Electron-Diffraction Study of the Polymorphism of Native Celluloses. *Macromolecules* 1991, 24, 2461-2466.

93. Horii, F.; Yamamoto, H.; Kitamaru, R.; Tanahashi, M.; Higuchi, T., Transformation of native cellulose crystals induced by saturated steam at high temperatures. *Macromolecules* 1987, 20, 2946-2949.

94. Yamamoto, H.; Horii, F.; Odani, H., Structural-Changes of Native Cellulose Crystals Induced by Annealing in Aqueous Alkaline and Acidic Solutions at High-Temperatures. *Macromolecules* 1989, 22, 4130-4132.

95. Debzi, E.; Chanzy, H.; Sugiyama, J.; Tekely, P.; Excoffier, G., The Iα→ Iβ transformation of highly crystalline cellulose by annealing in various mediums. *Macromolecules* 1991, 24, 6816-6822.

96. Aulin, C. Novel oil resistant cellulosic materials. KTH, 2009.

97. Siqueira, G.; Bras, J.; Dufresne, A., Cellulosic Bionanocomposites: A Review of Preparation, Properties and Applications. *Polymers-Basel* 2010, 2, 728-765.

98. Finkenstadt, V.; Millane, R., Crystal structure of Valonia cellulose Iβ. *Macromolecules* 1998, 31, 7776-7783.

99. Langan, P.; Nishiyama, Y.; Chanzy, H., X-ray structure of mercerized cellulose II at 1 Å resolution. *Biomacromolecules* 2001, 2, 410-416.

100. Wada, M.; Heux, L.; Isogai, A.; Nishiyama, Y.; Chanzy, H.; Sugiyama, J., Improved structural data of cellulose IIII prepared in supercritical ammonia. *Macromolecules* 2001, 34, 1237-1243.

101. Chanzy, H.; Henrissat, B.; Vincendon, M.; Tanner, S. F.; Belton, P. S., Solid-state 13C-NMR and electron microscopy study on the reversible cellulose I→ cellulose IIII transformation in Valonia. *Carbohyd Res* 1987, 160, 1-11.

102. Kondo, T.; Togawa, E.; Brown, R. M., "Nematic ordered cellulose": A concept of glucan chain association. *Biomacromolecules* 2001, 2, 1324-1330.

103. Sekiguchi, Y.; Sawatari, C.; Kondo, T., A gelation mechanism depending on hydrogen bond formation in regioselectively substituted O-methylcelluloses. *Carbohyd Polym* 2003, 53, 145-153.

104. Kondo, T., Hydrogen bonds in cellulose and cellulose derivatives. In *Polysaccharides*, CRC Press: 2004; pp 81-110.

105. Zhang, H.; Wu, J.; Zhang, J.; He, J. S., 1-Allyl-3-methylimidazolium chloride room temperature ionic liquid: A new and powerful nonderivatizing solvent for cellulose. *Macromolecules* 2005, 38, 8272-8277.

106. Saalwächter, K.; Burchard, W., Cellulose in new metal-complexing solvents. 2. Semidilute behavior in Cd-tren. *Macromolecules* 2001, 34, 5587-5598.

107. Zhang, L. N.; Ruan, D.; Zhou, J. P., Structure and properties of regenerated cellulose films prepared from cotton linters in NaOH/Urea aqueous solution. *Ind Eng Chem Res* 2001, 40, 5923-5928.

108. Yang, Q. L.; Fukuzumi, H.; Saito, T.; Isogai, A.; Zhang, L. N., Transparent Cellulose Films with High Gas Barrier Properties Fabricated from Aqueous Alkali/Urea Solutions. *Biomacromolecules* 2011, 12, 2766-2771.

109. Qi, H.; Chang, C.; Zhang, L., Properties and applications of biodegradable transparent and photoluminescent cellulose films prepared via a green process. *Green Chem* 2009, 11, 177-184.

110. Cai, J.; Zhang, L. N.; Zhou, J. P.; Li, H.; Chen, H.; Jin, H. M., Novel fibers prepared from cellulose in NaOH/urea aqueous solution. *Macromol Rapid Comm* 2004, 25, 1558-1562.

111. Cai, J.; Zhang, L. N.; Zhou, J. P.; Qi, H. S.; Chen, H.; Kondo, T.; Chen, X. M.; Chu, B., Multifilament fibers based on dissolution of cellulose in NaOH/urea aqueous solution: Structure and properties. *Adv Mater* 2007, 19, 821-825.

112. Habibi, Y.; Lucia, L. A.; Rojas, O. J., Cellulose Nanocrystals: Chemistry, Self-Assembly, and Applications. *Chem Rev* 2010, 110, 3479-3500.

113. Rånby, B. G., Fibrous macromolecular systems. Cellulose and muscle. The colloidal properties of cellulose micelles. *Discussions of the Faraday Society* 1951, 11, 158-164.

114. Dufresne, A.; Cavaille, J. Y.; Vignon, M. R., Mechanical behavior of sheets prepared from sugar beet cellulose microfibrils. *J Appl Polym Sci* 1997, 64, 1185-1194.

115. Paakko, M.; Ankerfors, M.; Kosonen, H.; Nykanen, A.; Ahola, S.; Osterberg, M.; Ruokolainen, J.; Laine, J.; Larsson, P. T.; Ikkala, O.; Lindstrom, T., Enzymatic hydrolysis combined with mechanical shearing and high-pressure homogenization for nanoscale cellulose fibrils and strong gels. *Biomacromolecules* 2007, 8, 1934-1941.

116. Zimmermann, T.; Bordeanu, N.; Strub, E., Properties of nanofibrillated cellulose from different raw materials and its reinforcement potential. *Carbohyd Polym* 2010, 79, 1086-1093.

117. Iwamoto, S.; Nakagaito, A. N.; Yano, H., Nano-fibrillation of pulp fibers for the processing of transparent nanocomposites. *Appl Phys a-Mater* 2007, 89, 461-466.

118. Alemdar, A.; Sain, M., Isolation and characterization of nanofibers from agricultural residues - Wheat straw and soy hulls. *Bioresource Technol* 2008, 99, 1664-1671.

119. Chen, W. S.; Yu, H. P.; Liu, Y. X.; Hai, Y. F.; Zhang, M. X.; Chen, P., Isolation and characterization of cellulose nanofibers from four plant cellulose fibers using a chemical-ultrasonic process. *Cellulose* 2011, 18, 433-442.

120. Wang, W. X.; Mozuch, M. D.; Sabo, R. C.; Kersten, P.; Zhu, J. Y.; Jin, Y. C., Production of cellulose nanofibrils from bleached eucalyptus fibers by hyperthermostable endoglucanase treatment and subsequent microfluidization. *Cellulose* 2015, 22, 351-361.

121. Abitbol, T.; Kloser, E.; Gray, D. G., Estimation of the surface sulfur content of cellulose nanocrystals prepared by sulfuric acid hydrolysis. *Abstr Pap Am Chem S* 2013, 245.

122. Tang, Y. J.; Yang, S. J.; Zhang, N.; Zhang, J. H., Preparation and characterization of nanocrystalline cellulose via low-intensity ultrasonic-assisted sulfuric acid hydrolysis. *Cellulose* 2014, 21, 335-346.

123. Montanari, S.; Rountani, M.; Heux, L.; Vignon, M. R., Topochemistry of carboxylated cellulose nanocrystals resulting from TEMPO-mediated oxidation. *Macromolecules* 2005, 38, 1665-1671.

124. Wang, B.; Sain, M., Isolation of nanofibers from soybean source and their reinforcing capability on synthetic polymers. *Compos Sci Technol* 2007, 67, 2521-2527.

125. Espinosa, S. C.; Kuhnt, T.; Foster, E. J.; Weder, C., Isolation of Thermally Stable Cellulose Nanocrystals by Phosphoric Acid Hydrolysis. *Biomacromolecules* 2013, 14, 1223-1230.

126. Tang, Y. J.; Shen, X. C.; Zhang, J. H.; Guo, D. L.; Kong, F. G.; Zhang, N., Extraction of cellulose nano-crystals from old corrugated container fiber using phosphoric acid and enzymatic hydrolysis followed by sonication. *Carbohyd Polym* 2015, 125, 360-366.

127. Sadeghifar, H.; Filpponen, I.; Clarke, S. P.; Brougham, D. F.; Argyropoulos, D. S., Production of cellulose nanocrystals using hydrobromic acid and click reactions on their surface. *J Mater Sci* 2011, 46, 7344-7355.

128. Habibi, Y.; Vignon, M. R., Optimization of cellouronic acid synthesis by TEMPO-mediated oxidation of cellulose III from sugar beet pulp. *Cellulose* 2008, 15, 177-185.

129. Leung, A. C. W.; Hrapovic, S.; Lam, E.; Liu, Y. L.; Male, K. B.; Mahmoud, K. A.; Luong, J. H. T., Characteristics and Properties of Carboxylated Cellulose Nanocrystals Prepared from a Novel One-Step Procedure. *Small* 2011, 7, 302-305.

130. Xie, H. X.; Du, H. S.; Yang, X. G.; Si, C. L., Recent Strategies in Preparation of Cellulose Nanocrystals and Cellulose Nanofibrils Derived from Raw Cellulose Materials. *Int J Polym Sci* 2018.

131. Dong, X. M.; Revol, J. F.; Gray, D. G., Effect of microcrystallite preparation conditions on the formation of colloid crystals of cellulose. *Cellulose* 1998, 5, 19-32.

132. Beck-Candanedo, S.; Roman, M.; Gray, D. G., Effect of reaction conditions on the properties and behavior of wood cellulose nanocrystal suspensions. *Biomacromolecules* 2005, 6, 1048-1054.

133. Ramires, E. C.; Dufresne, A., A review of cellulose nanocrystals and nanocomposites. *Tappi J* 2011, 10, 9-16.

134. Araki, J.; Wada, M.; Kuga, S.; Okana, T., Influence of surface charge on viscosity behavior of cellulose microcrystal suspension. *J Wood Sci* 1999, 45, 258-261.

135. Araki, J.; Wada, M.; Kuga, S., Steric stabilization of a cellulose microcrystal suspension by poly(ethylene glycol) grafting. *Langmuir* 2001, 17, 21-27.

136. Heux, L.; Chauve, G.; Bonini, C., Nonflocculating and chiral-nematic self-ordering of cellulose microcrystals suspensions in nonpolar solvents. *Langmuir* 2000, 16, 8210-8212.

137. Lima, A. M. D.; Wong, J. T.; Paillet, M.; Borsali, R.; Pecora, R., Translational and rotational dynamics of rodlike cellulose whiskers. *Langmuir* 2003, 19, 24-29.

138. Roohani, M.; Habibi, Y.; Belgacem, N. M.; Ebrahim, G.; Karimi, A. N.; Dufresne, A., Cellulose whiskers reinforced polyvinyl alcohol copolymers nanocomposites. *Eur Polym J* 2008, 44, 2489-2498.

139. Elazzouzi-Hafraoui, S.; Nishiyama, Y.; Putaux, J. L.; Heux, L.; Dubreuil, F.; Rochas, C., The shape and size distribution of crystalline nanoparticles prepared by acid hydrolysis of native cellulose. *Biomacromolecules* 2008, 9, 57-65.

140. Li, Q.; Zhou, J. P.; Zhang, L. N., Structure and Properties of the Nanocomposite Films of Chitosan Reinforced with Cellulose Whiskers. *J Polym Sci Pol Phys* 2009, 47, 1069-1077.

141. Habibi, Y.; Goffin, A.-L.; Schiltz, N.; Duquesne, E.; Dubois, P.; Dufresne, A., Bionanocomposites based on poly (ε-caprolactone)-grafted cellulose nanocrystals by ring-opening polymerization. *J Mater Chem* 2008, 18, 5002-5010.

142. de Menezes, A. J.; Siqueira, G.; Curvelo, A. A. S.; Dufresne, A., Extrusion and characterization of functionalized cellulose whiskers reinforced polyethylene nanocomposites. *Polymer* 2009, 50, 4552-4563.

143. Araki, J.; Kuga, S., Effect of trace electrolyte on liquid crystal type of cellulose microcrystals. *Langmuir* 2001, 17, 4493-4496.

144. Kroonbatenburg, L. M. J.; Kroon, J.; Northolt, M. G., Chain Modulus and Intramolecular Hydrogen-Bonding in Native and Regenerated Cellulose Fibers. *Polym Commun* 1986, 27, 290-292.

145. Tashiro, K.; Kobayashi, M., Theoretical evaluation of three-dimensional elastic constants of native and regenerated celluloses: role of hydrogen bonds. *Polymer* 1991, 32, 1516-1526.

146. Reiling, S.; Brickmann, J., Theoretical Investigations on the Structure and Physical-Properties of Cellulose. *Macromol Theor Simul* 1995, 4, 725-743.

147. Neyertz, S.; Pizzi, A.; Merlin, A.; Maigret, B.; Brown, D.; Deglise, X., A new all-atom force field for crystalline cellulose I. *J Appl Polym Sci* 2000, 78, 1939-1946.

148. Eichhorn, S. J.; Davies, G. R., Modelling the crystalline deformation of native and regenerated cellulose. *Cellulose* 2006, 13, 291-307.

149. Tanaka, F.; Iwata, T., Estimation of the elastic modulus of cellulose crystal by molecular mechanics simulation. *Cellulose* 2006, 13, 509-517.

150. Bergenstråhle, M.; Berglund, L. A.; Mazeau, K., Thermal response in crystalline Iβ cellulose: a molecular dynamics study. *The Journal of Physical Chemistry B* 2007, 111, 9138-9145.

151. Ganster, J.; Blackwell, J. In *NpH-MD-Simulations of the Elastic Moduli of Cellulose II at Room Temperatue*, Molecular modeling annual, Springer: 1996; pp 278-285.

152. Sakurada, I.; Nukushina, Y.; Ito, T., Experimental determination of the elastic modulus of crystalline regions in oriented polymers. *J Polym Sci* 1962, 57, 651-660.

153. Nishino, T.; Takano, K.; Nakamae, K., Elastic-Modulus of the Crystalline Regions of Cellulose Polymorphs. *J Polym Sci Pol Phys* 1995, 33, 1647-1651.

154. Matsuo, M.; Sawatari, C.; Iwai, Y.; Ozaki, F., Effect of orientation distribution and crystallinity on the measurement by X-ray diffraction of the crystal lattice moduli of cellulose I and II. *Macromolecules* 1990, 23, 3266-3275.

155. Sturcova, A.; Davies, G. R.; Eichhorn, S. J., Elastic modulus and stress-transfer properties of tunicate cellulose whiskers. *Biomacromolecules* 2005, 6, 1055-1061.

156. Diddens, I.; Murphy, B.; Krisch, M.; Muller, M., Anisotropic Elastic Properties of Cellulose Measured Using Inelastic X-ray Scattering. *Macromolecules* 2008, 41, 9755-9759.

157. Favier, V.; Canova, G. R.; Cavaille, J. Y.; Chanzy, H.; Dufresne, A.; Gauthier, C., Nanocomposite Materials from Latex and Cellulose Whiskers. *Polym Advan Technol* 1995, 6, 351-355.

158. Grunert, M.; Winter, W., Progress in the development of cellulose reinforced nanocomposites. *POLYMERIC MATERIALS SCIENCE AND ENGINEERING-WASHINGTON-* 2000, 82, 232-232.

159. Oksman, K.; Niska, K. O.; Sain, M., *Cellulose nanocomposites: processing, characterization, and properties*. Amer Chemical Society: 2006.

160. Samir, M. A. S. A.; Alloin, F.; Sanchez, J. Y.; Dufresne, A., Cellulose nanocrystals reinforced poly(oxyethylene). *Polymer* 2004, 45, 4149-4157.

161. Grunert, M.; Winter, W. T., Nanocomposites of cellulose acetate butyrate reinforced with cellulose nanocrystals. *J Polym Environ* 2002, 10, 27-30.

162. Choi, Y. J.; Simonsen, J., Cellulose nanocrystal-filled carboxymethyl cellulose nanocomposites. *J Nanosci Nanotechno* 2006, 6, 633-639.

163. Paralikara, S. A.; Simonsen, J.; Lombardi, J., Poly(vinyl alcohol)/cellulose nanocrystal barrier membranes. *J Membrane Sci* 2008, 320, 248-258.

164. de Rodriguez, N. L. G.; Thielemans, W.; Dufresne, A., Sisal cellulose whiskers reinforced polyvinyl acetate nanocomposites. *Cellulose* 2006, 13, 261-270.

165. Cao, X. D.; Habibi, Y.; Lucia, L. A., One-pot polymerization, surface grafting, and processing of waterborne polyurethane-cellulose nanocrystal nanocomposites. *J Mater Chem* 2009, 19, 7137-7145.

166. Favier, V.; Cavaille, J.; Canova, G.; Shrivastava, S., Mechanical percolation in cellulose whisker nanocomposites. *Polymer Engineering & Science* 1997, 37, 1732-1739.

167. Flandin, L.; Cavaillé, J.; Bidan, G.; Brechet, Y., New nanocomposite materials made of an insulating matrix and conducting fillers: processing and properties. *Polymer Composites* 2000, 21, 165-174.

168. Surve, M.; Pryamitsyn, V.; Ganesan, V., Universality in structure and elasticity of polymer-nanoparticle gels. *Physical review letters* 2006, 96, 177805.

169. Surve, M.; Pryamitsyn, V.; Ganesan, V., Polymer-bridged gels of nanoparticles in solutions of adsorbing polymers. *The Journal of chemical physics* 2006, 125, 064903.

170. Prasad, V.; Trappe, V.; Dinsmore, A.; Segre, P.; Cipelletti, L.; Weitz, D., Rideal Lecture Universal features of the fluid to solid transition for attractive colloidal particles. *Faraday discussions* 2003, 123, 1-12.

171. Barkhordari, M. R.; Fathi, M., Production and characterization of chitin nanocrystals from prawn shell and their application for stabilization of Pickering emulsions. *Food Hydrocolloid* 2018, 82, 338-345.

172. Fessi, N.; Nsib, M. F.; Chevalier, Y.; Guillard, C.; Dappozze, F.; Houas, A.; Palmisano, L.; Parrino, F., Photocatalytic degradation enhancement in Pickering emulsions stabilized by solid particles of bare TiO2. *Langmuir* 2019.

173. Marefati, A.; Bertrand, M.; Sjöö, M.; Dejmek, P.; Rayner, M., Storage and digestion stability of encapsulated curcumin in emulsions based on starch granule Pickering stabilization. *Food Hydrocolloid* 2017, 63, 309-320.

174. Zembyla, M.; Murray, B. S.; Sarkar, A., Water-In-Oil Pickering Emulsions Stabilized by Water-Insoluble Polyphenol Crystals. *Langmuir* 2018, 34, 10001-10011.

175. Wang, F.; Tang, J.; Liu, H.; Yu, G.; Zou, Y., Self-assembled polymeric micelles as amphiphilic particulate emulsifiers for controllable Pickering emulsions. *Materials Chemistry Frontiers* 2019.

176. Wu, J.; Ma, G. H., Recent studies of Pickering emulsions: particles make the difference. *Small* 2016, 12, 4633-4648.

177. Binks, B. P., Particles as surfactants - similarities and differences. *Curr Opin Colloid In* 2002, 7, 21-41.

178. Hu, Z.; Marway, H. S.; Kasem, H.; Pelton, R.; Cranston, E. D., Dried and Redispersible Cellulose Nanocrystal Pickering Emulsions. *Acs Macro Lett* 2016, 5, 185-189.

179. Tsuji, S.; Kawaguchi, H., Thermosensitive pickering emulsion stabilized by poly(N-isopropylacrylamide)-carrying particles. *Langmuir* 2008, 24, 3300-3305.

180. Guo, W.; Liu, J.; Zhang, P.; Song, L.; Wang, X.; Hu, Y., Multi-functional hydroxyapatite/polyvinyl alcohol composite aerogels with self-cleaning, superior fire resistance and low thermal conductivity. *Compos Sci Technol* 2018, 158, 128-136.

181. Liu, A.; Medina, L.; Berglund, L. A., High-Strength Nanocomposite Aerogels of Ternary Composition: Poly (vinyl alcohol), Clay, and Cellulose Nanofibrils. *Acs Appl Mater Inter* 2017, 9, 6453-6461.

182. Zhang, R.; Wan, W.; Qiu, L.; Wang, Y.; Zhou, Y., Preparation of hydrophobic polyvinyl alcohol aerogel via the surface modification of boron nitride for environmental remediation. *Appl Surf Sci* 2017, 419, 342-347.

183. Yang, Q. L.; Lue, A.; Qi, H. S.; Sun, Y. X.; Zhang, X. Z.; Zhang, L. N., Properties and Bioapplications of Blended Cellulose and Corn Protein Films. *Macromol Biosci* 2009, 9, 849-856.

184. Lemke, C. H.; Dong, R. Y.; Michal, C. A.; Hamad, W. Y., New insights into nano-crystalline cellulose structure and morphology based on solid-state NMR. *Cellulose* 2012, 19, 1619-1629.

185. Nguyen, K. T.; West, J. L., Photopolymerizable hydrogels for tissue engineering applications. *Biomaterials* 2002, 23, 4307-4314.

186. Wang, Y. X.; Chen, L. Y., Impacts of nanowhisker on formation kinetics and properties of all-cellulose composite gels. *Carbohyd Polym* 2011, 83, 1937-1946.

187. Cai, J.; Liu, Y. T.; Zhang, L. N., Dilute solution properties of cellulose in LiOH/urea aqueous system. *J Polym Sci Pol Phys* 2006, 44, 3093-3101.

188. Zhao, H. B.; Kwak, J. H.; Wang, Y.; Franz, J. A.; White, J. M.; Holladay, J. E., Effects of crystallinity on dilute acid hydrolysis of cellulose by cellulose ball-milling study. *Energ Fuel* 2006, 20, 807-811.

189. Gavillon, R.; Budtova, T., Aerocellulose: New highly porous cellulose prepared from cellulose-NaOH aqueous solutions. *Biomacromolecules* 2008, 9, 269-277.

190. Rinaldi, R.; Schuth, F., Acid Hydrolysis of Cellulose as the Entry Point into Biorefinery Schemes. *Chemsuschem* 2009, 2, 1096-1107.

191. Bungay, H. R., Biomass Refining. *Science* 1982, 218, 643-646.

192. Favier, V.; Chanzy, H.; Cavaille, J. Y., Polymer Nanocomposites Reinforced by Cellulose Whiskers. *Macromolecules* 1995, 28, 6365-6367.

193. Bondeson, D.; Mathew, A.; Oksman, K., Optimization of the isolation of nanocrystals from microcrystalline cellulose by acid hydrolysis. *Cellulose* 2006, 13, 171-180.

194. French, A. D., Idealized powder diffraction patterns for cellulose polymorphs. *Cellulose* 2014, 21, 885-896.

195. Fernandes, A. N.; Thomas, L. H.; Altaner, C. M.; Callow, P.; Forsyth, V. T.; Apperley, D. C.; Kennedy, C. J.; Jarvis, M. C., Nanostructure of cellulose microfibrils in spruce wood. *P Natl Acad Sci USA* 2011, 108, E1195-E1203.

196. Ruan, D.; Lue, A.; Zhang, L., Gelation behaviors of cellulose solution dissolved in aqueous NaOH/thiourea at low temperature. *Polymer* 2008, 49, 1027-1036.

197. Weng, L. H.; Zhang, L. N.; Ruan, D.; Shi, L. H.; Xu, J., Thermal gelation of cellulose in a NaOH/thiourea aqueous solution. *Langmuir* 2004, 20, 2086-2093.

198. Skouri, R.; Schosseler, F.; Munch, J. P.; Candau, S. J., Swelling and Elastic Properties of Polyelectrolyte Gels. *Macromolecules* 1995, 28, 197-210.

199. Emileh, A.; Vasheghani-Farahani, E.; Imani, M., Swelling behavior, mechanical properties and network parameters of pH- and temperature-sensitive hydrogels of poly((2-dimethyl amino) ethyl methacrylate-co-butyl methacrylate). *Eur Polym J* 2007, 43, 1986-1995.

200. Svensson, A.; Nicklasson, E.; Harrah, T.; Panilaitis, B.; Kaplan, D. L.; Brittberg, M.; Gatenholm, P., Bacterial cellulose as a potential scaffold for tissue engineering of cartilage. *Biomaterials* 2005, 26, 419-431.

201. Sanabria-DeLong, N.; Crosby, A. J.; Tew, G. N., Photo-Cross-Linked PLA-PEO-PLA Hydrogels from Self-Assembled Physical Networks: Mechanical Properties and Influence of Assumed Constitutive Relationships. *Biomacromolecules* 2008, 9, 2784-2791.

202. Lewis, M. A., Chronic and Sublethal Toxicities of Surfactants to Aquatic Animals - a Review and Risk Assessment. *Water Res* 1991, 25, 101-113.

203. Roberts, C. L.; Rushworth, S. L.; Richman, E.; Rhodes, J. M., Hypothesis: Increased consumption of emulsifiers as an explanation for the rising incidence of Crohn's disease. *J Crohns Colitis* 2013, 7, 338-341.

204. Tang, J. T.; Lee, M. F. X.; Zhang, W.; Zhao, B. X.; Berry, R. M.; Tam, K. C., Dual Responsive Pickering Emulsion Stabilized by Poly[2-(dimethylamino)ethyl methacrylate] Grafted Cellulose Nanocrystals. *Biomacromolecules* 2014, 15, 3052-3060.

205. Murray, B. S.; Durga, K.; Yusoff, A.; Stoyanov, S. D., Stabilization of foams and emulsions by mixtures of surface active food-grade particles and proteins. *Food Hydrocolloid* 2011, 25, 627-638.

206. Cunha, A. G.; Mougel, J. B.; Cathala, B.; Berglund, L. A.; Capron, I., Preparation of Double Pickering Emulsions Stabilized by Chemically Tailored Nanocelluloses. *Langmuir* 2014, 30, 9327-9335.

207. Visanko, M.; Liimatainen, H.; Sirvio, J. A.; Heiskanen, J. P.; Niinimaki, J.; Hormi, O., Amphiphilic Cellulose Nanocrystals from Acid-Free Oxidative Treatment: Physicochemical Characteristics and Use as an Oil-Water Stabilizer. *Biomacromolecules* 2014, 15, 2769-2775.

208. Yoon, J. Y.; Park, H. Y.; Kim, J. H.; Kim, W. S., Adsorption of BSA on highly carboxylated microspheres - Quantitative effects of surface functional groups and interaction forces. *J Colloid Interf Sci* 1996, 177, 613-620.

209. Salajkova, M.; Berglund, L. A.; Zhou, Q., Hydrophobic cellulose nanocrystals modified with quaternary ammonium salts. *J Mater Chem* 2012, 22, 19798-19805.

210. Wang, Y. X.; Chen, L. Y., Cellulose Nanowhiskers and Fiber Alignment Greatly Improve Mechanical Properties of Electrospun Prolamin Protein Fibers. *Acs Appl Mater Inter* 2014, 6, 1709-1718.

211. Tasset, S.; Cathala, B.; Bizot, H.; Capron, I., Versatile cellular foams derived from CNC-stabilized Pickering emulsions. *Rsc Adv* 2014, 4, 893-898.

212. Kalashnikova, I.; Bizot, H.; Cathala, B.; Capron, I., Modulation of Cellulose Nanocrystals Amphiphilic Properties to Stabilize Oil/Water Interface. *Biomacromolecules* 2012, 13, 267-275.

213. Kazarian, A. A.; Taylor, M. R.; Haddad, P. R.; Nesterenko, P. N.; Paull, B., Ion-exchange and hydrophobic interactions affecting selectivity for neutral and charged solutes on three

structurally similar agglomerated ion-exchange and mixed-mode stationary phases. *Analytica chimica acta* 2013, 803, 143-153.

214. El-Nahhal, Y.; Nir, S.; Serban, C.; Rabinovitch, O.; Rubin, B., Montmorillonite−phenyltrimethylammonium yields environmentally improved formulations of hydrophobic herbicides. *Journal of Agricultural and Food Chemistry* 2000, 48, 4791-4801.

215. Aveyard, R.; Binks, B. P.; Clint, J. H., Emulsions stabilised solely by colloidal particles. *Adv Colloid Interfac* 2003, 100, 503-546.

216. Frelichowska, J.; Bolzinger, M. A.; Chevalier, Y., Effects of solid particle content on properties of o/w Pickering emulsions. *J Colloid Interf Sci* 2010, 351, 348-356.

217. Midmore, B. R., Effect of aqueous phase composition on the properties of a silica-stabilized W/O emulsion. *J Colloid Interf Sci* 1999, 213, 352-359.

218. Wollenweber, C.; Makievski, A. V.; Miller, R.; Daniels, R., Adsorption of hydroxypropyl methylcellulose at the liquid/liquid interface and the effect on emulsion stability. *Colloid Surface A* 2000, 172, 91-101.

219. Shopsowitz, K. E.; Qi, H.; Hamad, W. Y.; MacLachlan, M. J., Free-standing mesoporous silica films with tunable chiral nematic structures. *Nature* 2010, 468, 422-U246.

220. Boluk, Y.; Lahiji, R.; Zhao, L. Y.; McDermott, M. T., Suspension viscosities and shape parameter of cellulose nanocrystals (CNC). *Colloid Surface A* 2011, 377, 297-303.

221. Monteiro, N.; Martins, A.; Reis, R. L.; Neves, N. M., Liposomes in tissue engineering and regenerative medicine. *J R Soc Interface* 2014, 11.

222. Fortunati, E.; Puglia, D.; Monti, M.; Santulli, C.; Maniruzzaman, M.; Kenny, J. M., Cellulose nanocrystals extracted from okra fibers in PVA nanocomposites. *J Appl Polym Sci* 2013, 128, 3220-3230.

223. Bai, X.; Ye, Z. F.; Li, Y. F.; Ma, Y. X., Macroporous Poly(vinyl alcohol) Foam Crosslinked with Epichlorohydrin for Microorganism Immobilization. *J Appl Polym Sci* 2010, 117, 2732-2739.

224. Wang, Y. X.; Chang, C. Y.; Zhang, L. N., Effects of Freezing/Thawing Cycles and Cellulose Nanowhiskers on Structure and Properties of Biocompatible Starch/PVA Sponges. *Macromol Mater Eng* 2010, 295, 137-145.

225. Chang, C. Y.; Lue, A.; Zhang, L., Effects of crosslinking methods on structure and properties of cellulose/PVA hydrogels. *Macromol Chem Physic* 2008, 209, 1266-1273.

226. Joshi, M. K.; Tiwari, A. P.; Pant, H. R.; Shrestha, B. K.; Kim, H. J.; Park, C. H.; Kim, C. S., In Situ Generation of Cellulose Nanocrystals in Polycaprolactone Nanofibers: Effects on Crystallinity, Mechanical Strength, Biocompatibility, and Biomimetic Mineralization. *Acs Appl Mater Inter* 2015, 7, 19672-19683.

227. Chang, C. Y.; Duan, B.; Cai, J.; Zhang, L. N., Superabsorbent hydrogels based on cellulose for smart swelling and controllable delivery. *Eur Polym J* 2010, 46, 92-100.

228. Qin, X. Z.; Lu, A.; Zhang, L. N., Gelation behavior of cellulose in NaOH/urea aqueous system via cross-linking. *Cellulose* 2013, 20, 1669-1677.

229. Zheng, Q. F.; Javadi, A.; Sabo, R.; Cai, Z. Y.; Gong, S. Q., Polyvinyl alcohol (PVA)-cellulose nanofibril (CNF)-multiwalled carbon nanotube (MWCNT) hybrid organic aerogels with superior mechanical properties. *Rsc Adv* 2013, 3, 20816-20823.

230. Yang, X.; Shi, K. Y.; Zhitomirsky, I.; Cranston, E. D., Cellulose Nanocrystal Aerogels as Universal 3D Lightweight Substrates for Supercapacitor Materials. *Adv Mater* 2015, 27, 6104-6109.

231. Si, Y.; Yu, J. Y.; Tang, X. M.; Ge, J. L.; Ding, B., Ultralight nanofibre-assembled cellular aerogels with superelasticity and multifunctionality. *Nat Commun* 2014, 5.

232. Zhu, C.; Han, T. Y. J.; Duoss, E. B.; Golobic, A. M.; Kuntz, J. D.; Spadaccini, C. M.; Worsley, M. A., Highly compressible 3D periodic graphene aerogel microlattices. *Nat Commun* 2015, 6.

233. Gong, X. Y.; Wang, Y. X.; Chen, L. Y., Enhanced emulsifying properties of wood-based cellulose nanocrystals as Pickering emulsion stabilizer. *Carbohyd Polym* 2017, 169, 295-303.

234. Calcagnile, P.; Fragouli, D.; Bayer, I. S.; Anyfantis, G. C.; Martiradonna, L.; Cozzoli, P. D.; Cingolani, R.; Athanassiou, A., Magnetically Driven Floating Foams for the Removal of Oil Contaminants from Water. *Acs Nano* 2012, 6, 5413-5419.

235. Yang, Y.; Deng, Y. H.; Tong, Z.; Wang, C. Y., Multifunctional foams derived from poly(melamine formaldehyde) as recyclable oil absorbents. *J Mater Chem A* 2014, 2, 9994-9999.

236. Zhang, Z.; Sebe, G.; Rentsch, D.; Zimmermann, T.; Tingaut, P., Ultralightweight and Flexible Silylated Nanocellulose Sponges for the Selective Removal of Oil from Water. *Chem Mater* 2014, 26, 2659-2668.

237. Duan, B.; Gao, H. M.; He, M.; Zhang, L. N., Hydrophobic Modification on Surface of Chitin Sponges for Highly Effective Separation of Oil. *Acs Appl Mater Inter* 2014, 6, 19933-19942.

238. Korhonen, J. T.; Kettunen, M.; Ras, R. H. A.; Ikkala, O., Hydrophobic Nanocellulose Aerogels as Floating, Sustainable, Reusable, and Recyclable Oil Absorbents. *Acs Appl Mater Inter* 2011, 3, 1813-1816.

239. Wen, Q.; Di, J. C.; Jiang, L.; Yu, J. H.; Xu, R. R., Zeolite-coated mesh film for efficient oil-water separation. *Chem Sci* 2013, 4, 591-595.

240. Rajakovic-Ognjanovic, V.; Aleksic, G.; Rajakovic, L., Governing factors for motor oil removal from water with different sorption materials. *J Hazard Mater* 2008, 154, 558-563.

241. Huang, X. F.; Lim, T. T., Performance and mechanism of a hydrophobic-oleophilic kapok filter for oil/water separation. *Desalination* 2006, 190, 295-307.

242. Lee, M. W.; An, S.; Latthe, S. S.; Lee, C.; Hong, S.; Yoon, S. S., Electrospun Polystyrene Nanofiber Membrane with Superhydrophobicity and Superoleophilicity for Selective Separation of Water and Low Viscous Oil. *Acs Appl Mater Inter* 2013, 5, 10597-10604.

243. Zhou, H.; Wang, H. X.; Niu, H. T.; Gestos, A.; Wang, X. G.; Lin, T., Fluoroalkyl Silane Modified Silicone Rubber/Nanoparticle Composite: A Super Durable, Robust Superhydrophobic Fabric Coating. *Adv Mater* 2012, 24, 2409-2412.

244. Abitbol, T.; Johnstone, T.; Quinn, T. M.; Gray, D. G., Reinforcement with cellulose nanocrystals of poly(vinyl alcohol) hydrogels prepared by cyclic freezing and thawing. *Soft Matter* 2011, 7, 2373-2379.

245. Artus, G. R. J.; Jung, S.; Zimmermann, J.; Gautschi, H. P.; Marquardt, K.; Seeger, S., Silicone nanofilaments and their application as superhydrophobic coating. *Adv Mater* 2006, 18, 2758-2762.

246. Gurav, J. L.; Rao, A. V.; Nadargi, D. Y.; Park, H. H., Ambient pressure dried TEOS-based silica aerogels: good absorbents of organic liquids. *J Mater Sci* 2010, 45, 503-510.

247. Schaedler, T. A.; Jacobsen, A. J.; Torrents, A.; Sorensen, A. E.; Lian, J.; Greer, J. R.; Valdevit, L.; Carter, W. B., Ultralight Metallic Microlattices. *Science* 2011, 334, 962-965.

248. Choi, S. J.; Kwon, T. H.; Im, H.; Moon, D. I.; Baek, D. J.; Seol, M. L.; Duarte, J. P.; Choi, Y. K., A Polydimethylsiloxane (PDMS) Sponge for the Selective Absorption of Oil from Water. *Acs Appl Mater Inter* 2011, 3, 4552-4556.

249. Li, A.; Sun, H. X.; Tan, D. Z.; Fan, W. J.; Wen, S. H.; Qing, X. J.; Li, G. X.; Li, S. Y.; Deng, W. Q., Superhydrophobic conjugated microporous polymers for separation and adsorption. *Energ Environ Sci* 2011, 4, 2062-2065.

250. Wu, T.; Chen, M. X.; Zhang, L.; Xu, X. Y.; Liu, Y.; Yan, J.; Wang, W.; Gao, J. P., Three-dimensional graphene-based aerogels prepared by a self-assembly process and its excellent catalytic and absorbing performance. *J Mater Chem A* 2013, 1, 7612-7621.

251. Zhu, Q.; Chu, Y.; Wang, Z. K.; Chen, N.; Lin, L.; Liu, F. T.; Pan, Q. M., Robust superhydrophobic polyurethane sponge as a highly reusable oil-absorption material. *J Mater Chem A* 2013, 1, 5386-5393.

252. Gui, X. C.; Wei, J. Q.; Wang, K. L.; Cao, A. Y.; Zhu, H. W.; Jia, Y.; Shu, Q. K.; Wu, D. H., Carbon Nanotube Sponges. *Adv Mater* 2010, 22, 617-621.

253. Liu, Y.; Ma, J. K.; Wu, T.; Wang, X. R.; Huang, G. B.; Liu, Y.; Qiu, H. X.; Li, Y.; Wang, W.; Gao, J. P., Cost-Effective Reduced Graphene Oxide-Coated Polyurethane Sponge As a Highly Efficient and Reusable Oil-Absorbent. *Acs Appl Mater Inter* 2013, 5, 10018-10026.

254. Zhu, Q.; Pan, Q. M.; Liu, F. T., Facile Removal and Collection of Oils from Water Surfaces through Superhydrophobic and Superoleophilic Sponges. *J Phys Chem C* 2011, 115, 17464-17470.

Appendix

Content of phenyltrimethylammonium (CP)

The content of phenyltrimethylammonium (CP) was calculated according to the following equation:

$$CP\%=N\%/14\times136 \qquad (1)$$

where N% is the nitrogen content (%), 14 and 136 stand for the relative atomic mass of nitrogen and molecular weight of phenyltrimethylammonium group, respectively. The content of phenyltrimethylammonium (CP) on the surface of m-O-CNCs-1, m-O-CNCs-2 and m-O-CNCs-3 was calculated to be 9.42%, 15.36%, and 18.77%, respectively.

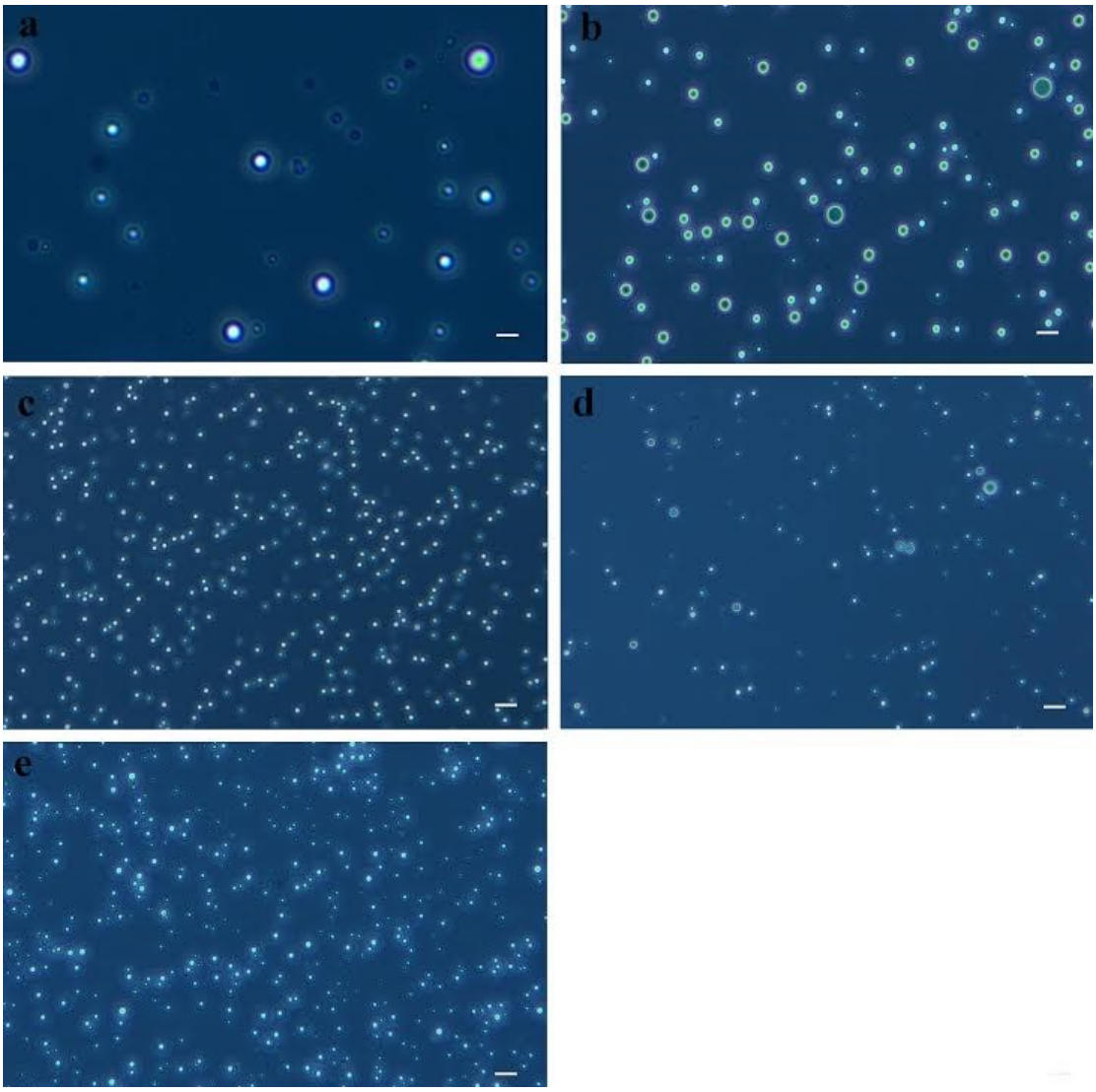

Figure S 1 (a-e) Optic microscopic images of the hexadecane/water Pickering emulsions stabilized by m-O-CNC-1 at various concentrations. (a) 0.5 g/L (b) 1.0 g/L(c) 2.0 g/L (d)4.0 g/L (e) 5.0 g/L. Scale bar: 10 μm.

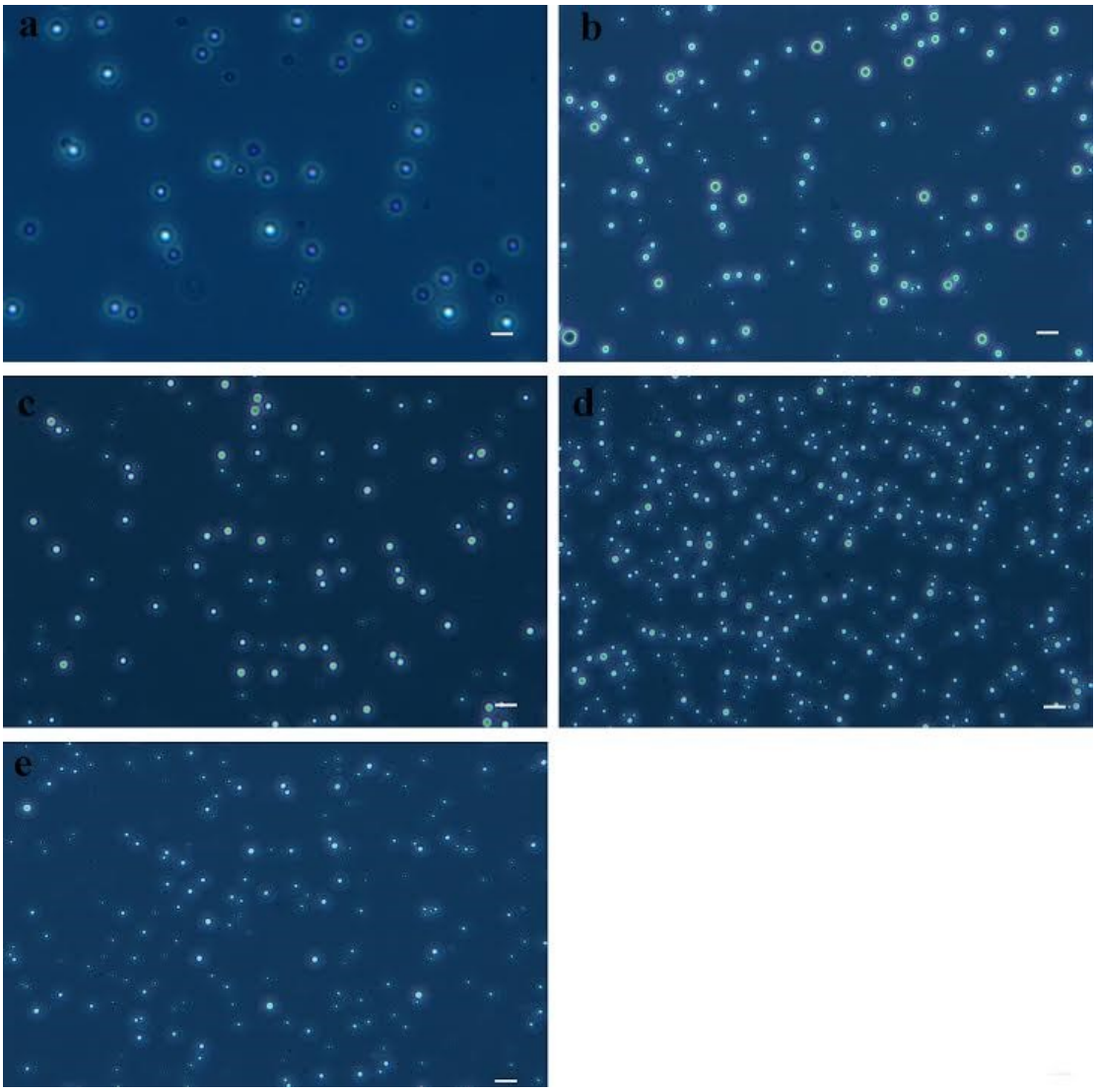

Figure S 2 (a-e) Optic microscopic images of the hexadecane/water Pickering emulsions stabilized by m-O-CNC-3 at various concentrations. (a) 0.5 g/L (b) 1.0 g/L(c) 2.0 g/L (d)4.0 g/L (e) 5.0 g/L. Scale bar: 10 μm.

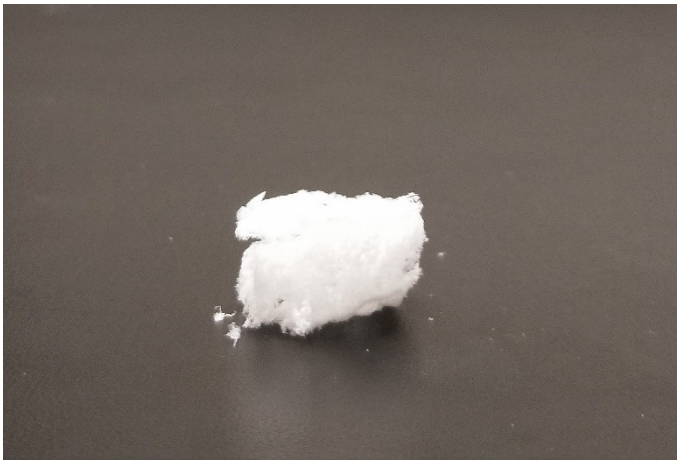

Figure S 3 Image of CNCs/ECH.

Figure S 4 Compression images of the Aerogel-6 (a) and PVA-ECH sponge (b).

Video S 1 Removal of oil-red-colored chloroform from deionized water with Aerogel-2.

Video S 2 Rinsing Aerogel-2 with ethanol to remove the red-oil-colored chloroform and maintain its absorption capacity.